Hydrogeochemical Characterization of Water Resources in the Pra Basin (Ghana) for Quality Assessment and Water Management: Field Observations and Geochemical Modelling

---

Hydrogeochemische Charakterisierung der Wasserressourcen im Pra-Becken (Ghana) zur Qualitätsbewertung und Wasserbewirtschaftung: Feldbeobachtungen und Geochemische Modellierung

Kumulative Dissertation

zur Erlangung des akademischen Grades

doctor rerum naturalium (Dr. rer. nat.)

in der Wissenschaftsdisziplin Hydrogeologie

eingereicht an der

Mathematisch-Naturwissenschaftlichen Fakultät

der Universität Potsdam

vorgelegt von

Manu Evans

Potsdam, 18. December 2023

Gutachter

Prof. Dr. Michael Kuhn
Deutsches GeoForschungsZentrum GFZ
Department Geochemie
Sektion Fluidsystemmodellierung

und

Universitat Potsdam
Mathematisch-Naturwissenschaftliche Fakultat
Institut fur Geowissenschaften

Prof. Dr. Maria-Theresia Schafmeister
Universitat Greifswald
Mathematisch-Naturwissenschaftliche Fakultat
Institut fur Geographie und Geologie

Prof. Bruce Kofi Banoeng-Yakubo
University of Ghana
School of Physical and Mathematical Sciences
College of Basic and Applied Sciences

Published online on the
Publication Server of the University of Potsdam:
https://doi.org/10.25932/publishup-62806
https://nbn-resolving.org/urn:nbn:de:kobv:517-opus4-628062

Abstract

Watershed management requires an understanding of key hydrochemical processes. The Pra Basin is one of the five major river basins in Ghana with a population of over 4.2 million people. Currently, water resources management faces challenges due to surface water pollution caused by the unregulated release of untreated household and industrial waste into aquatic ecosystems and illegal mining activities. This has increased the need for groundwater as the most reliable water supply. Our understanding of groundwater recharge mechanisms and chemical evolution in the basin has been inadequate, making effective management difficult. Therefore, the main objective of this work is to gain insight into the processes that determine the hydrogeochemical evolution of groundwater quality in the Pra Basin.

The combined use of stable isotope, hydrochemistry, and water level data provides the basis for conceptualizing the chemical evolution of groundwater in the Pra Basin. For this purpose, the origin and evaporation rates of water infiltrating into the unsaturated zone were evaluated. In addition, Chloride Mass Balance (CMB) and Water Table Fluctuations (WTF) were considered to quantify groundwater recharge for the basin. Indices such as water quality index (WQI), sodium adsorption ratio (SAR), Wilcox diagram, and salinity (USSL) were used in this study to determine the quality of the resource for use as drinking water and for irrigation purposes. Due to the heterogeneity of the hydrochemical data, the statistical techniques of hierarchical cluster and factor analysis were applied to subdivide the data according to their spatial correlation. A conceptual hydrogeochemical model was developed and subsequently validated by applying combinatorial inverse and reaction pathway-based geochemical models to determine plausible mineral assemblages that control the chemical composition of the groundwater.

The interactions between water and rock determine the groundwater quality in the Pra Basin. The results underline that the groundwater is of good quality and can be used for drinking water and irrigation purposes. It was demonstrated that there is a large groundwater potential to meet the entire Pra Basin's current and future water demands. The main recharge area was identified as the northern zone, while the southern zone is the discharge area. The predominant influence of weathering of silicate minerals plays a key role in the chemical evolution of the groundwater.

The work presented here provides fundamental insights into the hydrochemistry of the Pra Basin and provides data important to water managers for informed decision-making in planning and allocating water resources for various purposes. A novel inverse modelling approach was used in this study to identify different mineral compositions that determine the chemical evolution of groundwater in the Pra Basin. This modelling technique has the potential to simulate the composition of groundwater at the basin scale with large hydrochemical heterogeneity, using average water composition to represent established spatial groupings of water chemistry.

Kurzfassung

Die Bewirtschaftung von Wassereinzugsgebieten erfordert ein Verständnis der wichtigsten hydrochemischen Prozesse. Das Pra-Becken ist eines der fünf großen Flusseinzugsgebiete Ghanas mit einer Bevölkerung von über 4,2 Millionen Menschen. Die Bewirtschaftung der Wasserressourcen wird derzeit durch die Verschmutzung der Oberflächengewässer erschwert, die durch die unkontrollierte Einleitung von unbehandelten Haushalts- und Industrieabfällen in die aquatischen Ökosysteme und durch illegale Bergbauaktivitäten entsteht. Dies hat den Bedarf an Grundwasser als zuverlässigste Wasserversorgung erhöht. Unser Verständnis der Mechanismen der Grundwasserneubildung und der chemischen Entwicklung im Einzugsgebiet ist bislang unzureichend, was eine wirksame Bewirtschaftung erschwert. Daher ist das Hauptziel dieser Arbeit Einblicke in die Prozesse zu bekommen, welche die hydrogeochemische Entwicklung der Grundwasserqualität im Pra-Becken bestimmen.

Die kombinierte Verwendung von Daten stabiler Isotope, der Hydrochemie und von Wasserständen bildet die Grundlage für die Konzeption der chemischen Entwicklung des Grundwassers im Pra-Becken. Dafür wurden die Herkunft und die Verdunstungsraten des in die ungesättigte Zone infiltrierenden Wassers bewertet. Darüber hinaus wurden die Chlorid-Massenbilanz und die Wasserspiegelschwankungen betrachtet, um die Grundwasserneubildung für das Einzugsgebiet zu quantifizieren. Indizes wie der Wasserqualitätsindex (WQI), das Natriumadsorptionsverhältnis (SAR), das Wilcox-Diagramm und der Salzgehalt (USSL) wurden in dieser Studie verwendet, um die Qualität der Ressource für die Verwendung als Trinkwasser und zu Bewässerungszwecken zu bestimmen. Aufgrund der Heterogenität der hydrochemischen Daten wurden die statistischen Verfahren der hierarchischen Cluster- und Faktorenanalyse angewandt, um die Daten entsprechend ihrer räumlichen Korrelation zu unterteilen. Ein konzeptionelles hydrogeochemisches Modell wurde entwickelt und anschließend durch Anwendung kombinatorischer inverser und reaktionspfadbasierter geochemischer Modelle validiert, um plausible mineralische Assemblagen zu bestimmen, welche die chemische Zusammensetzung des Grundwassers kontrollieren.

Die Wechselwirkungen zwischen Wasser und Gestein bestimmen die Grundwasserqualität im Pra-Becken. Die Ergebnisse unterstreichen, dass das Grundwasser eine gute Qualität aufweist und als Trinkwasser und für Bewässerungszwecke genutzt werden kann. Es wurde nachgewiesen, dass ein großes Grundwasserpotenzial vorhanden ist, um den derzeitigen und künftigen Wasserbedarf des gesamten Pra-Beckens zu decken. Als Hauptneubildungsgebiet wurde die nördliche Zone im Gebiet identifiziert, während die südliche Zone das Abflussgebiet ist. Der vorherrschende Einfluss der Verwitterung von Silikatmineralen spielt bei der chemischen Entwicklung des Grundwassers eine zentrale Rolle.

Die hier vorgestellte Arbeit gibt grundlegende Einblicke in die Hydrochemie des Pra-Beckens und liefert für das Wassermanagement wichtige Daten für eine fundierte Entscheidungsfindung bei der Planung und Zuweisung von Wasserressourcen für verschiedene Zwecke. Ein neuartiger Ansatz zur inversen Modellierungwurde in dieser Studie eingesetzt, um unterschiedliche Mineralzusammensetzungen zu ermitteln, welche die chemische Entwicklung des Grundwassers im Pra-Becken bestimmen. Diese Modellierungstechnik hat das Potenzial, die Zusammensetzung eines Grundwassers auf der Skala eines Beckens mit großer hydrochemischer Heterogenität zu simulieren, wobei die durchschnittliche Wasserzusammensetzung zur Darstellung der etablierten räumlichen Gruppierungen der Wasserchemie verwendet wird.

Table of contents

Abstract I

Kurzfassung III

List of Figures IX

List of Tables XIII

List of Acronyms and Symbols XV

1 Introduction and Motivation 1
- 1.1 Water Resources Potential and Uses in the Pra Basin . . . 1
- 1.2 Sources of Water Pollution . . . 2
- 1.3 Regional Geology and Hydrogeology . . . 3
- 1.4 Previous Works and Knowledge Gap . . . 6
- 1.5 Relevance of this Study . . . 8
- 1.6 Thesis Objectives . . . 9
- 1.7 Geochemical Modelling of Water Chemistry . . . 9
- 1.8 Approaches to Estimate Groundwater Recharge . . . 10
- 1.9 Structure of the Thesis and Scientific Contribution . . . 11

2 Stable Isotopes and Water Level Monitoring Integrated to Characterize Groundwater Recharge in the Pra Basin, Ghana 13
- 2.1 Introduction . . . 14
- 2.2 Materials and Methods . . . 15
  - 2.2.1 Study Area . . . 15
  - 2.2.2 Data Collection and Analysis . . . 17
  - 2.2.3 Quantification of Evaporation Losses of Sampled Water . . . 18
  - 2.2.4 Groundwater Recharge Estimation Using CMB Method . . . 19
  - 2.2.5 Groundwater Recharge Estimation Using Water Table Fluctuation Method 20
- 2.3 Results . . . 21
  - 2.3.1 Climatology of Precipitation and Temperature in the Pra Basin . . . 21
  - 2.3.2 Variability in Surface Water and Groundwater $\delta^{18}O$ and $\delta^{2}H$ Values . . . 22
  - 2.3.3 Correlation Between $\delta^{18}O$ and $\delta^{2}H$ of Water . . . 23
  - 2.3.4 Estimations of the Rate of Evaporation in Surface Water and Groundwater 25
  - 2.3.5 Groundwater Recharge Estimate Using Chloride Mass Balance Method . 25
  - 2.3.6 Groundwater Recharge Estimate from Water Table Fluctuation Method . 26
- 2.4 Discussion . . . 28
  - 2.4.1 Regional Climatic Conditions, Present and the Past . . . 28
  - 2.4.2 Isotopic Characterization of the Surface Water and Groundwater . . . 28
  - 2.4.3 Groundwater Recharge Estimates . . . 30
- 2.5 Conclusions . . . 32
- 2.6 Appendix . . . 34
  - 2.6.1 Groundwater Recharge Estimates Using the CMB Method . . . 34

2.6.2 A Decadal Mean Monthly Precipitation Climatology in the Pra Basin from 1964 to 2013 . . . 35
2.6.3 A Decadal Mean Monthly Temperature Climatology in the Pra Basin from 1964 to 2013 . . . 36
2.6.4 Stable Oxygen-18 and Deuterium Isotopes Plot Against Elevation for Surface Water and Groundwater . . . 37

3 Hydrochemical Characterization of Surface Water and Groundwater in the Crystalline Basement Aquifer System in the Pra Basin (Ghana) 39
3.1 Introduction . . . 39
3.2 Materials and Methods . . . 41
3.2.1 Location and Physical Setting . . . 41
3.2.2 Geology . . . 42
3.2.3 Surface Water and Groundwater Sampling . . . 42
3.2.4 Instrumentation and Measurements . . . 43
3.2.5 Computation of Water Quality Indices . . . 43
3.2.6 Cluster Analysis of the Groundwater Hydrochemical Data . . . 45
3.3 Results . . . 45
3.3.1 Surface Water Chemistry . . . 46
3.3.2 Groundwater Chemistry . . . 46
3.3.3 Calculation of Surface Water Quality Indices for Drinking and Irrigation . . . 46
3.3.4 Calculation of Groundwater Quality Indices for Drinking and Irrigation . . . 48
3.3.5 Hierarchical Cluster Analysis (HCA) of the Groundwater Hydrochemical Data . . . 48
3.3.6 Groundwater Chemical Variation Within the Three Defined Zones . . . 49
3.3.7 Groundwater Types . . . 52
3.3.8 Mineral Weathering Processes . . . 53
3.3.9 Factor Analysis . . . 53
3.4 Discussion . . . 55
3.4.1 Sampling and Measurements . . . 55
3.4.2 Assessment of Surface Water Quality for Drinking and Irrigation . . . 55
3.4.3 Assessment of Groundwater Quality for Drinking and Irrigation . . . 56
3.4.4 Mechanism Controlling Groundwater Chemistry . . . 57
3.4.5 Chemical Processes Driving Groundwater Evolution . . . 57
3.4.6 Statistical Analysis Explaining the Causes of Spatial Variability in Groundwater Composition . . . 58
3.5 Conclusions . . . 59

4 Water-Rock Interactions Driving Groundwater Composition in the Pra Basin (Ghana) Identified by Combinatorial Inverse Geochemical Modelling 61
4.1 Introduction . . . 61
4.2 Materials and Methods . . . 63
4.2.1 Study Area . . . 63
4.2.2 Geological Setting . . . 63
4.2.3 Hydrogeologic Conditions . . . 64
4.2.4 Field Work . . . 65
4.2.5 Modelling Input Data Sources . . . 65

4.2.6 Geochemical Code and Thermodynamic Data . . . 67
4.2.7 Combinatorial Inverse Modelling Approach . . . 67
4.2.8 Calibration Based on Reaction Path Scheme . . . 69
4.3 Results . . . 70
4.3.1 Mineral Assemblages Identified from the Combinatorial Inverse Modelling 70
4.3.2 Reaction Path Modelling . . . 72
4.4 Discussion . . . 74
4.5 Model Limitations . . . 77
4.6 Conclusions . . . 78
4.7 Appendix . . . 80
4.7.1 Additional Mineral Phases Included in the `phreeqc.dat` Thermodynamic Data Base . . . 80

5 Discussion **81**
5.1 Water Quality and Groundwater Recharge Dynamics . . . 82
5.2 Complexities of Conceptual Groundwater Flow Path . . . 83
5.3 A Novel Model for the assessment of Water Quality Evolution . . . 84
5.4 Implications for Water Resources Management . . . 86

6 Conclusions and outlook **89**

References **93**

Publications of the candidate **103**

Acknowledgements **105**

Selbstständigkeitserklärung

List of Figures

1.1 Sources of water supply in the Pra Basin include mechanized boreholes fitted with hand pumps for community water supply with depths usually less than 60 m (A) and hand-dug wells usually completed to a depth of less than 20 m (B). Picture taken on March 17, 2020. 3

1.2 A degraded land from illegal mining activities in search of economic minerals. Picture taken on March 14, 2020. 4

1.3 Polluted surface water bodies mainly resulted from the activities of illegal mining operations. Picture taken on March 03, 2020. 5

1.4 Geological map of the Pra Basin showing the three dominant lithologies, the Birimian Supergroup composed of the meta-sediments and the volcanic rocks, the Granitoid consisting of the Cape Coast granitoid and the Tarkwain Group. 6

2.1 The location of the main Pra Basin in Ghana (**A**), the study area representing the Birim and the Lower Pra catchments of the Pra Basin (**B**), the geological map of the area showing the predominant rock types and the surface water and groundwater sampling locations (**C**). Modified after Manu et al. (2023d). . . 16

2.2 A topographic map showing the distribution of the sampling points (modified after Manu et al. (2023e)). The northern boundary of the basin forms part of the Kwahu Mountain Range, with elevations reaching 850 m above sea level. Also visible is the river network with major flow direction from the north to the south of the basin. 17

2.3 Mean monthly precipitation **(a)** and temperature **(b)** climatology for the past fifty years (1964-2013) in the study area. Data source: Princeton University's land surface modelling group, which has been biased corrected and down-scaled according to the observation-based global forcing dataset of Sheffield et al. (2006) 22

2.4 Box-and-whisker plots of the variation in the $\delta^{18}O$ and $\delta^{2}H$ ratios and the calculated d-excess for the surface water **(a)** and groundwater **(b)** samples for the three zones. 23

2.5 Groundwater **(a)** ($\delta^{18}O$) and **(b)** ($\delta^{2}H$) values of the Pra Basin do not show significant correlation with elevation. 24

2.6 (**a**) Surface water and groundwater $\delta^{18}O$ and $\delta^{2}H$ relationship plots used to infer the origin and evaporation influence. Also featured are the local (Akiti 1986) and the global (Craig 1961) meteoric water lines. Both water sources defined an evaporation line with lower slopes, indicating the change in the $\delta^{18}O$ and $\delta^{2}H$ isotope ratios in the initial precipitation. (**b**) The d-excess vrs. $\delta^{18}O$ plot provide information about the influence of evaporation. Almost all samples plot below the d-excess of the LMWL, indicating that the precipitation that recharged the surface water and groundwater experienced evaporation. The intercept of the surface water and groundwater lines (A and B) indicates precipitation's initial isotopic signature before recharge. 24

2.7 (**a**) Conceptual diagram showing the potential recharge pathway affecting changes in groundwater isotopic composition and Cl^{-} concentration (modified after Love et al. (1993)). (**b**) Deuterium vs. Cl^{-} shows no dominant process influencing groundwater recharge. 25

2.8 Spatial interpolation of groundwater recharge based on the CMB approach as a percentage of the long-term mean precipitation (1500 mm) using the inverse distance weighting (IDW) method. 26

2.9 Groundwater hydrographs and observed averaged monthly precipitation at some selected locations (**a**) Abaam, (**b**) Asuboni, (**c**) Atutumirem and (**d**) Kwaben in the Pra Basin for the water year 2022. 27

2.10 Decadal mean monthly precipitation climatology from (**a**) 1964 to 1973, (**b**) 1974 to 1983, (**c**) 1984 to 1993, (**d**) 1994 to 2003 and (**e**) 2004 to 2013, respectively in the Pra Basin for the three defined zones (northern, central and southern) after Manu et al. (2023d). The northern zones are at higher elevations while the southern zones are at lower elevations, respectively. 35

2.11 Decadal mean monthly temperature climatology from (**a**) 1964 to 1973, (**b**) 1974 to 1983, (**c**) 1984 to 1993, (**d**) 1994 to 2003 and (**e**) 2004 to 2013, respectively in the Pra Basin for the three defined zones (northern, central and southern) after Manu et al. (2023d). The northern zones are at higher elevations, while the southern ones are at lower elevations. 36

2.12 Surface water stable oxygen-18 (**a**) and deuterium (**b**) isotopes plot against elevation show no clear correlation between them. The sample located in the highest elevation measured the least stable isotope of oxygen and deuterium ratios. 37

2.13 Groundwater stable oxygen-18 (**a**) and deuterium (**b**) isotopes plot against elevation show no significant correlation between them. Very few samples in the southern zone (low elevation) showed relative enrichment of the stable oxygen-18 and deuterium isotope ratios. 37

3.1 The location of the main Pra Basin in Ghana and the international boundaries (**A**), the study area representing the Birim and the Lower Pra catchments of the Pra Basin (**B**), the digital elevation model (DEM) of the study area and the river networks, including some notable districts (**C**). 41

3.2 Geological map of the study area showing the predominant rock types and the sampling locations. The Birimian Supergroup consist of meta-sediments, mainly phyllite, schists and greywacke. The Tarkwain Group consist of sandstones, conglomerates and argillites, the Cape Coast granitoid of quartz and dioritic gneiss and the Dyke is made of dolerite. 42

3.3 The box- and-whisker plots show the relative abundance of major ions, trace metals and silica in surface water (**a**) and groundwater (**b**). The horizontal solid line and the x symbol on the box-and-whisker plot represent the average and the median concentrations, respectively. Outliers are defined by points that fall more than 1.5*IQR above the third quartile or below the first quartile. All the ion concentrations are measured in mg/L except pH. 47

3.4 Surface water spatial distribution maps of (**a**) Water Quality Index (WQI) and (**b**) Sodium Adsorption Ratio (SAR) for the assessment of water quality for drinking and irrigation purposes 47

3.5 Irrigation water classification diagrams showing surface water and groundwater quality acceptable for irrigation (**a**) USSL classification (Allison and Richards 1954) and (**b**) Wilcox classification (Wilcox 1955) 48

3.6 Groundwater spatial distribution maps of (**a**) Water Quality Index (WQI) and (**b**) Sodium Adsorption Ratio (SAR) for the assessment of water quality for drinking and irrigation purposes. 49

3.7 Hierarchical cluster analysis (HCA) of the hydrochemical dataset. (**A**) Taking into account only hydrochemical data, three clusters are identified with no apparent geographical proximity, highlighting large variability across the basin. (**B**) Considering elevation for the HCA, three spatially distinct clusters appear, dividing the basin into three zones: northern, central and southern. The elevation is highest in the northern zone and decreases towards the southern zone. 50

3.8 Box-and-whisker plots displaying the variations in the (**a**) physical parameters and silica content, and (**b**) major cations in the groundwater. The interpretation of the box-and-whisker plots follows the legend presented in Figure 3.3. The horizontal solid line and the x symbol on the box-and-whisker plot represents the average and the median concentrations, respectively. Outliers are defined by points that fall more than 1.5*IQR above the third quartile or below the first quartile. NZ, CZ and SZ denote the northern zone, central zone and southern zone, respectively. All chemical parameters are measured in mg/L except for pH and EC µS/cm. 51

3.9 Box-and-whisker plots highlighting the variations in the major anions (HCO_3^-, Cl^-, SO_4^{2-} and NO_3^-) in groundwater for the three identified zones. The horizontal solid line and the x symbol on the box-and-whisker plot represents the average and the median concentrations, respectively. Outliers are defined by points that fall more than 1.5*IQR above the third quartile or below the first quartile. NZ, CZ and SZ denote the northern zone, central zone and southern zone, respectively. All chemical parameters are measured in mg/L. 51

3.10 Piper diagram presenting the dominant ion species in the groundwater. 52

3.11 Gibbs diagram for groundwater samples used to determine the main controls of water chemistry highlight rock weathering as the main mechanism controlling groundwater chemistry in the Pra Basin. 53

3.12 Bi-variate ion plots showing the most probable geochemical processes, including silicate weathering (a), and ion exchange (b and c) in the groundwater system. 54

4.1 Geological map showing the dominant rock formations and the sampling locations. The Birimian rocks are composed of metasediments, while the Cape Coast granitoid is composed of granite, and the Dyke is made of dolerite (modified after Manu et al. (2023d)). 64

4.2 Three demarcated zones from the previous study by Manu et al. (2023d) show the spatial distribution of groundwater sampling sites. The northern zone is characterized by high elevations, while the southern zone has low elevations. The groundwater flow is assumed to mimic the topography. 66

4.3 Thin sections of rock outcrops (adopted from Manu et al. (2023e)). The first row shows the mineralogy of the Birimian metasediments (**B1**, **B2**,**B3**), including quartz (Qz), biotite (Bt), K-feldspar (Ksp), sericite (Ser), chlorite (Chl), and calcite (Cal). The second row shows the mineral composition of the granitoid (**G1**,**G2**,**G3**) comprising quartz (Qz), K-feldspar (Ksp), plagioclase (Pl), muscovite (Ms), and biotite (Bt). 67

4.4 Conceptual reaction path models considering the rainwater origin of the groundwater. The northern zone is assumed to be the recharge area at high elevations. Vertical flow in the central and southern zones is assumed to have no significant impact on groundwater chemical evolution. 69

4.5 Frequency distribution of the 50 best inverse equilibrium models. For the northern zone (Flowpath I), no model matched all the aqueous components; however, the best simulations are shown in (**A**). Simulations matching all the measured aqueous components in the groundwater and mineral reactions for the overall best-matched for the central (Flowpath II) and southern zones (Flowpath III) are shown in (**B**,**C**), respectively. The minerals with a higher number of occurrences underscore the likelihood of a reactive mineral phase. Negative and positive mole transfers indicate mineral dissolution and precipitation, respectively. 71

4.6 Comparison of the predicted aqueous groundwater components (red circles) from the reaction pathway calibration model and the range of observed composition (box plot) for the northern zone (**a**), central zone (**b**), and southern zone (**c**). 73

4.7 Conceptual model of hydrogeochemical evolution and groundwater flow path in the crystalline basement aquifer system of the Pra Basin in Ghana. Groundwater is assumed to flow from the northeast to the south of the basin. . . 77

List of Tables

2.1 Monitored well characteristics in Ghana's Pra Basin. The meta-sediment comprises weathered phyllite, shale, schist, while the granite comprises granitic to quartz dioritic gneiss. 20

2.2 List of specific yield values used in groundwater recharge estimate in India (modified after Sinha and Sharma (1988). 21

2.3 Groundwater recharge values estimated for the Pra Basin for the water year 2022 27

2.4 Groundwater recharge values estimated for the Pra Basin using the CMB method. We utilized an average long-term precipitation of 1500 mm (Benneh and Dickson 1995) and a chloride concentration in rainwater of 1.13 mg/L (Duah et al. 2021) for the recharge estimates. Cl_{GW} is the chloride in groundwater. 34

3.1 List of parameters used to calculate the WQI, their standard drinking water reference values. 44

3.2 Correlation coefficients between the hydrochemical parameters in the groundwater, highlighting the relationships between them. They were tested at a significance level of $p < 0.05$ with $r > 0.7$ and $r < 0.5$ indicating stronger and weaker correlations (Okofo et al. 2021; Wang 2014), respectively. Only the correlations with r-values > 0.7 are considered significant and presented here. 52

3.3 Rotated Component Matrix (Extraction method: Principal component Analysis, Rotation Method: Varimax with Kaiser Normalization) generated from the factor analysis explaining significant relationships between the hydrochemical parameters. The dash symbols (-) indicate that the parameter loaded a communality less than 0.5 and was deemed statistically insignificant and thus was not considered for the factor analysis. 55

4.1 Hydrochemical data from rainwater and groundwater used for the modelling. The rainwater (RW) and groundwater (comprising northern, central, and southern) data were adopted from Akoto and Adiyiah (2007) and Manu et al. (2023e). ND denotes not determined. 66

4.2 List of additional phases included in the `phreeqc.dat` database for the simulations. 80

List of Acronyms and Symbols

Abbreviations

WRC	Water Resources Commission
GIDA	Ghana Irrigation Development Authority
GH	Ghana
DDT	Dichlorodiphenyltrichloroethane
WTF	Water Table Fluctuation
CMB	Chloride Mass Balance
N	North
W	West
IDW	Inverse distance weighting
LMWL ‘	Local meteoric water line
GMWL	Global meteoric water line
V-SMOW	Vienna Standard Mean Ocean Water
WQI	Water quality index
SAR	Sodium adsorption ratio
USSL	United States Salinity Level
HCA	Hierarchical cluster analysis
ICP-OES	Inductively Coupled Plasma Optical Emission Spectroscopy
n	Number of samples
DO	Dissolved oxygen
EC	Electrical conductivity
CBE	Charge balance error
WHO	World Health Organization
CAI	Chloro-alkaline indices
SPSS	Statistical Package for Social Science
IQR	Inter quartile range
NZ	Northern zone
CZ	Central zone
SZ	Southern zone
TDS	Total Dissolved Solids
UTM	Universal Transverse Mercator
RRMSE	Relative root mean square error
CH_2O	Organic matter

Symbols

R	Recharge	mm
P	Precipitation	mm
Cl_p	Chloride in precipitation	mg/l
Cl_{gw}	Chloride in groundwater	mg/l
S_y	Specific yield	-
Δh	Rise in water level	m
Δt	Time duration of recharge	year
f	Fraction of water loss through evaporation	-
δ_L	Initial isotopic signature of surface water and groundwater	‰
δ_P	Initial isotopic signature of precipitation	‰
ϵ_k	Kinetic isotopic fractionation factor	‰
^{18}O	Stable oxygen-18 isotope	‰
^{2}H	Stable deuterium isotope	‰
T	Temperature	°C
ϵ	Total isotopic enrichment factor	‰
ϵ_{eq}	Equilibrium isotopic enrichment factor	‰
q_i	Quality rating value	-
C_i	Parameter concentration	mg/l
S_i	WHO standard values	mg/l
w_i	Assigned weights	-
W_i	Relative weights	-
y_i	Observed aqueous concentration	mol/kw
$\hat{y}_i$	Simulated aqueous concentration	mol/kgw

Chapter 1

Introduction and Motivation

Water resources play a pivotal role in the survival of humans, socioeconomic development and the functioning of many ecosystems. The Pra Basin is one of Ghana's five major river basins with high economic importance. Due to urbanization, expansion of industries such as mining, increased population with growing demand for water supply, and climate change, a comprehensive evaluation of the water resources would be required. This endeavour is imperative to ensure the judicious and sustainable utilization of water resources while safeguarding the integrity of the surrounding environmental ecosystem.

Implementation of sustainable and effective water resources management can be a daunting task, particularly in sub-Saharan Africa where there is limited knowledge about the hydrogeological and hydrochemical processes of aquifer systems (Chacha et al. 2018; Ligate et al. 2021), a scenario aptly exemplified by the Pra Basin. In the basin, this challenge is further compounded by the absence of adequate measures to regulate the impact of human activities. Uncontrolled anthropogenic activities such as improper farming practices, illegal mining, dewatering at mine sites and indiscriminate sewage disposal contribute significantly to the challenges in managing water resources in the basin (Duncan 2020; Golow and Mingle 2003; Tay and Hayford 2016).

The hydrogeochemical characterization of water resources provides the fundamental information required for sustainable water resource management (Okwir et al. 2023; Pisciotta et al. 2019; Ruidas et al. 2022). To achieve this, a holistic strategy that synergistically integrates hydrochemistry, stable isotopes and geochemical simulations proves to be a key tool to elucidate the primary hydrochemical factors affecting the various quality parameters of water sources (Okofo et al. 2022; Yidana et al. 2012c). The large heterogeneity that characterizes the groundwater composition is a particular challenge in basin-scale hydrogeochemical characterisation. Therefore, the combination of stable isotope interpretations and classical hydrochemical ion plots allows the conceptualization of the hydrogeochemical system (Dragon 2021; Okofo et al. 2021; Todd 1980; Xiao et al. 2018; Yidana et al. 2008), which could be used as a basis for further geochemical simulation investigations tailored for water management (Li et al. 2010; Roy et al. 2020; Zaghlool et al. 2020). The outcomes derived from this robust methodological approach provide a comprehensive grasp of the factors driving the chemical evolution of water quality, thereby facilitating effective and sustainable water resource management.

1.1 Water Resources Potential and Uses in the Pra Basin

The Pra Basin has an abundant water resource consisting of dense river networks, groundwater and two rain seasons accounting for an annual long-term average rainfall of 1,500 mm (Benneh and Dickson 1995). Surface waters, including rivers, lakes, ponds and dams, are recharged by precipitation. The total annual runoff for the entire country is estimated at 56.4 billion m^3 (MWRWH 2007). Over the long term, the average annual rainfall is approximately 1,500 mm, contributing to a total annual volume of 34,786 million m^3 across the entire basin.

Of this amount, 72% representing about 25,046 million m^3 evaporates into the atmosphere (WRC 2012). The Pra River, which flows for a total distance of 240 km before entering the Gulf of Guinea, records an average annual discharge of 4,174 million m^3 (WRC 2012) representing 1% of the total annual precipitation. Major tributaries that contribute to the flow of the main Pra River include Anum, Offin, Birim and Oda. Regarding groundwater resources, the basin is located within the crystalline basement aquifer, which has great potential for groundwater development (Dapaah-Siakwan and Gyau-Boakye 2000). In Ghana, crystalline aquifers play a key role in the water supply system. The study area predominantly comprises Birimian meta-sediments and granitic rocks, which have major porosities that regulate groundwater circulation. Dapaah-Siakwan and Gyau-Boakye (2000) had previously demonstrated a 75% success rate in drilling productive wells in the Birimian aquifers, with yields ranging from 0.4 to 30 m^3/h, averaging 13 m^3/h. The annual groundwater recharge was estimated by WRC (2012) to be 16% of the long-term annual precipitation, equating to a substantial amount of 5,566 million m^3, highlighting significant groundwater potential for water supply.

Water resources in the Pra Basin are used mainly for domestic, mining/industrial and agricultural (irrigation) purposes (WRC 2012). The domestic water supply comes mainly from surface water and groundwater. Several reservoirs have been constructed from surface water resources to store water to augment urban water supply. Many riparian communities draw water from the rivers, mostly from perennial tributaries. Groundwater is sourced for community water supply through hand-dug wells, mechanized boreholes equipped with hand pumps (Figure 1.1) and wells installed with submersible pumps. For industrial and mining purposes, permits have been granted by the WRC to several companies, including AngloGold Ashanti (GH), Bonte Gold Mines Company Ltd, AngloGold Ashanti (Iduaprem), Abore Mining Company Ltd, Xtra Gold Mining Ltd and Central Ashanti Gold Ltd, Central African Gold Ltd and Benso Oil Pal Plantation Ltd (WRC 2012). According to WRC (2012), the industrial water consumption amounts to a total of 49.2 million m^3/year for both surface water and groundwater representing 1.2% of the total surface water for the basin. In recent times, many commercial water bottling companies have also used groundwater for their production. Regarding agricultural water uses, surface water and groundwater are tapped for irrigation and livestock watering. According to WRC (2012), three formal irrigation schemes are operated by the Ghana Irrigation Development Authority (GIDA). These include the Adiembra Irrigation Project, the Anum Valley-Bottom Irrigation Project and the Gyadam Irrigation Project. These projects draw their water from the Offin, Anum and Birim rivers.

1.2 Sources of Water Pollution

Water pollution is pervasive across the basin, primarily driven by illegal mining activities (Duncan 2020; Golow and Mingle 2003; Tay and Hayford 2016). Historically, prior to the surge in mining operations, factors such as poor farm management practices (e.g., inappropriate application of fertilizer and pesticides), the utilization of toxic substances like dichlorodiphenyltrichloroethane (DDT) for fishing and the indiscriminate discharge of untreated solid and liquid waste into water bodies were significant contributors to water pollution in the area. However, more recently, the increase in illegal mining activities targeting valuable minerals like gold and diamond has significantly exacerbated the deterioration of the basin's surface water and groundwater quality (Asare 2021; Bessah et al. 2021; Darko et al. 2021; Donkor et al. 2006; Duncan 2020; Golow and Mingle 2003; Tay and Hayford 2016). Major water pollutants include,

Figure 1.1: Sources of water supply in the Pra Basin include mechanized boreholes fitted with hand pumps for community water supply with depths usually less than 60 m (A) and hand-dug wells usually completed to a depth of less than 20 m (B). Picture taken on March 17, 2020.

mercury, arsenic, iron, lead, manganese, aluminium, cadmium and selenium. Notably, mercury and selenium are linked to human activities (Affum et al. 2016; Tay and Hayford 2016), while the origins of the remaining trace metals are geogenic in nature (Affum et al. 2016). Figure 1.2 portrays extensively disrupted soil resulting from illegal mining operations. During rain periods, a significant portion of the excavated soil is washed into the rivers, resulting in high turbidity loads and brownish colouration of the water (see Figure 1.3). A significant concern lies in the lack of reclamation for most of these excavated sites, which most likely will serve as a transport medium for contaminants into the aquifers. Therefore, investigating the various sources of recharge and characterizing the chemical processes of the water resources serves as the starting point to better control the impact of the widespread water pollution in the basin.

1.3 Regional Geology and Hydrogeology

Geologically, the Pra Basin is underlain by three distinct lithological formations: the Birimian Supergroup, the Cape Coast granitoid, and the Tarkwain Group (Figure 1.4). The distribution of these lithologies is such that the Birimian System predominantly underlies the northern zone, the Cape Coast granitoid is prevalent in the southern parts, while the Tarkwain occurs at the eastern and western fringes of the study area. According to Banoeng-Yakubo et al. (2010), the Birimian Supergroup consists of meta-sedimentary and

Figure 1.2: A degraded land from illegal mining activities in search of economic minerals. Picture taken on March 14, 2020.

metamorphosed volcanic rocks, forming five subparallel belts of volcanic rocks separated by broad basins of sedimentary rocks. The sedimentary belts within the Birimian include greywackes with turbidite features, phyllites, slates, schists, weakly metamorphosed tuffs, and sandstones. The metavolcanic rocks consist of lava flows and dyke rocks of basaltic and andesitic composition (Banoeng-Yakubo et al. 2010; Kesse 1985).

The Tarkwain formation is characterized by clastic sedimentary rocks, occurring in troughs and lying on top of the Birimian System. Notably, the Tarkwain rocks host most of Ghana's paleo-placer gold deposits, believed to have formed from the erosional products of the Birimian System, dominated by coarse clastic sediments (Kesse 1985).

Various types of granitoids have been identified in association with the Birimian sedimentary basin in Ghana, including the Cape Coast, Winneba, Bongo, and Dixcove granitoids (Junner 1940; Kesse 1985). The Cape Coast granites, occurring exclusively in the Birimian System, are mostly biotite-bearing and sometimes appear migmatitic in certain localities. Junner (1940) and subsequent studies by Kesse (1985) proposed that the Cape Coast granitoid intruded the Birimian System during regional deformation.

In Ghana, the hydrogeological landscape is broadly categorized into five provinces as outlined in Banoeng-Yakubo et al. (2010): the Birimian Province, the Crystalline Basement Granitoid Complex Province, the Voltaian Province, the Pan African Province, and the Coastal Sedimentary Province. This research focuses on the Birimian and the Basement Complex

Figure 1.3: Polluted surface water bodies mainly resulted from the activities of illegal mining operations. Picture taken on March 03, 2020.

Provinces. The Birimian Province encompasses aquifers within the Birimian meta-sedimentary, meta-volcanic, and Tarkwain rocks, while the Basement Complex includes aquifers within the granitoid formation. Generally, these lithologies exhibit low inherent permeability, and groundwater occurrence is facilitated through secondary porosity, such as faults, fractures, and shearing, developed during regional tectonic processes (Banoeng-Yakubo et al. 2010).

In the Birimian Province, groundwater is mainly found at the bottom of the saprolite and the top of the saprock. The clay-rich upper saprolite layer is a semi-confining layer for this aquifer zone. The Basement Complex granitoid comprises three aquifer types: the weathered rock aquifers related to fractures, fractured quartz vein aquifers, and fractured unweathered aquifers. Generally, Birimian aquifer systems exhibit higher yields than the granitoid, with the Birimian rocks showing deeper weathering and weathered layers (Banoeng-Yakubo et al. 2010).

According to the study by Banoeng-Yakubo et al. (2008) in the Akyem area of the Pra Basin, the authors highlighted three major flow regimes: local, intermediate, and regional. Due to aquifer heterogeneity resulting from the complex geological setting and groundwater flow dependence on secondary permeability, barriers to continuous groundwater flow exist (Banoeng-Yakubo et al. 2008). Consequently, the local groundwater flow system likely aligns with the topography pattern, with the regional flow mimicking the northeast-to-southwest direction of the geological structural entities in Ghana.

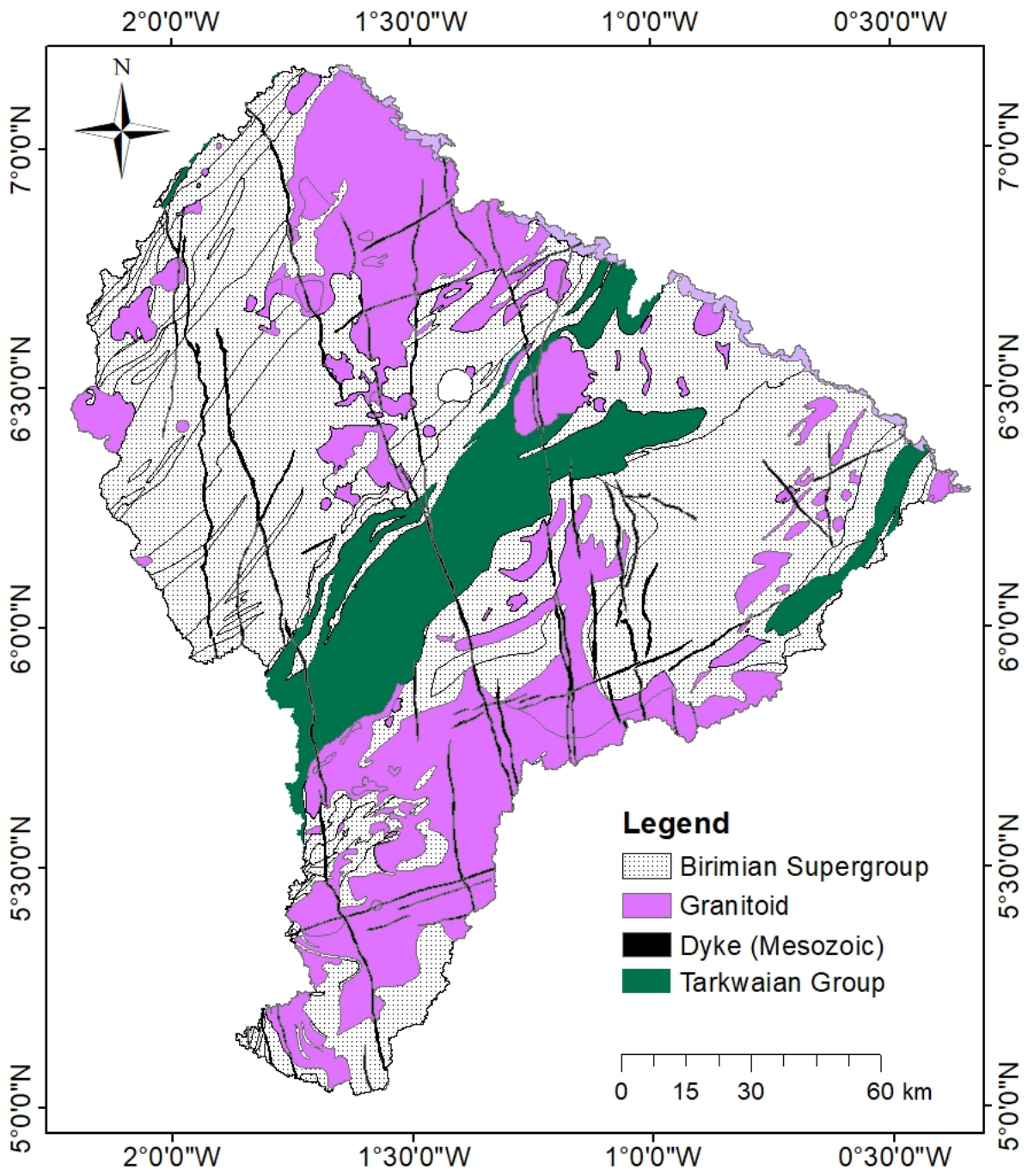

Figure 1.4: Geological map of the Pra Basin showing the three dominant lithologies, the Birimian Supergroup composed of the meta-sediments and the volcanic rocks, the Granitoid consisting of the Cape Coast granitoid and the Tarkwain Group.

1.4 Previous Works and Knowledge Gap

Broadly, comprehensive basin-wide information about hydrogeochemical controls on water quality parameters is scarce in the Pra Basin. Existing studies are limited in scope, poorly coordinated, and predominantly conducted on a local scale. Researchers in the Pra Basin have employed classical bivariate ion plots and multivariate statistical analysis to gain insights into the hydrochemical controls of both surface water and groundwater quality. For instance, Tay et al. (2015) applied groundwater geochemistry and stable isotopes to investigate the origin of dissolved ions in the lower part of the Pra Basin, identifying major processes such as silicate weathering, ion exchange reactions, sea aerosol spray, and the oxidations of

pyrite (FeS_2) and arsenopyrite (FeAsS) as significant contributors to groundwater chemistry. Additionally, studies by Ahialey et al. (2010) and Okofo et al. (2021) delved into the natural baseline chemistry of groundwater in some parts of the Pra Basin. Ahialey et al. (2010) found elevated iron concentrations in groundwater samples in the Lower Pra Basin, with a dominant Na-Cl water type. Okofo et al. (2021) utilized multivariate statistical analysis and classical ion plots to identify three spatial hydrochemical groupings, indicating hypothetical chemical evolutions. They concluded that rock-water interaction is the primary driver of groundwater chemistry, with minimal influence from anthropogenic activities. The authors employed inverse geochemical modelling and highlighted plausible mineral assemblages, including the dissolution of minerals like dolomite, plagioclase, halite, and gypsum and the precipitation of calcite and chlorite. Other researchers (Loh et al. 2021; Tay et al. 2018) reported similar findings in different parts of the Pra Basin, reinforcing the consensus that water-rock interactions are central in controlling groundwater chemistry.

In water quality assessment, groundwater consistently exhibits good quality based on several authors' comparative assessments and calculations of water quality indices. Conversely, surface water is generally deemed poor quality, with most studies attributing this to the prevalence of mining activities in the Pra Basin. It is noteworthy that these water quality assessments have predominantly focused on specific areas rather than adopting a regional-scale perspective. Dorleku et al. (2019) specifically evaluated nutrient levels in groundwater within the Lower Pra sub-catchment, concluding that nitrate, phosphate, and sulfate levels fall within acceptable limits set by the World Health Organization (WHO). Their assessment relied on a comparative analysis using established WHO standards for drinking water (WHO 2017). Okofo et al. (2021) conducted a study in the Bosome Freho District, a localized area in the Pra Basin, assessing groundwater quality for irrigation and drinking purposes. Utilizing the Water Quality Index (WQI) and Wilcox diagram, they concluded that the groundwater in this region is of good quality for drinking and irrigation. Another study by Dorleku et al. (2018) investigated the impact of small-scale gold mining on heavy metal levels in groundwater in the Lower Pra sub-catchment. High concentrations of iron, manganese, lead, aluminium, and mercury were recorded, indicating a significant influence from mining activities. Asante-Annor et al. (2018) explored the hydrochemistry of the Basin granitoid, focusing on 25 groundwater samples from the Assin and Breman Districts. They found that all physico-chemical parameters were within permissible limits set by the Ghana Standards Authority and the WHO, except for pH, iron (Fe), and manganese (Mn). As discussed so far, the studies conducted for water quality assessment are only qualitative and do not reveal the controlling factors that drive chemical evolution. Therefore, a more robust approach incorporating numerical simulations is always a step in the right direction to understand the most likely geochemical processes affecting water quality.

Quantitative assessment employing classical recharge estimates and numerical groundwater flow models has not been conducted on the Pra Basin, except for water availability and demand analysis projects undertaken by the Water Resources Commission of Ghana in 2012. One regional survey used the Water and Evaluation (WEAP) model to assess the basin's water availability and demand projections (WRC 2012). The key input variables of this model include hydrometeorological data (precipitation, temperature, humidity and cloud cover), land use (agriculture, grasslands, human settlements and forests), demographics and domestic water needs, as well as irrigation and mining water needs. These analyzes are based exclusively on surface water and do not include any groundwater components. The WRC (2012) reported that water requirements for mining and other industrial uses are negligible compared to agricultural

and domestic uses. The authors also found that Kumasi, the most urbanized area in the basin, derives most of its water supply from surface water. In another study, Obuobie et al. (2012b) used the Falkenmark indicator to assess the Pra Basin's vulnerability to water scarcity under climate change between 2006 and 2035. The authors concluded that the Pra Basin is already water-stressed without climate change and is expected to reach absolute water scarcity by 2050. All analyzes were based on surface water resources and did not capture components of groundwater and precipitation.

To date, hydrogeochemical investigations in the Pra Basin have predominantly relied on qualitative interpretations of hydrochemical data, overlooking the thermodynamics of the groundwater system. This study addresses lingering questions, contributing to an enhanced understanding of the basin's hydrochemistry. Most of the conclusions drawn thus far suggest that the primary process governing the hydrogeochemical evolution of groundwater is the weathering of silicate minerals. These conclusions lack detailed identification of the specific minerals involved in the reactions. For instance, Okofo et al. (2021) proposed mineral assemblages, such as halite, dolomite, and gypsum, lacking substantiation from petrographical analysis. This study integrated field investigations involving outcrop sampling for petrographic studies to identify constraints on mineral phases. Concurrently, numerical simulations, based on the local thermodynamic equilibrium hypothesis, are conducted to quantify reactions and identify plausible mineral assemblages influencing groundwater chemical composition.

Another speculative assertion concerns the oxidation of pyrite (FeS2) and arsenopyrite (FeAsS) as a significant factor impacting groundwater quality in the area, as suggested by Tay et al. (2015). This aspect is better elucidated through a numerical modelling approach. To augment current knowledge, geochemical simulations are performed to understand the evolution of water chemistry along a defined hypothetical flow path, leveraging a novel combinatorial inverse modelling and reaction path modelling. In the combinatorial modelling approach, a predefined pool of mineral phases is screened under the local thermodynamic equilibrium hypothesis of water-rock interaction to identify plausible mineral assemblages responsible for observed chemical changes in water composition. The outcomes derived from the reaction path and combinatorial inverse modelling are then utilized to construct the Pra Basin's baseline basin-scale hydrogeochemical conceptual model.

1.5 Relevance of this Study

This study represents a pioneering effort in hydrogeochemical characterization of water resources within the Pra Basin at a basin-wide scale. It involves analyzing stable oxygen ($\delta^{18}O$) and deuterium ($\delta^{2}H$) isotope ratio from 90 water samples, along with water level measurements and geochemical modelling, to gain insights into the chemical evolution of groundwater. The comprehensive sampling of surface and groundwater sources in the basin marks a significant milestone, providing a robust regional dataset (Manu et al. 2023e) for assessing water resources in the area. Diverging from prior methods relying on classical interpretations of chemical parameters, this study employs statistical data treatment alongside traditional knowledge to construct a conceptual hydrogeochemical model for the basin. The model is rigorously tested using numerical simulations. Employing combinatorial inverse and reaction path modelling, the study discerns plausible mineral assemblages and potential regional groundwater flow paths in the basin. This research is important as it introduces an innovative approach to evaluating water quality in the Pra Basin and beyond. It delivers high-quality regional hydrochemical and isotopic data, offering interpretations crucial for policy formulation to enhance water quality

management in the basin. In summary, a conceptual hydrogeochemical model is presented that explains the plausible evolution of groundwater chemistry along a hypothetical flow path and serves as a baseline model to facilitate water resource management and other hydrochemical research in the Pra Basin.

1.6 Thesis Objectives

To ensure the sustainable management of water resources, a thorough understanding of their genesis, recharge mechanisms and the chemical processes that drive their evolution is required. Using only traditional hydrochemical interpretations may not provide a thorough and accurate knowledge of the major factors influencing the chemical behaviour of a water system. As a result, a combined approach including statistical analysis, classical hydrochemistry, stable isotope analysis and geochemical modelling is rudimentary. This approach allows for a comprehensive evaluation of the many controls on water chemistry, resulting in the development of effective and sustainable water resource management strategies. The overall research objective is to gain insight into the processes that determine the hydrogeochemical evolution of groundwater quality in the Pra Basin. Three objectives are derived to provide the scientific background information needed to formulate and implement water resources management policies:

- The **first objective** is to determine the origin and recharge processes of the groundwater in the basin. For this purpose, the stable oxygen-18 and deuterium isotope ratios in surface water and groundwater are analyzed. The Chloride Mass Balance (CMB) and Water Table Fluctuation (WTF) methods are used to quantify the recharge to groundwater and to infer potential recharge areas.
- The **second objective** focuses on assessing the hydrochemistry of the Pra Basin in order to gain insight into spatial variations in surface water and groundwater quality and geochemical processes affecting its evolution. This is achieved by integrating multivariate statistical analysis, including hierarchical cluster and factor analysis, classical bivariate ion plots and water quality indices to learn the chemical variations and water quality for drinking and irrigation purposes.
- The **third objective** is to determine plausible mineral assemblages and quantify their reactions that drive the chemical evolution of groundwater by utilizing a conceptual model developed from the knowledge gained in the previous two objectives. For this purpose, combinatorial inverse geochemical and reaction path modelling was used under the local thermodynamic equilibrium hypothesis to consistently reproduce the chemical composition of groundwater along the flow regime.

1.7 Geochemical Modelling of Water Chemistry

Chemical reactions resulting from interactions between water and rocks play a critical role in shaping the distribution, presence, and overall properties of chemical elements in water (Merkel et al. 2005). The quantification and understanding of these reactions are effectively achieved by applying geochemical models that include mass balance, thermodynamic equilibrium, kinetics and reactive mass transport (Appelo and Postma 2005; Parkhurst 1995). This work employs equilibrium models to analyze the chemical evolution of groundwater resources.

The mass balance modelling approach is employed to identify the mineral phases responsible for alterations in water chemistry between two distinct end members. This method assumes a connection between the two end-member solutions along the same flow path. The PHREEQC code (Parkhurst 1995), widely utilized for inverse calculations, relies on its underlying database, which varies based on the solution's mineral phases and ionic strength. For instance, solutions with high ionic strength are best modelled with the pitzer.dat thermodynamic database, while freshwater systems are typically best modelled with the phreeqc.dat database. This approach relies solely on the mass balance of the chemical reaction equation and does not necessitate thermodynamics for its computations.

Alternatively, thermodynamic equilibrium conditions are sometimes assumed, relying on equilibrium constants to predict concentrations of species and phases in the solution. Both methodologies can be seamlessly implemented using the PHREEQC geochemical modelling code (Parkhurst 1995). A system is considered in chemical equilibrium when its Gibbs free energy, representing the probability of a reaction occurring, is zero (Merkel et al. 2005). During a chemical reaction at equilibrium, the products formed convert into the original reactants until both the forward and reverse reactions occur at the same rate. While natural systems rarely reach thermodynamic equilibrium in principle, there are regions within the solution where equilibrium reactions occur, called local thermodynamic equilibria (Merkel et al. 2005).

1.8 Approaches to Estimate Groundwater Recharge

Quantifying the available water that recharges groundwater is essential for water resource management. Different approaches are often used to estimate groundwater recharge from rainwater infiltration and through baseflow. In general, comprehensive investigations of the hydrogeological conditions provide possible ways to recharge groundwater (Chenini et al. 2015). Recharge estimation can also be achieved through water balance modelling, using the water balance equation considering input parameters such as precipitation and outputs such as evapotranspiration in a watershed (Finch 1998; Szilagyi et al. 2003). In some cases, tracers have been used to estimate the rate and location of groundwater recharge (Sukhija et al. 1996; Wu et al. 2016). This approach involves placing markers in the subsurface and tracking the direction of their movement along a defined flow path. Soil moisture measurements by monitoring fluctuations in soil moisture content can infer the amount of water likely to recharge aquifer systems (Andreasen et al. 2013; Zhang et al. 1999). By studying isotopes in groundwater, it is possible to determine the origin and age of groundwater, which are key elements for understanding groundwater recharge mechanisms. For more robust calculations, numerical modelling approaches utilizing advanced codes such as MODFLOW (Harbaugh et al. 2000) offer a sophisticated means of simulating groundwater flow and estimating recharge rates. This method considers the intricate hydrogeological conditions specific to the study area, providing a detailed understanding of groundwater dynamics.

In the context of the present study, groundwater recharge was estimated by applying the Chloride Mass Balance (CMB) and Water Table Fluctuation (WTF) methods. The CMB method relies on chloride concentrations in groundwater and precipitation, along with long-term average annual precipitation data. This method assumes that chloride in groundwater is solely derived from precipitation and that no chloride is stored in the unsaturated zone (Duah et al. 2021; McNamara 2005; Obuobie et al. 2010). The WTF method utilizes well-monitoring records over at least one year to determine the rise in water level, which is then multiplied by the specific yield of the aquifer materials (Delin et al. 2007; Obuobie et al. 2012b). This method assumes that the

rise in groundwater is attributed to precipitation reaching the saturated zone. The stable $\delta^{18}O$ and $\delta^{2}H$ isotopes ratio of surface water and groundwater have also been utilized to determine the source of the groundwater and recharge mechanism affecting the infiltrating water before entering the aquifer system.

1.9 Structure of the Thesis and Scientific Contribution

This cumulative doctoral thesis consists of three published articles in peer-reviewed journals. The main findings and discussions of the dissertation are presented in **Chapters 2** to **4**, with the combined discussions of the three articles being elaborated in **Chapter 5**. Conclusions from the objectives of the thesis as well as prospects for future research, are presented in **Chapter 6**.

The authors' contributions are the same for all three manuscripts, and they are only listed once, as indicated below. As the first author, I was primarily responsible for collecting field data, doing laboratory measurements, conceptualizing and analyzing data, and running the simulations. In addition, I was in charge of the manuscript drafting and revision process. Marco De Lucia, as a co-author, contributed to the development of the code and actively participated in the preparation and revision of the manuscripts. Michael Kühn, as my primary scientific supervisor, provided valuable guidance throughout the research process and contributed significantly to the manuscript's conceptualization, development and revision.

This research introduces a novel regional dataset encompassing chemical parameters and the study area's stable isotopic ratios of surface water and groundwater. Additionally, it incorporates petrographic analysis of outcrop samples from the terrain. The published data (*Hydrochemistry and stable oxygen ($\delta^{18}O$) and hydrogen ($\delta^{2}H$) isotopic composition of surface water and groundwater and mineralogy, in the Pra Basin (Ghana) West Africa*) forms the cornerstone for discussions in chapters **Chapters 2** to **4**.

In **Chapter 2**, the origin of surface water and groundwater, as well as their recharge processes, are determined. For this purpose, the stable oxygen-18 and deuterium isotope ratios in surface water and groundwater were analyzed and their linear relationships were used to infer the origin and likely recharge processes. Both surface water and groundwater in the catchment area originate from precipitation that has undergone significant evaporation. The groundwater is relatively depleted in the heavier isotopes compared to the surface water, pointing towards a shorter residence time of the infiltrating water within the evaporation extinction depth in the vadose zone. The mean evaporative loss of surface water and groundwater (prior to recharge) is estimated at 65%. Estimation of groundwater recharge shows that the studied catchment area, which includes Birim and Lower Pra, has an annual recharge of 228 million m^3, which is higher than the total water consumption for the entire Pra Basin, indicating a large groundwater potential. This chapter is published as *"Stable Isotopes and Water Level Monitoring Integrated to Characterize Groundwater Recharge in the Pra Basin, Ghana"* in *Water* and cited as Manu et al. (2023b). In **Chapter 3**, hydrochemical characterization of surface water and groundwater was performed to gain insight into the quality of the water and the geochemical processes that control its evolution. Water quality analysis shows that groundwater is generally of high drinking and irrigation quality, while surface water needs to be treated before it can be used. Manganese and iron are considered to be the main contaminants affecting surface water quality in the catchment area. From the hierarchical cluster analysis, three spatial groupings of the hydrochemical data can be identified, representing distinct spatial associations based

on elevation. The trilinear Piper diagram of the groundwater samples clarifies the chemical evolution from Ca-HCO_3 to Na-HCO_3 and finally to the Na-Cl water type along the flow path from the recharge point to the discharge point. Silicate weathering, carbonate dissolution and ion exchange are identified as likely hydrogeochemical processes driving groundwater chemical evolution. This chapter is published as *"Hydrochemical characterization of surface water and groundwater in the crystalline basement aquifer system in the Pra basin (Ghana)"* in *Water* and cited in the following as Manu et al. (2023d).

In **Chapter 4**, geochemical simulations are performed to identify the plausible mineral assemblages that reacted or dissolved to account for the groundwater chemical evolution along the defined flow path. For this, combinatorial inverse modelling under the local thermodynamic equilibrium hypothesis using the averaged water composition for the three clusters identified in **Chapter 3** was employed to determine all plausible mineral assemblages from a given pool of mineral phases that explain the groundwater composition. The weathering of silicate minerals, including albite, anorthite, plagioclase, K-feldspar and chalcedony, as the dominant minerals that explain the groundwater composition in the transition and the discharge zones. The combinatorial inverse model approach enables the implementation of algorithms associated with geochemical models, such as error analysis, parameter calibration, and statistical modelling, to comprehensively study mineral reactions driving groundwater chemical evolution. This chapter is published as *"Water-rock interactions driving groundwater composition in the Pra Basin (Ghana) identified by combinatorial inverse geochemical modelling"* in *Minerals* and cited in the following as Manu et al. (2023c).

Chapter 2

Stable Isotopes and Water Level Monitoring Integrated to Characterize Groundwater Recharge in the Pra Basin, Ghana

ABSTRACT

In the Pra Basin of Ghana, groundwater is increasingly becoming the alternative water supply due to the continual pollution of surface water resources through illegal mining and indiscriminate waste discharges into rivers. However, our understanding of hydrogeology and the dynamics of groundwater quality remains inadequate, posing challenges for sustainable water resource management. This study aims to characterize groundwater recharge by determining its origin and mechanism of recharge prior to entering the saturated zone and to provide spatial estimates of groundwater recharge using stable isotopes and water level measurements relevant to groundwater management in the basin. Ninety (90) water samples (surface water and groundwater) were collected to determine stable isotope ratios of oxygen (δ^{18}O) and hydrogen (δ^{2}H) and chloride concentration. In addition, ten boreholes were installed with automatic divers to collect time series data on groundwater levels for the 2022 water year. The Chloride Mass Balance (CMB) and the Water Table Fluctuation (WTF) methods were employed to estimate the total amount and spatial distribution of groundwater recharge for the basin. Analysis of the stable isotope data shows that the surface water samples in the Pra Basin have oxygen (δ^{18}O) and hydrogen (δ^{2}H) isotope ratios ranging from -2.8 to 2.2‰ vs V-SMOW for δ^{18}O and from -9.4 to 12.8‰ vs V-SMOW for δ^{2}H, with a mean of -0.9‰ vs V-SMOW and 0.5‰ vs V-SMOW, respectively. Measures in groundwater ranges from -3.0 to -1.5‰ vs V-SMOW for δ^{18}O and from -10.4 to -2.4‰ vs V-SMOW for δ^{2}H, with a mean of -2.3 and -7.0‰ vs V-SMOW, respectively. The water in the Pra Basin originates from meteoric source. Groundwater has a relatively depleted isotopic signature compared to surface water due to the short residence time of infiltration within the extinction depth of evaporation in the vadose zone. Estimated evaporative losses in the catchment range from 51 to 77%, with a mean of 62% for surface water and from 55 to 61% with a mean of 57% for groundwater, respectively. Analysis of the stable isotope data and water level measurements suggests a potential hydraulic connection between surface water and groundwater. This hypothesis is supported by the fact that the isotopes of groundwater have comparatively lower values than surface water. Furthermore, the observation that the groundwater level remains constant in months with lower rainfall further supports this conclusion. The estimated annual groundwater recharge in the catchment ranges from 9 to 667 mm (average 165 mm) and accounts for 0.6% to 33.5% (average 10.7%) of mean annual precipitation. The total estimated mean recharge for the study catchment is 228 Mm^3, higher than the estimated total surface water use for the entire Pra Basin of 144 Mm^3 for 2010, indicating vast groundwater potential. Overall, our study provides a novel insight into the recharge mechanism and spatial quantification of groundwater recharge, which can be used to constrain groundwater flow and hydrogeochemical evolution models, which are crucial for effective groundwater management within the framework of the Pra Basin's Integrated Water Resources Management Plan.

2.1 Introduction

Estimating groundwater recharge and identifying its origin and recharge processes are required in managing groundwater systems. The Pra Basin hosts most of the valuable mineral deposits that partly drive Ghana's economy. Recently, the basin has faced many water management challenges resulting from the excessive land degradation from illegal mining activities (Manu et al. 2023d). Most of the surface water the indigenous people once used for their water supply is polluted and no longer potable (Manu et al. 2023d). This situation has placed heightened pressure on the utilization of groundwater as an alternative water supply across the basin. Quantifying groundwater recharge and identifying its origin and recharge processes is supposed to provide sustainable use of the resource (Afrifa et al. 2017).

Determining the sustainable yield of aquifers requires accurate information on groundwater recharge at both spatial and temporal scales in response to changing climatic conditions (Afrifa et al. 2017). To properly characterize aquifer systems, several techniques for quantifying groundwater recharge as well as studying recharge processes, have been proposed. Most of these methods involve numerical simulations (Mace et al. 2000; Okofo and Martienssen 2022; Yidana et al. 2014; Yidana et al. 2011) and the application of natural tracers (Addai et al. 2016; Adomako et al. 2010; Afrifa et al. 2017; Gibrilla et al. 2022; Obuobie et al. 2010). Afrifa et al. (2017) emphasized that the most accurate groundwater recharge estimates can be obtained through a calibrated numerical groundwater flow model. However, these estimates are limited by the governing hypotheses and conditions and the availability of adequate hydrogeological data (Afrifa et al. 2017). A combined interpretation of stable isotope data and the groundwater recharge estimation using the classical Chloride Mass Balance (CMB) and Water Table Fluctuation (WTF) methods have been used here to develop a conceptual model for the groundwater system.

Stable isotopes of oxygen and hydrogen are key water constituents that can be used to determine groundwater origin (Afrifa et al. 2017; Gibrilla et al. 2022), recharge processes (Addai et al. 2016; Yidana 2013), identify potential end-member mixing between aquifers and surface water bodies (Love et al. 1993; Yidana 2013) and provide valuable information about hydrological systems at the local or regional scale (Yidana 2013). However, isotopic data might not offer straightforward source interpretation due to the complexity of most hydrogeological systems. This is because multiple end-member solutions, each with different isotopic enrichment, can contribute to groundwater recharge along the flow path. These different sources further complicate the interpretation of the groundwater sources, which is based solely on isotope data (Davisson et al. 1999). Against this background, the interpretation of regional surface water and groundwater isotope data must consider the prevailing climatic conditions and the surface and sub-surface processes.

In various geological terrains around the world, the CMB method has been employed to evaluate groundwater recharge (Dassi 2010; Duah et al. 2021; Eriksson and Khunakasem 1969; Marei et al. 2010; Obuobie et al. 2010). The CMB method was postulated by Eriksson and Khunakasem (1969), who used it to estimate groundwater recharge in the saturated zone of a coastal plain in Israel. Since then, several researchers in sub-Saharan Africa have adopted this technique to estimate groundwater recharge (Gebru and Tesfahunegn 2019; Obuobie et al. 2010; Uugulu and Wanke 2020). The approach runs on the hypothesis that the groundwater chloride concentration is mainly derived from atmospheric deposition and is conservative (McNamara 2005; Zhu et al. 2003). The method estimates groundwater recharge

over a large temporal and spatial range, from one year to thousands of years and from a few metres to several kilometres (Obuobie et al. 2010).

The WTF method is used to quantify groundwater recharge by analyzing the rise in the water level (Delin et al. 2007). This technique assumes that the groundwater level rise is exclusively a result of precipitation infiltrating the aquifer while disregarding other factors of the groundwater budget, such as lateral flows during recharge (Healy and Cook 2002; Obuobie et al. 2012a; Scanlon et al. 2002). The method is most effective when applied to unconfined aquifers that exhibit rapid fluctuations in water levels over a relatively short period (Healy and Cook 2002; Scanlon et al. 2002). One key limitation of the WTF is the need for an accurate estimate of the specific yield of the geologic material in order to compute the recharge (Obuobie et al. 2012a; Risser et al. 2005). Several researchers have utilized the WTF technique to quantify groundwater recharge in various climatic and geological terrains across the world (Afrifa et al. 2017; Healy and Cook 2002; Obuobie et al. 2012a; Risser et al. 2005; Scanlon et al. 2002). The widespread use of the WTF method stems from the fact that groundwater level data is easy to collect and recharge rates can be easily estimated based on temporal or spatial variations in water levels (Healy and Cook 2002). It has been proposed that the WTF's recharge estimate is more accurate than estimates derived from other alternative methods (Obuobie et al. 2012a).

In this paper, we used the stable isotopes as a proxy to assess groundwater origin and potential recharge processes, including quantifying the evaporative losses of surface water and groundwater prior to recharge. In addition, the CMB and WTF methods are used to provide estimates of groundwater recharge in the basin. A fifty-year precipitation and temperature record is also examined to learn about changes in climatology, climate variability, and its impacts on water resources. The results obtained from this study will be crucial in conceptualizing the basin's hydrogeological and hydrochemical framework, which are currently not well-studied.

2.2 Materials and Methods

2.2.1 Study Area

Our investigation focuses on the Birim and the main Pra sub-catchments, which lie between 5°N and 6°44′18.30″ N, and 0°20′7.8″ W, and 1°52′26.50″ W in the Pra Basin of Ghana (Figure 2.1). The total land area is about 10,703 km^2. Both rivers originate in the highlands of Ghana's Kwahu Mountain Range in the Eastern Region and flow approximately 240 kilometres south into the ocean (WRC 2012). Further information on the physical setting can be found in Manu et al. (2023e).

The northern zone of the area is characterized by relatively high elevations, reaching 800 m above mean sea level, while the southern areas are relatively flat, with elevations down to 0 m (Figure 2.2). The vegetation is a moist deciduous forest type with isolated reserves. Three air masses, including monsoon, equatorial and northeast trade winds, drive the region's climate (Kankam-Yeboah et al. 2013). According to Kankam-Yeboah et al. (2013), the region can be classified as a humid semi-equatorial climate with bimodal rainfall peaking in May/June and September/October. The average yearly rainfall is 1500 mm and ranges from 1300 to 1900 mm (Benneh and Dickson 1995; WRC 2012). In most months, potential evapotranspiration (PET) surpasses precipitation, averaging 1650 mm (Kankam-Yeboah et al. 2013). The basin is generally warm and moist, with an annual relative humidity between 70% and 80% (WRC 2012). The

mean temperature is 28 °C with minimum and maximum values of 26 °C and 32 °C (Benneh and Dickson 1995).

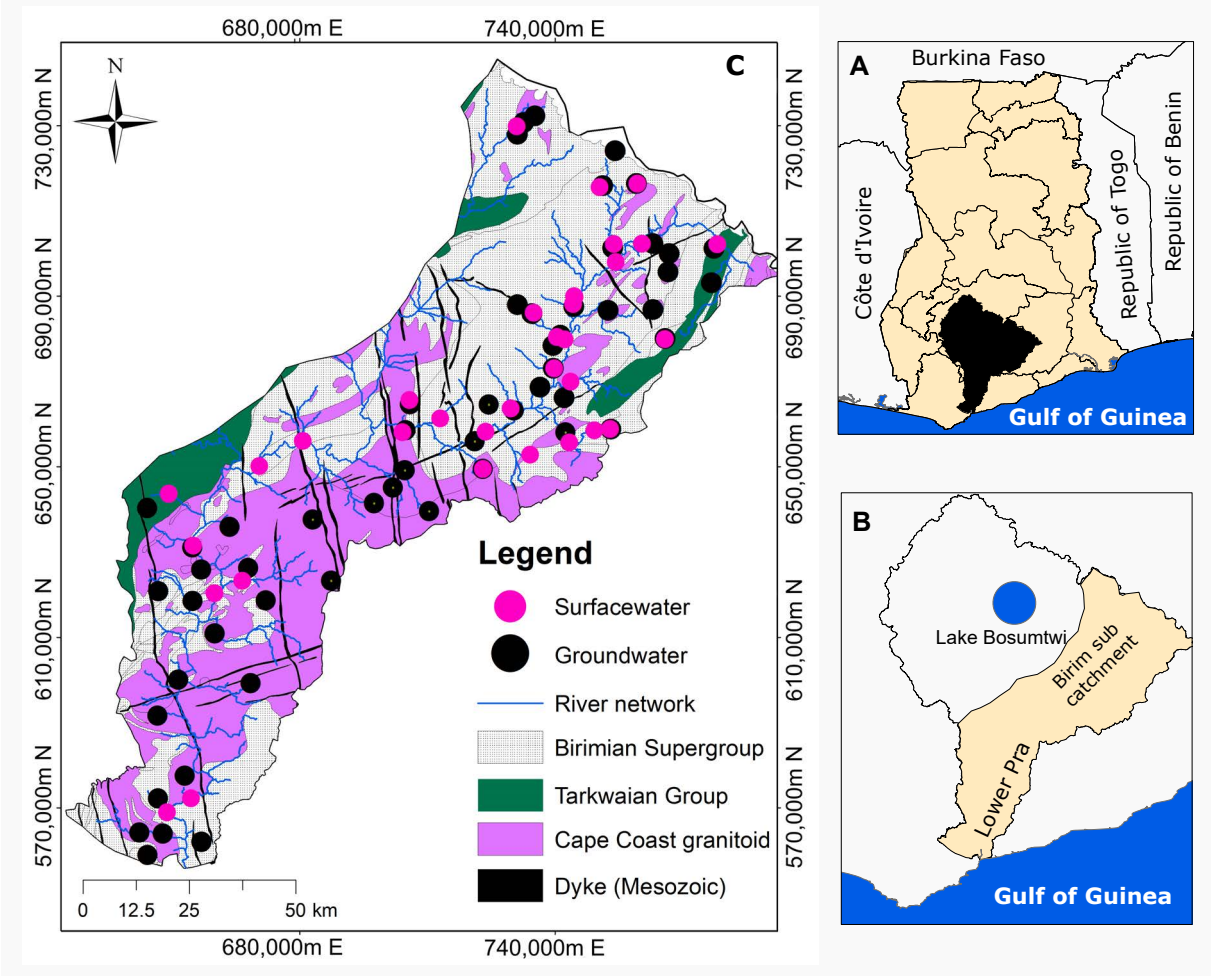

Figure 2.1: The location of the main Pra Basin in Ghana (**A**), the study area representing the Birim and the Lower Pra catchments of the Pra Basin (**B**), the geological map of the area showing the predominant rock types and the surface water and groundwater sampling locations (**C**). Modified after Manu et al. (2023d).

The geology consists primarily of Birimian meta-sediments and the Cape Coast granitoid (Figure 2.1). These rocks are crystalline and typically lack primary porosity (Banoeng-Yakubo et al. 2010). However, secondary porosities have developed due to compressional and tensional activities during regional tectonic processes. Given this, groundwater in the area is governed by secondary structures in the form of fractures, shears and faults. Notably, the Birimian meta-sediments exhibit a substantial weathered zone between these two rock formations, ranging from 90 to 120 m (Banoeng-Yakubo et al. 2009b). This weathered zone is characterized by significantly higher permeability than the massive granitoids. Investigations have shown that the most productive groundwater zones in the Birimian are the layer between the lower part of the saprolite and the upper part of the saprock (Banoeng-Yakubo et al. 2009b). This aquifer zone complements the fracture zone aquifer within the bedrock and is an important water source for domestic and agricultural uses. For the granitoids, the weathered zone has a thickness ranging from 20 to 80 m (Kortatsi 2007). It is worth mentioning that most of the groundwater wells were drilled for domestic purposes and that the total depths of the wells are determined when sufficient water is obtained. Given this, the reported borehole depths may not have penetrated the entire aquifer in the terrain.

Nonetheless, studies by Banoeng-Yakubo et al. (2010) revealed that the depths of boreholes in the Birimian formation generally range from 35 to 62 m with an average of 42 m. In contrast, boreholes in the granitoid formation typically range from 35 to 55 m in depth, with an average of 50 m (Carrier et al. 2008). According to Banoeng-Yakubo et al. (2010), the rocks' water-yielding capacity depends on the secondary permeabilities. In the terrain, Borehole yield is variable, ranging from 8 to 360 lpm in the Birimian formation and from 12 to 150 lpm in the granitoids (Dapaah-Siakwan and Gyau-Boakye 2000; Ganyaglo et al. 2010). Between the two rock types, the Birimian has a higher groundwater-yielding potential than the granitoid due to differences in secondary permeabilities.

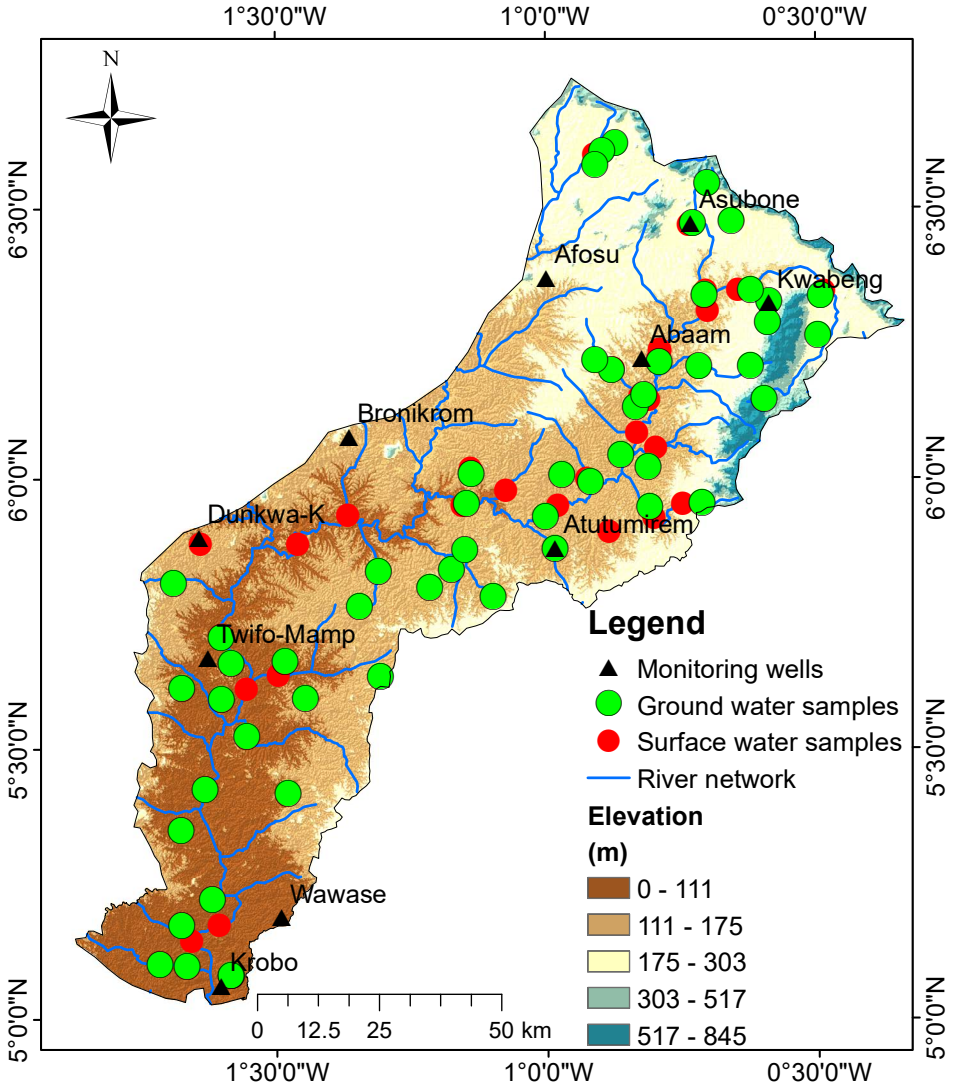

Figure 2.2: A topographic map showing the distribution of the sampling points (modified after Manu et al. (2023e)). The northern boundary of the basin forms part of the Kwahu Mountain Range, with elevations reaching 850 m above sea level. Also visible is the river network with major flow direction from the north to the south of the basin.

2.2.2 Data Collection and Analysis

In this study, a total of 90 water samples were collected from boreholes and rivers (Figure 2.2). The sampling campaign was conducted in March 2020 and marked the beginning of the first wet season in the study region. The water samples were analyzed for their $\delta^{18}O$ and $\delta^{2}H$ isotope ratios using the Picarro L-2140i Ringdown Spectrometer. All the measurements

are presented in permille (‰) relative to the Vienna Standard Mean Ocean Water 2 Standard (V-SMOW2). The analytical accuracy of the instrument is ±0.19‰ for δ^{18}O, and ±0.49‰ for δ^{2}H, respectively. The measurement uncertainty was assessed by conducting ten repeated analyzes with international reference materials SLAP2 and V-SMOW2. In addition, the instrument's performance was verified against an international laboratory standard. The stable isotope ratios' concentrations were then calculated using Equation (2.1):

$$\delta = \left(\frac{R_{\text{sample}} - R_{\text{std}}}{R_{\text{std}}} \right) \cdot 1000‰ \tag{2.1}$$

where R_{sample} and R_{std} are the stable isotopic ratios of oxygen and deuterium of the water samples and the standard concentration, respectively. The chloride concentrations in groundwater and precipitation were taken from Manu et al. (2023d) and Duah et al. (2021), respectively. Bivariate plots were used to construct surface water and groundwater regression lines using the δ^{18}O vs. δ^{2}H plot. The water samples' isotopic composition was interpreted considering the local and the global meteoric water lines established by Akiti (1986) and Craig (1961), respectively.

Total precipitation amounts and minimum and maximum temperature data from 1964 to 2013 were acquired from Princeton University's land surface modelling group. The data have been bias-corrected and down-scaled according to the observation-based global forcing dataset of Sheffield et al. (2006). A total of 14 observation stations distributed evenly across the basin were used for the analysis. Ten rain gauges were installed at or near the locations of the wells being monitored to measure daily precipitation and temperature (minimum and maximum).

2.2.3 Quantification of Evaporation Losses of Sampled Water

This study used the isotopic signature of the precipitation that recharged the sampled surface and groundwater and the annual average humidity and temperature of the prevailing climatic conditions to estimate the evaporation rate of these two water sources. The procedure used in the calculation is akin to the model proposed by Craig, Gordon, et al. (1965). For a detailed step-wise approach, refer to Fellman et al. (2011). The fraction of water loss through evaporation can be quantified using the equation reformulated by Gibson and Reid (2010) for a non-steady-state condition and adopted by several authors (Dogramaci et al. 2012; Loh et al. 2022; Yidana 2013), as shown in Equation (2.2):

$$\mathrm{f} = 1 - \left(\frac{\delta_{\mathrm{L}} - \delta^{*}}{\delta_{\mathrm{P}} - \delta^{*}} \right)^{\frac{1}{\mathrm{m}}} \tag{2.2}$$

where δ_L and δ_P indicate the initial signatures of δ^{18}O and δ^{2}H ratios of the sampled surface water and groundwater, respectively. The indices m and δ^{*} are estimated from Equations (4.1) and (2.4) respectively (Allison and Leaney 1982; Dogramaci et al. 2012; Gibson and Reid 2010; Welhan and Fritz 1977; Yidana 2013):

$$\mathrm{m} = \frac{(\mathrm{h} - \frac{\epsilon}{1000})}{(1 - h + \frac{\epsilon_{\mathrm{k}}}{1000})} \tag{2.3}$$

$$\delta^{*} = \frac{(\mathrm{h}\delta_{\mathrm{A}} + \epsilon)}{(\mathrm{h} - \frac{\epsilon}{1000})} \tag{2.4}$$

where h represents the basin's mean relative humidity, δ_A represents the stable $\delta^{18}O$ and $\delta^{2}H$ ratios for the ambient air/vapor, ϵ_k is the kinetic isotopic fractionation factor, which is linked to the relative humidity between water (w) and vapor (v) for ^{18}O and ^{2}H, estimated using Equations (2.5) and (2.6), respectively:

$$\epsilon_k{}^{18}O_{w\text{-}v} = 14.2(1-h)‰ \tag{2.5}$$

$$\epsilon_k{}^{2}H_{w\text{-}v} = 12.5(1-h)‰ \tag{2.6}$$

$\epsilon_k{}^{18}O_{w\text{-}v}$ and $\epsilon_k{}^{2}H_{w\text{-}v}$ were estimated at 4.3 and 3.8, respectively, by adopting a local humidity of 70% (Turner et al. 1996). The total isotopic enrichment factor, ϵ (Gonfiantini 1986) is calculated using Equation (2.7):

$$\epsilon = \epsilon_{eq} + \epsilon_k \tag{2.7}$$

where ϵ_{eq} is expressed as $\epsilon_{eq} = 1000(1-\alpha^{-1}{}_{w\text{-}v})$, which is a function of temperature (in Kelvin) expressed for $\delta^{18}O$ by Equation (2.8) (Loh et al. 2022; Yidana 2013):

$$10^{10} ln\alpha^{18}O_{w\text{-}v} = \left(\frac{1.534\times10^{6}}{T^{2}}\right) - \left(\frac{3.206\times10^{3}}{T}\right) + 2.644 \tag{2.8}$$

Using a mean yearly temperature of 298.15 K, the kinetic fractionation factor (ϵ_k) was calculated to be 9.11‰ vrs V-SMOW, resulting in a fractionation enrichment factor (f) of −13.37‰ vrs V-SMOW (Loh et al. 2022).

Determining the isotopic signature of ambient air moisture (δ_A) can be a daunting task since it is seldom directly measured in field settings. Typically, it is estimated based on the initial isotopic composition of recent rainfall. It's crucial to emphasize that the isotopic composition of ambient air can undergo notable variations at various heights above a surface water body (Adsiz et al. 2023). According to the proposal by Peng et al. (2012), an isotopic equilibrium exists between the isotopic signature of the initial precipitation δ_A and the ambient air vapor δ_{IP} which is expressed by Equation (2.9):

$$\delta_A \cong \delta_{IP} - 10^{3}(\alpha_{w\text{-}v} - 1) \tag{2.9}$$

where $\alpha_{w\text{-}v}$ is the fractionation factor. For the estimation, we adopted the initial isotopic signature of rainwater, which was sampled in April 2012 around the Lake Bosumtwi area from Loh et al. (2022) and returned a value of −12.40‰vs V-SMOW for $\delta^{18}O$.

2.2.4 Groundwater Recharge Estimation Using CMB Method

The CMB method relies on the mass balance principle to estimate groundwater recharge using precipitation and groundwater chloride data (Obuobie et al. 2010). The basic assumptions guiding the application of the CMB method are as follows: (1) the unsaturated zone has no Cl^{-} in storage; (2) in groundwater it is derived primarily from precipitation and dry atmospheric deposition; (3) its concentration in surface water is the same as in the precipitation and (4) the depth of groundwater is large enough that seasonal variation is regarded as small (McNamara 2005; Obuobie et al. 2010).

Considering steady-state equilibrium conditions with advection as the dominant Cl^{-} transport in the system and disregarding other sources such as dry atmospheric deposition

and human activities like irrigation and animal watering (Obuobie et al. 2010), the recharge to groundwater is thus calculated using Equation (2.10):

$$R = P \cdot \frac{Cl_p}{Cl_{gw}} \tag{2.10}$$

where R denotes the total estimated recharge (mm), P is the long-term average precipitation (mm), Cl_p and Cl_{gw} are the precipitation and groundwater chloride concentration measured in mg/L, respectively (Obuobie et al. 2010). In the calculation, we utilized the average annual precipitation of 1500 mm as reported by Dickson et al. (1988). In addition, the average chloride concentration in precipitation (1.13 mg/L) was taken from Duah et al. (2021), which was estimated using records from meteorological stations in the adjacent Densu Basin. The chloride concentration in groundwater was obtained from 56 samples collected by ourselves (Manu et al. 2023e).

The calculated recharge values were further interpolated using the inverse distance weighting (IDW) method to determine the spatial distribution of groundwater recharge. Mainly because of data paucity, a simple interpolation scheme, IDW was chosen instead of interpolation schemes that assume a statistical correlation between the data points.

2.2.5 Groundwater Recharge Estimation Using Water Table Fluctuation Method

The WTF method entails tracking and measuring changes in groundwater levels over time, often months to a year. In this investigation, data loggers were installed in ten boreholes in August 2020 to record and store data on water level fluctuations every four hours. In addition, four wells had barometer data recorders installed to track air pressure, and this information was used for correction. The information about the location and geological formation for the monitored wells are shown in Table 2.1.

Table 2.1: Monitored well characteristics in Ghana's Pra Basin. The meta-sediment comprises weathered phyllite, shale, schist, while the granite comprises granitic to quartz dioritic gneiss.

Community	Well ID	Longitude	Latitude	Elevation (m)	Well depth (m)	Geology
Abaam	PTB 20	-0.82403	6.22183	146	70.8	Meta-sediment
Asubone Rail	PTB 30	-0.73244	6.47144	191	27.0	Meta-sediment
Krobo	PTB 21	-1.60335	5.06144	13	56.0	Meta-sediment
Kwabeng	PTB 31	-0.58864	6.32337	207	37.0	Meta-sediment
Wawase	PTB 25	-1.48185	5.14681	59	20.0	Meta-sediment
Bronikrom	PTB 28	-1.36528	6.07804	140	80.0	Meta-sediment
Afosu	PTB 29	-1.00022	6.37052	187	48.0	Meta-sediment
Dunkwa-K	PTB 26	-1.67817	5.92007	105	36.7	Sandstone
Twifo-Mamp	PTB 17	-1.62684	5.66945	88	28.6	Granite
Atuntumirem	PTB 19	-0.98522	5.87161	133	40.5	Granite

The WTF approach assumes that the rise in the groundwater table over a period of time is driven solely by groundwater recharge and that it is directly related to the aquifer's specific yield (Delin et al. 2007). Groundwater recharge can thus be estimated using Equation (2.11):

$$R = S_y \cdot \frac{\Delta h}{\Delta t} \tag{2.11}$$

where R designate the recharge amount from precipitation, S_y represents the specific yield, (Δh) is the head difference throughout the recharge period and Δt is the time duration of the recharge. For each monitoring well, the graphical extrapolation approach was used to approximate the increase in water level (Δh). We examined the water level data visually and manually stretched the recession curve. The rise in the water level during the recharge phase is determined by the difference between the lowest point on the extrapolated antecedent recession curve and the peak of the water rise (Obuobie et al. 2012a). More information regarding the use of the WTF method is well explained in Delin et al. (2007).

As there are currently no records of specific yield for the aquifer materials in the basin, it was adopted from the literature (Table 2.2) (Sinha and Sharma 1988). The values were adopted using the geologic material of the area's aquifers, which was primarily granite and meta-sediments (Table 2.2) (Sinha and Sharma 1988). With this in mind, we used specific yield (Sy) values of 0.02 in the range of 0.01 to 0.03 for weathered phyllite, schist and associated rocks, 0.02 in the range of 0.02 – 0.04 for granite and 0.05 in the range of 0.01 - 0.08 for sandstone (Sinha and Sharma 1988), respectively.

Table 2.2: List of specific yield values used in groundwater recharge estimate in India (modified after Sinha and Sharma (1988).

Material	Range of specific yield
Sandy alluvium	0.12–0.18
Valley fills	0.10–0.14
Silt/clay rich alluvium	0.05–0.12
Sandstone	0.01–0.08
Limestone	0.03
Highly karstified limestone	0.07
Granite	0.02–0.04
Basalt	0.01–0.03
Laterite	0.02–0.04
Weathered phyllite, shale, schist, and associated rocks	0.01–0.03

2.3 Results

2.3.1 Climatology of Precipitation and Temperature in the Pra Basin

Figure 2.3a,b displays decadal mean monthly precipitation and temperature for the past 50 years. The bimodal precipitation pattern remains visible in the precipitation climatology (Figure 2.3a). The wet season has two halves, the first of which starts in March and peaks in June, and the second in September and peaks in October. However, analysis of the decadal variability in precipitation patterns reveals a decrease in the precipitation amount at the peak of the first wet season and an increase during the second wet period.

According to our observations, the second half of the wet season has gotten noticeably wetter in the past decade compared to the previous four decades. The first decade, between 1964 and 1973, recorded the highest peak of the first wet season, with a mean precipitation of 257 mm, while the last decade, between 2004 and 2013, recorded the lowest peak, with a mean of 193 mm. The second wet season's highest peak, with an average rainfall of 184 mm, occurred between 2004 and 2013. The mean monthly precipitation for the past decades for the three zones (northern, central and southern) are shown in Figure 2.10 (Appendix 2.6.2). Analysis of extreme

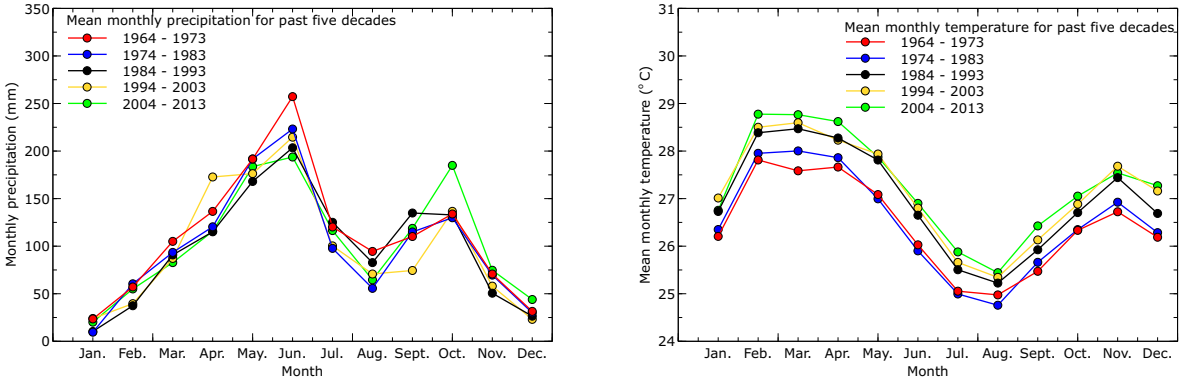

(a) **(b)**

Figure 2.3: Mean monthly precipitation **(a)** and temperature **(b)** climatology for the past fifty years (1964-2013) in the study area. Data source: Princeton University's land surface modelling group, which has been biased corrected and down-scaled according to the observation-based global forcing dataset of Sheffield et al. (2006)

precipitation events reveals that the southern zone, located closer to the sea, experiences higher precipitation amounts, particularly in June, which gradually decreases towards the northern part of the basin. Conversely, during the first dry period from July to September, the northern zone exhibits relatively higher precipitation than the central and southern parts.

We discovered that the mean monthly temperatures in the basin have been rising over the past 50 years (Figure 2.3b). The bimodal pattern of the basin's temperature climatology has not changed. In the months of February and November, two peaks are visible. In the most recent ten years, between 2004 and 2013, February had the highest temperatures, with an average monthly value for the season of 28.8 °C, while the average monthly value for the second season was 27.54 °C. Generally, the wet season records the lowest temperatures, while the dry season records the highest. The temperature variations in the three zones are shown in Figure 2.11 (Appendix 2.6.3) and show the trend from the northern topographically high to the southern topographically low of the region. Across all five decades, temperatures are highest in the lowlands and lowest in the highlands.

2.3.2 Variability in Surface Water and Groundwater δ^{18}O and δ^{2}H Values

Surface water (Figure 2.4a) shows large variability in stable isotopic composition. The δ^{18}O and δ^{2}H ratios in surface water samples range from -2.8 to 2.2‰ vrs V-SMOW for δ^{18}O and from -9.4 to 12.8‰ vrs V-SMOW for δ^{2}H, with a mean of -0.9‰ vrs V-SMOW and 0.5‰ vrs V-SMOW, respectively. The deuterium excess (d-excess) is between -5.0‰ vrs V-SMOW and 12.6‰ vrs V-SMOW, with a mean of 7.5‰ vrs V-SMOW. The δ^{2}H values show the largest variability in the dataset and this occurs in the northern zone. No significant variations exist in the mean isotopic composition of the stable O-18 isotope ratios in the northern zones. The computed d-excess values exhibit a relatively consistent level of variability across the three zones. When plotting stable isotopes against elevation (see Figure 2.12a in Appendix 2.6.4), no distinct correlation is observed. Nonetheless, the sample taken from the Apapaw River, which serves as the source of the Birim River and is located at a higher elevation, displays a notably depleted isotopic composition.

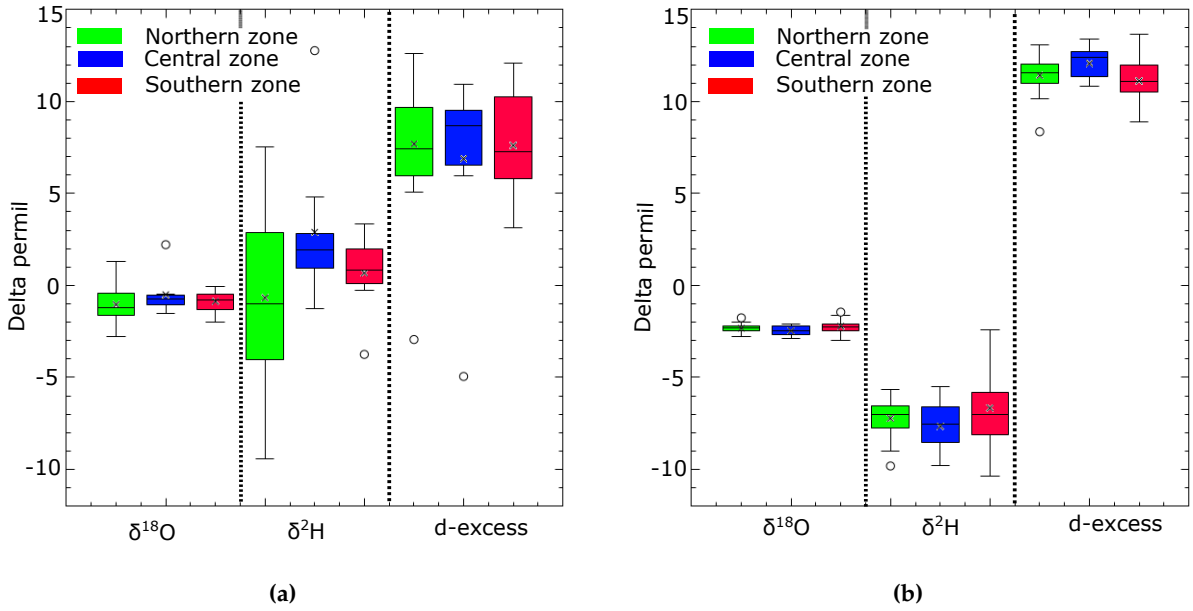

Figure 2.4: Box-and-whisker plots of the variation in the δ^{18}O and δ^{2}H ratios and the calculated d-excess for the surface water **(a)** and groundwater **(b)** samples for the three zones.

Groundwater (Figure 2.4b) shows less variability in the stable isotopes than surface water. The δ^{18}O and δ^{2}H isotope ratios in groundwater range from -3.0 to -1.5‰ vrs V-SMOW and from -10.4 to -2.4‰ vrs V-SMOW with an estimated mean of -2.3‰ vrs V-SMOW and -7.0‰ vrs V-SMOW, respectively. The d-excess ranges from 8.3 to 13.6‰ vrs V-SMOW, with a mean of 11.4‰ vrs V-SMOW. The δ^{18}O values are generally enriched relative to δ^{2}H values in all the three zones. Groundwater exhibits a higher d-excess than surface water. Figure 2.5 is a contour map displaying the distribution of δ^{18}O and δ^{2}H values in the Pra Basin groundwater. A plot of the stable isotopes against the elevation (see Figure 2.12b in Appendix 2.6.4) shows no positive correlation.

2.3.3 Correlation Between δ^{18}O and δ^{2}H of Water

The initial isotopic compositions of the precipitation that recharged the surface water and groundwater are estimated to be -2.6‰ vrs V-SMOW (δ^{18}O) and -6.4‰ vrs V-SMOW (δ^{2}H) and -3.1‰ vrs V-SMOW (δ^{18}O) and -10.8‰ vrs V-SMOW (δ^{2}H), respectively. These values are determined by the intersection of the evaporation lines of surface water and groundwater on the local meteoric water line (LMWL). Notably, these values indicate significant depletion compared to the measured isotopic signatures of surface water and groundwater. Figure 2.6a shows the linear regression models for the relationships between δ^{18}O and δ^{2}H for the water samples. Notably, the positions of the water samples are to the right of the LMWL, with surface waters showing the largest deviation from the initial isotopic composition. The regression analysis of the two water sources shows lower slope and intercept values compared to the LMWL. The calculated d-excess of all the water samples is lower than that of the LMWL. The surface water samples show a lower d-excess compared to the groundwater. Figure 2.6b illustrates the relationship between d-excess and δ^{18}O for surface water and groundwater. The Cl^{-} and δ^{2}H relationship depicted in Figure 2.7 does not exhibit a distinct influence of isotopic processes like evaporation, mixing, or transpiration on the groundwater. In general, stable surface water and

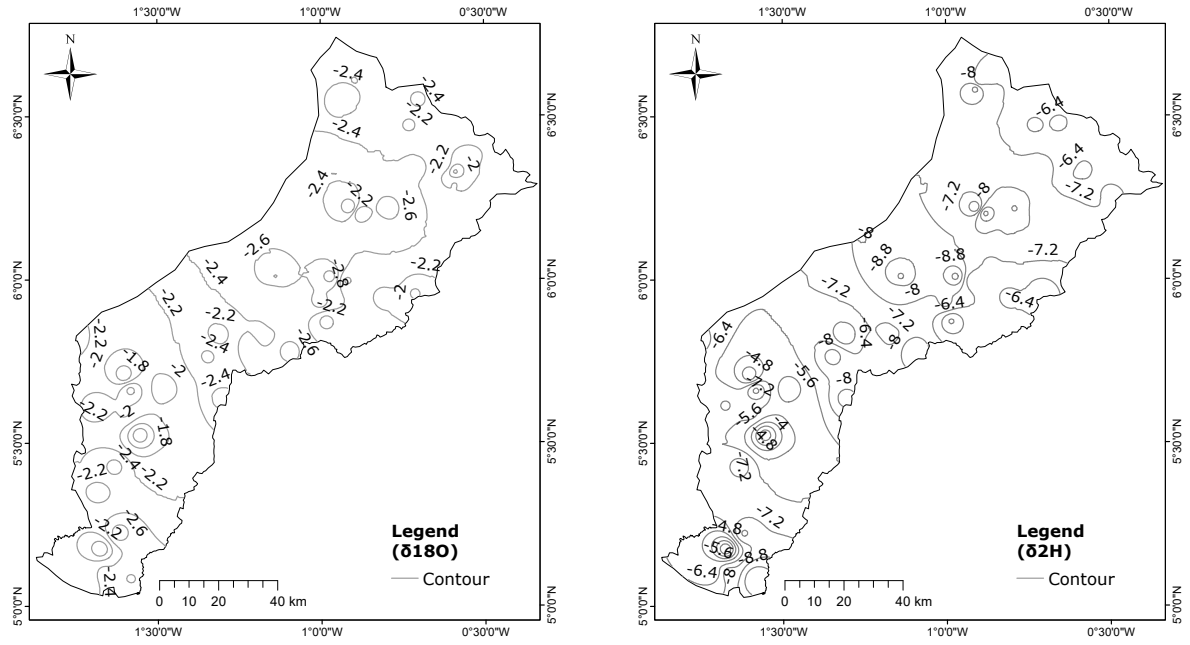

(a) (b)

Figure 2.5: Groundwater **(a)** (δ^{18}O) and **(b)** (δ^{2}H) values of the Pra Basin do not show significant correlation with elevation.

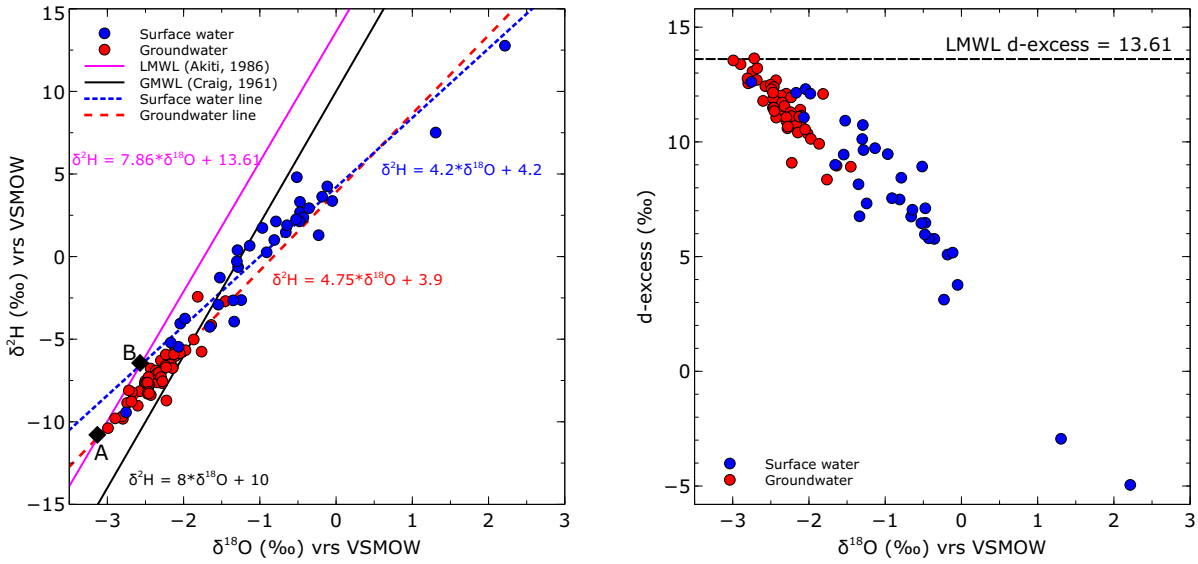

(a) (b)

Figure 2.6: (**a**) Surface water and groundwater δ^{18}O and δ^{2}H relationship plots used to infer the origin and evaporation influence. Also featured are the local (Akiti 1986) and the global (Craig 1961) meteoric water lines. Both water sources defined an evaporation line with lower slopes, indicating the change in the δ^{18}O and δ^{2}H isotope ratios in the initial precipitation. (**b**) The d-excess vrs. δ^{18}O plot provide information about the influence of evaporation. Almost all samples plot below the d-excess of the LMWL, indicating that the precipitation that recharged the surface water and groundwater experienced evaporation. The intercept of the surface water and groundwater lines (A and B) indicates precipitation's initial isotopic signature before recharge.

groundwater isotopes have undergone substantial alterations, enriching the heavier isotopes in contrast to their initial isotopic composition.

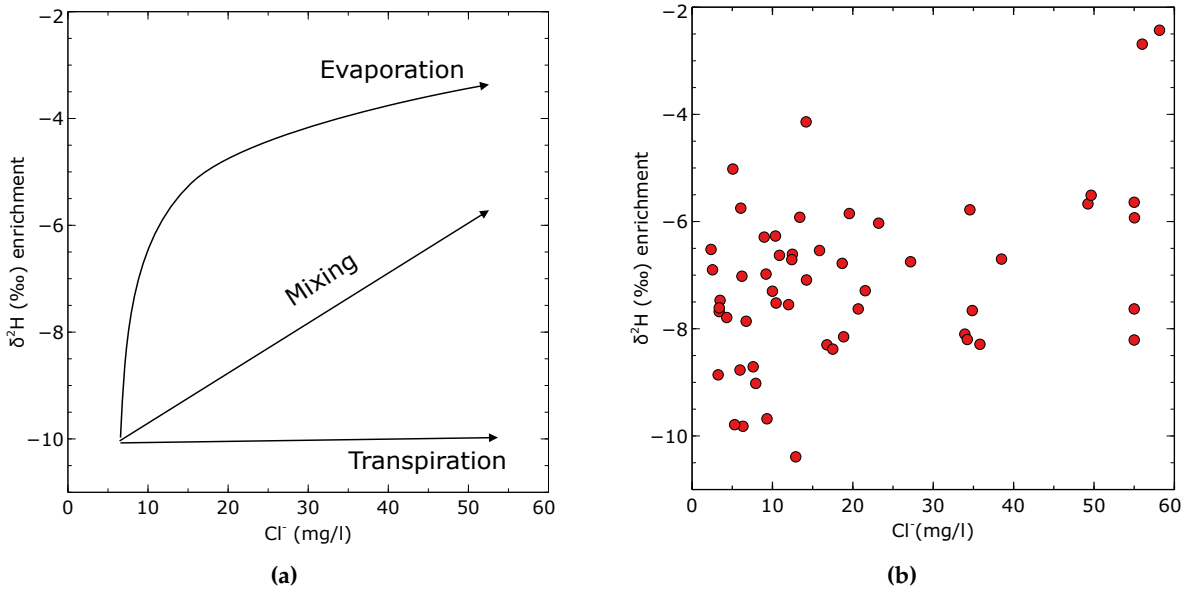

Figure 2.7: (**a**) Conceptual diagram showing the potential recharge pathway affecting changes in groundwater isotopic composition and Cl^- concentration (modified after Love et al. (1993)). (**b**) Deuterium vs. Cl^- shows no dominant process influencing groundwater recharge.

2.3.4 Estimations of the Rate of Evaporation in Surface Water and Groundwater

Surface water experiences higher rates of evaporation compared to groundwater. The calculated regional evaporation rates for surface water vary between 51% and 77%, averaging 62%, while for groundwater, it range from 55% to 61%, with an average of 57%. No significant disparities in mean evaporation rates were observed among the northern, central, and southern zones for groundwater. However, for surface water, there are slight variations in mean evaporation rates across these zones, specifically recording values of 61%, 64%, and 62% for the northern, central, and southern zones, respectively. An analysis of evaporation rates in relation to elevation did not reveal any discernible increasing or decreasing patterns.

2.3.5 Groundwater Recharge Estimate Using Chloride Mass Balance Method

The chloride in the groundwater range from 3.2 mg/L to 196.7 mg/L, with a mean of 26.9 mg/L. The lowest chloride concentrations were predominantly measured in the northern parts of the area, which are characterized by highly fractured meta-sedimentary rocks and are farthest away from the coast. The highest chloride concentrations were measured in the southern areas of the basin, which are underlain by granitoid rocks and are situated near the coast.

Groundwater recharge was highest in the northern zone and decreased down gradient towards the south. The estimated amount of recharge in the Pra Basin ranges between 9 mm and 666 mm, representing 0.6% to 33.5% of the average yearly rainfall. In Appendix 2.6, you can find Table 2.4, which provides the estimated recharge values for different borehole locations. The estimated average recharge for the entire study region is 165 mm, which is equivalent to 10.7% of the annual precipitation average of 1500 mm. Figure 2.8 shows the spatial groundwater recharge distribution based on the CMB calculations.

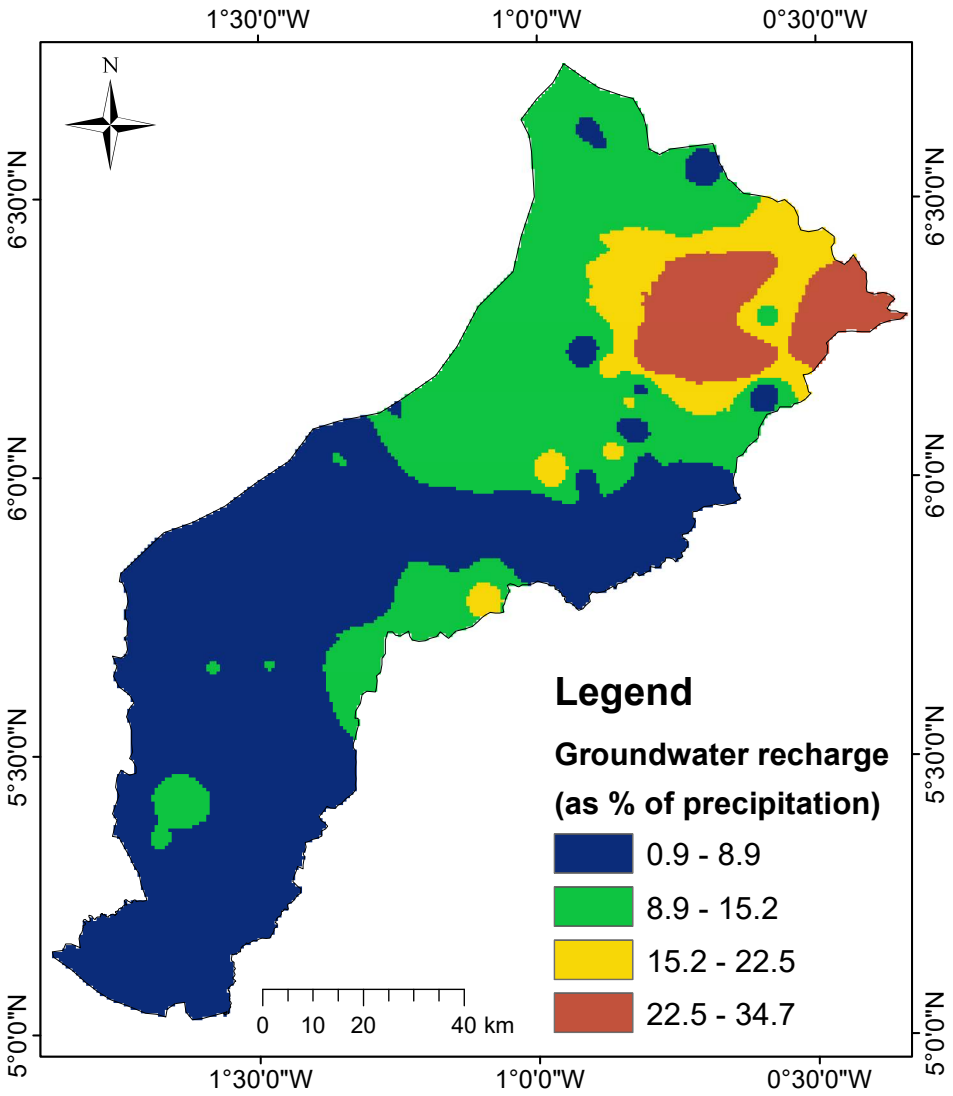

Figure 2.8: Spatial interpolation of groundwater recharge based on the CMB approach as a percentage of the long-term mean precipitation (1500 mm) using the inverse distance weighting (IDW) method.

2.3.6 Groundwater Recharge Estimate from Water Table Fluctuation Method

Generally, the rise in groundwater level coincides with the wet periods, with peak values in June and September. Figure 2.9 shows the hydrographs of groundwater level fluctuations from selected monitoring wells overlaid with the mean monthly precipitation for the water year 2022. The highest and lowest water level rises occurred in the first wet season (usually March–June), with values of 3.28 m and 0.12 m, respectively. It is also evident that the rise in groundwater level associated with a precipitation event occurred with a delay of 1–2 months between January and February and from November to December.

Groundwater recharge rate is higher in the first half (March-June) of the wet season than in the second (September-November), reflecting the rise in water levels in both seasons. Table 2.3 presents the estimated groundwater recharge values using the WTF method. The mean recharge range from 0.23 to 3.60% of the mean annual precipitation. The highest estimated mean recharge for the two wet seasons occurred in Kwaben, with 54.1 mm, accounting for 3.6% of the annual rainfall in the basin. We observed that the highest value was associated with the well

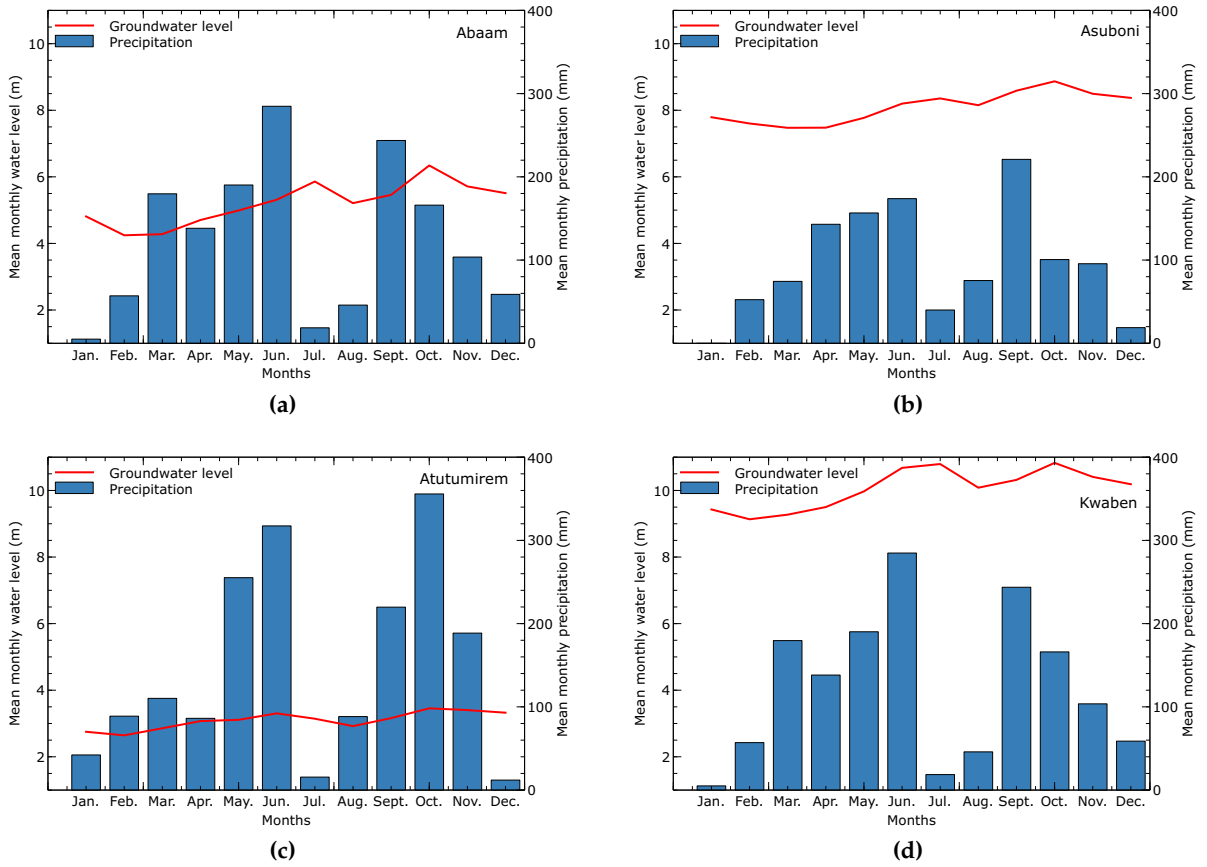

Figure 2.9: Groundwater hydrographs and observed averaged monthly precipitation at some selected locations (**a**) Abaam, (**b**) Asuboni, (**c**) Atutumirem and (**d**) Kwaben in the Pra Basin for the water year 2022.

located in the Birimian meta-sediment, with a depth of 37 m. In contrast, the deepest well at 80 m depth located at Bronikrom had the lowest estimated mean recharge, also found in the Birimian meta-sediment. No significant correlation was obtained between the well depth and the recharge.

Table 2.3: Groundwater recharge values estimated for the Pra Basin for the water year 2022

Well location	Aquifer material	Specific yield S_y	Δh (m) 1st wet season	Δh (m) 2nd wet season	Recharge (mm) 1st wet season	Recharge (mm) 2nd wet season	Mean recharge (mm)	% of annual rainfall
Abaam	Meta-sediments	0.02	1.60	1.13	32.0	22.6	27.3	1.82
Asuboni	Meta-sediments	0.02	0.87	1.07	17.4	21.4	19.4	1.29
Krobo	Meta-sediments	0.02	1.85	0.15	37.0	3.0	20.0	1.33
Kwaben	Meta-sediments	0.02	3.29	2.12	65.8	42.4	54.1	3.60
Wawaase	Meta-sediments	0.02	1.24	0.92	24.8	18.4	21.6	1.44
Bronikrom	Meta-sediments	0.02	0.12	0.23	2.4	4.6	3.5	0.23
Afosu	Meta-sediments	0.02	0.85	0.74	17.0	14.8	15.9	1.06
Dunkwa-K	Sandstone	0.05	0.73	0.49	36.5	24.5	30.5	2.00
Twifo Mamp	Granite	0.03	1.47	0.77	44.1	23.1	33.6	2.20
Atutumirem	Granite	0.03	1.05	0.98	21.0	19.9	20.5	1.40

Note(s): Meta-sediments are composed of weathered phyllite, shale, schist and associated rocks. Δh designates the water level rise.

2.4 Discussion

2.4.1 Regional Climatic Conditions, Present and the Past

The climatology of temperature and precipitation of the study area has not changed over the past five decades. Ghana's Fourth National Communication to the United Nations Framework Convention on Climate Change reports that temperatures increased by 1.0 °C between 1960 and 2003, with an average of 0.21 °C per decade (Bergesen et al. 2018). The report also highlights that hot days have increased by 48 per year (Bergesen et al. 2018). This change is largely consistent with the results presented in this study (Figure 2.3b). The temperature for the past five decades has been observed to follow an increasing trend with the current climate getting hotter. These are reflected in the peak months in February and November, with the highest recorded temperatures. Since isotope fractionation is temperature-dependent, the current climatic conditions are likely to favour the enrichment of the heavier isotopes compared to earlier decades when temperatures were relatively lower. In addition to the temperature increase, there is also a noticeable variation in the amount of rainfall, with the current years experiencing a decrease in the first peak during the first wet season and an increase in the second season. This trend is consistent with the assertion that precipitation over the past three decades varied greatly on the inter-annual and inter-decade timescales (Bergesen et al. 2018). Here, we could argue that different seasons are likely to be associated with different concentrations of stable isotopes in precipitation due to the rising temperatures and the change in the precipitation, which has become erratic for the past five decades. The observed trends in the past extreme climate scenarios indicate that the study area has experienced higher temperatures and reduced rainfall, impacting both source vapor and precipitation. This will certainly enrich the isotopic composition of precipitation, which is the principal source of recharge of the Pra Basin's surface water and groundwater systems.

2.4.2 Isotopic Characterization of the Surface Water and Groundwater

The considerable variation in $\delta^{18}O$ and $\delta^{2}H$ values observed in the surface water samples, as opposed to the groundwater samples, can be attributed to the significant evaporation occurring in the region due to the elevated temperatures. In this study, we adopted the local meteoric water line developed by Akiti (1986) for southern Ghana as our reference for our interpretation. The slope and the intercept of $\delta^{18}O$ and $\delta^{2}H$ fitted for the surface water samples are less than the LMWL. This is primarily due to fractionation caused by evaporation, as supported by previous studies (Craig, Gordon, et al. 1965; Dogramaci et al. 2012). It has been established that the slope of surface water evaporation typically ranges from 4 to 6 (Barnes and Allison 1988), which is the case in this study. Since surface waters are open systems, the isotope fractionation upon evaporation is influenced by the prevailing atmospheric conditions. Studies have shown that lower slopes of surface water are associated with lower humidity (Fan et al. 2015). In general, an increase in humidity will cause a proportional increase in the slope of the evaporation line and vice versa. In the study area, where the relative humidity is generally between 70% and 80% year-round, the $\delta^{18}O$ and $\delta^{2}H$ isotope ratios are expected to produce a regression line with a lower slope than the LMWL (Yidana 2013) due to the influence of fractionation attending the continuous evaporation of the open river systems in the basin. The deuterium excess (d-excess) calculated for the surface water samples is used together with $\delta^{18}O$ to derive a relationship that can be used to understand the influence of evaporation on

the water's stable ^{18}O and ^{2}H isotope composition. In the case of this study, all surface water d-excess values are lower than the LMWL estimate of 13.61‰ vrs V-SMOW (Figure 2.6b), underlining an evaporation influence.

The estimated evaporation rate of the surface water reflects the influence of the prevailing high temperatures, resulting in a more enriched stable $\delta^{18}O$ and $\delta^{2}H$ ratios relative to the groundwater pointing to a likely discharge from groundwater into the surface water. The intercept of the surface water line with the LMWL indicates the initial isotopic signature of the precipitation that recharged the rivers before undergoing evaporation (Dogramaci et al. 2012; Yidana 2013). This is based on the assumption that the LMWL reflects the characteristics of recent rainfall. However, we acknowledge that there may be changes in the slope and intercept of the LMWL due to climate variability over the past five decades. Unfortunately, we could not conduct precipitation measurements over a longer period due to time constraints to allow a more representative characterization of the stable isotope composition of precipitation in the basin. Nevertheless, the intercept values of -3.1‰ vrs V-SMOW ($\delta^{18}O$) and -10.8‰ vrs V-SMOW ($\delta^{2}H$) obtained were within the range of $\delta^{18}O$ and $\delta^{2}H$ compositions in recent precipitation observed in the Densu Basin (Adomako et al. 2010) which shares similar climatic conditions with our study area. The large deviation of the surface water samples from the initial isotopic signature of precipitation indicates that the surface water in the basin has experienced evaporative enrichment of the heavier isotopes. This enrichment is attributed to the fractionation process associated with evaporation. Furthermore, it is plausible that biological organisms influenced the isotopic composition of the surface water by concentrating lighter isotopes and potentially distorting the isotope ratio data, especially under changing climatic conditions such as those prevalent in the study area (Dawson et al. 2002). As a result, the combined effects could lead to stable isotope depletion in the surface waters, which is the subject of a separate study. From the estimated evaporation losses, it is clear that the influence of living organisms may be masked by the evaporative enrichment of the heavier isotopes due to the high temperatures in the region. It is important to acknowledge the presence of potential sources of error in these estimates. These sources may include uncertainties in climatic parameters such as relative humidity and the isotopic composition of ambient water vapor. Furthermore, the plausibility of sampling surface water, which consists of a mixture of water from different sources (Yidana 2013), can make the analysis even more complex and uncertain. As expected, the stable isotope ratios are more enriched in the surface water than in groundwater, suggesting that any interaction between surface water and groundwater would likely favor groundwater discharge into the rivers.

The regional groundwater $\delta^{18}O$ and $\delta^{2}H$ data plots near the LMWL exhibit a lower slope and intercept relative to the LMWL indicating that the source of groundwater recharge is mainly from precipitation that has undergone some degree of evaporation prior to recharge. This is consistent with the signature of groundwater isotopic composition in semiarid regions caused by high temperatures and low relative humidity (Okofo et al. 2022; Yidana 2013). Research has shown that evaporation of infiltrating water prior to recharge generally exhibits a systematic enrichment of stable isotopes, resulting in a change in the evaporation line relative to the LMWL with a slope of typically 2 to 5 (Barnes and Allison 1988). In this study, the slope (4.7) of the groundwater evaporation line (Figure 2.6a) falls within this range and suggests that evaporation plays an important role in the groundwater recharge processes in the Pra Basin.

The significant departures of the slope and intercept relative to the LMWL are likely due to the effects of high evaporation rates attending high temperatures, low relative humidity and

the slow infiltration rate through the vadose zone (Afrifa et al. 2017; Yidana 2013). During the infiltration process, the infiltrating water can be affected by re-evaporation in the unsaturated zone due to the delayed transit time of the water. Yidana (2013) emphasized that the nature and thickness of the overburden material and its clay content determine the percentage of precipitation that reaches the saturated zone. When the aquifer system is less permeable, the vertical hydraulic conductivity is reduced, and infiltration is slowed, so water in the vadose zone above the evaporation extinction depth re-evaporates (Yidana 2013). In the event of significant evaporation, the water in the unsaturated zone becomes enriched with heavier isotopes, which are later transported into the aquifer by the infiltration of the late rains. In our study area, the northern and central zones are underlain primarily by meta-sedimentary rocks that are more permeable and porous to facilitate direct recharge from precipitation than the Cape Coast granitoids that underlie the southern parts of the basin. For this reason, the meta-sedimentary aquifers are expected to show more depleted isotopes than the granitoid. However, the isotopic composition of groundwater does not show significant variations in the terrain, suggesting that the factors leading to the isotopic fractionation of precipitation reaching the saturated zone are similar. However, the slight variability between the northern and southern zones can be explained by the differences in precipitation evolution processes from the vadose zone to the saturated zone (Yidana 2013). The intersection of the groundwater evaporation line with the LMWL indicates the isotopic signature of the source precipitation (Loh et al. 2022; Yidana 2013) that recharges the aquifers in the area. As indicated in Figure 2.6a, $\delta^{18}O$ and $\delta^{2}H$ at the intersection are $-3.1‰$ vrs V-SMOW and $-10.8‰$ vrs V-SMOW, respectively. Estimates of the fraction of precipitation that evaporates before groundwater recharge range from 57 to 65%. Although the precipitation evaporation rate on its way to the saturated zone is lower than surface waters, it remains a notable factor. This observation supports the notion that infiltration of precipitation through the vadose zone is a slow process that results in significant re-evaporation of the water before or during its passage through the unsaturated zone.

Multiple processes, including evaporation, mixing and transpiration, may affect the infiltrating water on the land surface or during percolation through the unsaturated to the saturated zone. The bivariate plot of Cl^- vrs. $\delta^{2}H$ was used to elucidate further on the likely processes affecting the infiltrating water prior to groundwater recharge (Figure 2.7a). Here we see in Figure 2.7b that $\delta^{2}H$ does not correlate with Cl^- concentration. Suppose the infiltrating water is affected by evaporation. In that case, we expect that an increase in Cl^- will correspond to the enrichment in ^{2}H along the evaporation line shown in Figure 2.7a (Love et al. 1993). If the infiltrating water is affected by transpiration prior to recharge, then the Cl^- concentration will increase without a corresponding change in the stable ^{2}H isotopic composition and the evaporation line will be horizontal (Love et al. 1993). If mixing two discrete end members is the sole dominant process, the strong positive correlation indicated by a straight line would be expected (Love et al. 1993). In the study area, the groundwater movement is structurally controlled so that the water samples probably consist of water from different aquifers. This will likely affect the mean isotopic composition of the final water. The transpiration process during recharge is reasonable as the dense vegetation cover in the study area likely facilitates the transpiration of infiltrated water in the root zone.

2.4.3 Groundwater Recharge Estimates

The estimated recharge values obtained from the CMB and WTF methods are largely consistent with values reported in other studies conducted in Ghana and semi-arid regions in

Africa. The CMB recharge estimates show larger variability, ranging from 0.6% to 34%, while the WTF method ranges from 0.2% to 3.6% of the mean long-term annual precipitation. The estimate of 10.7% mean recharge of the annual precipitation from the CMB is generally consistent with the mean basin recharge of 16% reported by the Water Resources Commission of Ghana, and our results are consistent with other studies carried out in different parts of Ghana. For example, Yidana et al. (2011) estimated an average recharge of 7.6% of annual precipitation using numerical groundwater flow models in south-east Ghana, while Afrifa et al. (2017), Obuobie et al. (2010), and Duah et al. (2021) reported similar figures in northern and southern Ghana, respectively.

The groundwater recharge estimates obtained from the CMB are reasonable compared to other studies. However, some uncertainties are expected due to other potential sources of Cl^- in groundwater that are not considered in the calculation. The main assumption for using the CMB is that the source of Cl^- in groundwater is mainly from precipitation and that Cl^- behaves conservatively, not being leached or absorbed from aquiferous sediments and not being affected by chemical reactions (Afrifa et al. 2017; Duah et al. 2021; Obuobie et al. 2010). Other sources of Cl^-, including deposition from marine aerosols and pollution from sewage, might contribute to the Cl^- loads as these wells are public wells exposed to unregulated disposal of solid and liquid waste on-site. While the weathering of chloride-containing minerals (e.g., halite) can impact chloride in groundwater, its effects have been neglected because no petrographic evidence of their occurrence is known in the terrain (Manu et al. 2023c). If Cl^- in groundwater increases, the estimated recharge, which is inversely proportional to the Cl^- concentration in groundwater, is expected to be low, leading to an overestimation of recharge and vice versa.

The basin-wide distribution of groundwater recharge shows high values in the northern parts, which are underlain by the Birimian meta-sedimentary rocks, while the lower recharge areas correspond to the granitoid. In a previous study (Manu et al. 2023d), the northern parts of the study area were proposed as a recharge zone likely to receive direct recharge from precipitation. With direct recharge, lower Cl^- values are expected than in waters with a high evaporation rate before reaching the aquifer. Among these two lithologies, the Birimian meta-sediments composed of phyllite have higher aquifer permeability than the granitoid (Banoeng-Yakubu et al. 2011; Yidana et al. 2011). Because secondary porosity governs the occurrence of groundwater in the terrain (Banoeng-Yakubu et al. 2011), it is likely that more vertical recharge is expected in the phyllite aquifers to the north than to the south, which is granitoid and less permeable compared to the Birimian rocks. The accuracy of the CMB estimates could be improved by using long-term data on chloride (Cl^-) instead of the one-time measurements used in this study. Unfortunately, long-term monitoring data on Cl^- in the Pra Basin was unavailable during this research.

The groundwater hydrographs show that the main driver of groundwater recharge is seasonal precipitation, although the contribution of river runoff is also a plausible factor. A close inspection of the hydrographs and rainfall patterns reveals that the peak of groundwater level rise occurs most during the two wet seasons, July and October. The current rainfall peak in the second part of the season is projected to occur in October; however, it happened in September. This trend suggests that the 2022 water year does not follow the mean climatology of the rainfall in the second season, which is supposed to peak in October. A similar characteristic was observed in the last three decades (Figure 2.3) when the peak in rainfall in the second period was slightly higher in September than expected in October. The continuous water level rise observed during the break of the wet seasons can be described as a delayed vertical recharge

from the preceding precipitation or horizontal component of the groundwater water recharge (Afrifa et al. 2017; Lee et al. 2005). A similar trend has been observed by Afrifa et al. (2017) in the Oti River Basin in Ghana. This observation is influenced by the thickness of the overburden and the nature of the material it is composed of Lee et al. (2005) emphasized that the thickness of the unsaturated zone partly controls the peak of the water level fluctuation during groundwater level monitoring. A thicker unsaturated zone is more likely to display a gradual peaking of the amplitude of the water level rise over monitoring periods than a shallow unsaturated zone, which would show a rapid peak in the amplitude (Afrifa et al. 2017; Lee et al. 2005). This assertion is largely consistent with the nature of the hydrographs (Figure 2.9) presented for the ten groundwater wells in this study. It is a well-known fact that every visible river basin on the earth's surface is accompanied by an underground basin, often as large or larger than its surface counterpart. At the same time, groundwater is one of the main components of the water balance in a river system, which is why some rivers also exist in the dry season. In the study area, the major rivers are the Birim River and Main Pra River, which could contribute some water to the aquifers. While isotope data predominantly suggest groundwater discharging into rivers, the results from the groundwater hydrographs suggest that the reverse is also plausible. This is supported by Figure 2.9, which shows that the groundwater level remains relatively stable even in months with low rainfall.

The groundwater recharge using the WTF method shows relatively little variability and agrees with the range of values estimated using the CMB method. This is reasonable and consistent with those obtained with WTF and other methods in many semi-arid regions (Afrifa et al. 2017; Duah et al. 2021; Obuobie et al. 2010). Using the average recharge estimate of 1.64% and the minimum annual precipitation of 1300 mm, the estimated mean annual recharge for the entire study catchment for the 2022 water year is 228 Mm^3, which is higher than the estimated total surface water use for the entire Pra Basin of approximately 144 Mm^3 for the year 2010 (WRC 2012). It is worth noting that the land size of the current study catchment (10,703 km^2) is less than half the size of the entire Pra Basin (23,000 km^2) and therefore indicates a great potential for developing groundwater for domestic and industrial purposes. The comparatively lower recharge amounts calculated by the WTF compared to the CMB can be partly attributed to the limited number of monitoring wells used in this current study. Here, conclusions on the spatial variability of groundwater recharge using the WTF can be improved by considering more data from evenly distributed monitoring wells across the basin. Furthermore, we would like to point out that the specific yield (Sy) used in the calculation was taken from the literature and not from measurements of the respective aquifer materials in the region. For this reason, some margin of error is predicted for the estimated groundwater recharge reported in this study. If the specific yield of the aquifer materials in the basin is measured, the accuracy of the WTF recharge calculations can be improved.

2.5 Conclusions

The use of stable isotope tracers oxygen ($\delta^{18}O$) and hydrogen ($\delta^{2}H$) and water level measurements have been applied in this study to ascertain the source, recharge mechanisms, and spatial estimates of groundwater recharge within the Pra Basin of Ghana. This study has presented regional stable isotope data of surface and groundwater for the first time, providing essential boundary conditions to conceptualize hydrogeochemical processes that drive groundwater evolution. Using chloride mass balance (CMB) and water table fluctuation (WTF) methods has enabled the quantification of groundwater recharge in the Pra Basin. Data

from past climate records were fully integrated into the study to evaluate the potential climatic variability over the past 50 years. Current data from 10 groundwater monitoring wells were provided for the recharge estimates and for understanding the source of the aquifer recharge. Our results allow the following conclusions:

1. The past fifty years show a temperature increase of about 1 degree Celsius. The climatology of precipitation and temperature remain unchanged; however, a gradual decrease in precipitation can be observed for the first peak of the rainy season in June.
2. Surface waters have experienced relatively high levels of evaporation due to the direct effects of prevailing climatic conditions. The relatively lower evaporation rate of groundwater is attributed to the short residence time of the infiltrating water within the evaporation extinguishing depth in the vadose zone.
3. Groundwater recharge from meteoric water tends to have higher concentrations of heavier isotopes relative to the LMWL. This enrichment occurs due to significant evaporation either at the land surface or during seepage through the vadose zone. The rate of evaporation of infiltrating water is likely influenced by factors such as the thickness and composition of the material between the surface and the saturated zone, as well as the high temperatures and low relative humidity prevailing in the region.
4. An integrated analysis of stable isotope data and water level measurements suggests a potential hydraulic connection between surface water and groundwater. This hypothesis is supported by the fact that the isotopes of groundwater have comparatively lower values than surface water. Furthermore, the observation that the groundwater level remains constant in months with lower rainfall further supports this conclusion.
5. The primary groundwater recharge area is in the northern zone, where the highest recharge occurs. The calculated recharge values show a gradual decline from the northern regions towards the southern areas of the basin.
6. Groundwater recharge for the study catchment, considering the average estimate of 1.64% (WTF) and minimum annual precipitation of 1300 mm, is 228 M m^3, which is higher than the estimated water use for the entire Pra Basin, underscoring a high potential for water supply.

The results presented in this study can be used to advance water management in the Pra Basin as they provide quantitative recharge estimates, which are prerequisites for planning and sustainable development of groundwater resources. For further studies, developing a numerical groundwater flow model is essential to gain a more comprehensive understanding of the water budget in the catchment. Such a model would enable accurate groundwater recharge estimates by integrating various water balance components, such as precipitation, river contributions, evapotranspiration, etc. Furthermore, this modelling approach would enable reliable delineation of groundwater flow patterns and the assessment of the hydrochemical evolution of groundwater in the Pra Basin.

2.6 Appendix

2.6.1 Groundwater Recharge Estimates Using the CMB Method

Table 2.4: Groundwater recharge values estimated for the Pra Basin using the CMB method. We utilized an average long-term precipitation of 1500 mm (Benneh and Dickson 1995) and a chloride concentration in rainwater of 1.13 mg/L (Duah et al. 2021) for the recharge estimates. Cl_{GW} is the chloride in groundwater.

Community	Northings (m)	Eastings (m)	Elevation (m)	Cl_{GW} (mg/l)	Recharge (mm)	as % of annual rainfall
Apapaw	765897.0	680069.0	362.0	34.9	48.6	3.2
Asiakwa SOS	776819.0	693156.0	238.0	3.5	486.6	32.4
Jejeti	759161.8	716496.3	204.0	9.0	188.8	12.6
Asubone	754144.0	724194.0	219.0	18.7	90.8	6.1
Kokrompe	751209.0	715992.0	205.0	10.4	163.4	10.9
Kofi dede	735301.0	732346.0	225.0	9.2	184.2	12.3
Kwahu Besease	732647.0	730776.0	220.0	38.5	44.0	2.9
Kwahu Oda	731178.0	728046.0	201.0	7.9	214.0	14.3
Kwaben	766831.0	700042.0	210.0	6.1	279.7	18.6
Akrofofo	763058.0	702365.0	181.0	3.5	666.2	32.0
Asunafo	753556.0	701388.0	171.0	3.4	502.5	33.5
Bomaa	766573.0	695707.0	248.0	10.9	155.9	10.4
Pamang	763069.0	686882.0	223.0	3.4	501.5	33.4
Kwamang	752530.0	686709.0	175.0	4.3	393.3	26.2
Okyinso	744419.0	687559.0	158.0	3.2	522.3	32.0
Akyem Abodom	741242.0	680849.7	143.0	18.9	89.9	6.0
Subi	739530.0	678458.8	164.0	6.7	251.9	16.8
Abompe	734625.3	685930.3	181.0	6.3	267.8	17.9
Otumi	731175.3	688002.9	186.0	34.6	49.0	3.3
Kade	739619.2	673085.2	132.0	35.0	48.4	3.2
Akwatia	742140.6	666200.2	169.0	14.2	119.1	7.9
Kusi	736501.7	668688.9	145.0	6.2	273.3	18.2
Awaham	753138.8	658835.2	198.0	49.2	34.4	2.3
Kakoasi	742452.0	658015.0	125.0	23.2	73.0	4.9
Etwereso	705906.0	664604.8	140.0	9.3	181.9	12.1
Zevor	704904.4	658538.3	112.0	16.8	101.0	6.7
Lebikrom	724448.3	664516.9	145.0	5.3	320.1	21.3
Soabe	730327.1	663168.4	136.0	15.9	106.9	7.1
Oda	721159.6	655929.2	121.0	98.0	17.3	1.2
Atutumirem	723063.7	649411.2	115.0	49.6	34.1	2.3
Aprade	710391.5	639605.4	165.0	6.0	284.1	18.9
Kenie	697462.6	641406.8	131.0	10.5	162.1	10.8
Obobakrokrowa	701896.6	645044.1	126.0	12.5	135.8	9.1
Akotikrom	704676.7	649089.0	129.0	21.5	78.7	5.2
Nyamebekyere	683039.0	637611.0	135.2	12.9	131.4	8.8
Ababuom	687388.0	623282.0	111.2	7.6	223.0	14.9
Bronokrom	656858.0	561969.0	14.0	55.0	30.8	2.1
Brunokrom	656856.0	561958.0	14.0	196.7	8.6	0.6
Kotogyina	644148.0	558902.0	32.5	87.9	19.3	1.3
Abotere	642296.0	564153.0	29.5	58.1	29.1	1.9
Dompin	647796.3	563871.1	14.0	33.9	50.0	3.3
Ewiadaso	646686.0	572168.0	60.0	27.2	62.4	4.2
Nyekompoe	652970.0	577496.0	38.4	20.7	82.0	5.5
Essamang	646554.0	591595.0	51.3	12.4	136.6	9.1
Mamponso	651448.0	600012.0	40.3	10.0	169.6	11.3
Anyanasi	654795.0	618484.0	68.1	34.2	49.5	3.3
Dokoro	646702.0	620785.0	97.0	14.2	119.5	8.0
Somnyamekor	656844.5	625862.5	84.0	12.0	141.3	9.4
Breman	654738.0	631093.0	75.0	79.5	21.3	1.4
Imbrain	636514.0	642921.0	141.9	17.5	96.9	6.5
Akonfudi	686960.0	644646.0	98.1	35.8	47.3	3.2
Kenkuase	671977.0	618658.0	94.2	19.6	86.6	5.8
Okyerekrom	667847.0	626235.0	79.2	5.1	334.0	22.3
Twifo Mamp	660003.0	610858.0	63.2	122.0	13.9	0.9
Wawase	668444.0	599214.0	105.0	13.4	126.5	8.4

2.6.2 A Decadal Mean Monthly Precipitation Climatology in the Pra Basin from 1964 to 2013

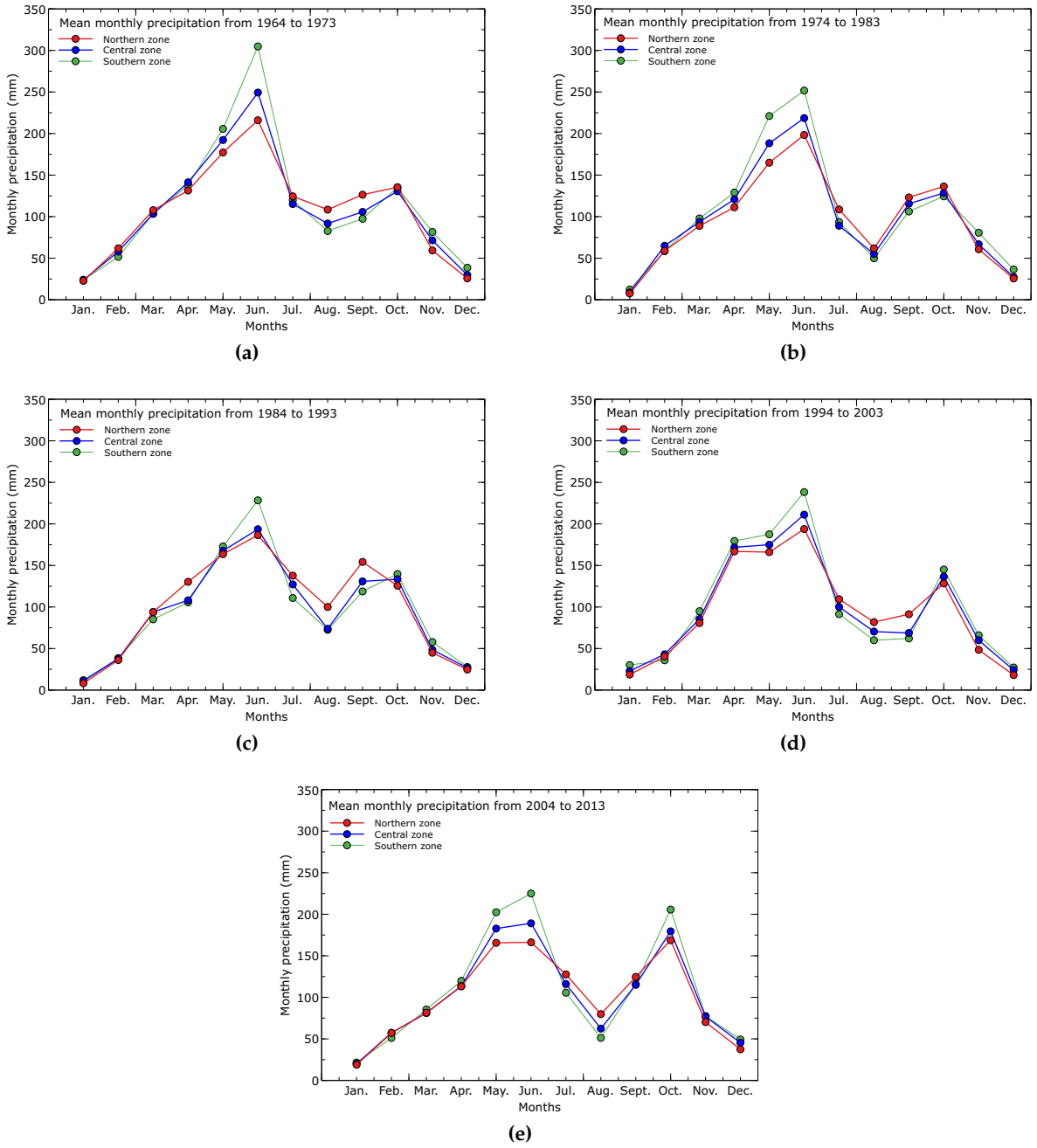

Figure 2.10: Decadal mean monthly precipitation climatology from (**a**) 1964 to 1973, (**b**) 1974 to 1983, (**c**) 1984 to 1993, (**d**) 1994 to 2003 and (**e**) 2004 to 2013, respectively in the Pra Basin for the three defined zones (northern, central and southern) after Manu et al. (2023d). The northern zones are at higher elevations while the southern zones are at lower elevations, respectively.

2.6.3 A Decadal Mean Monthly Temperature Climatology in the Pra Basin from 1964 to 2013

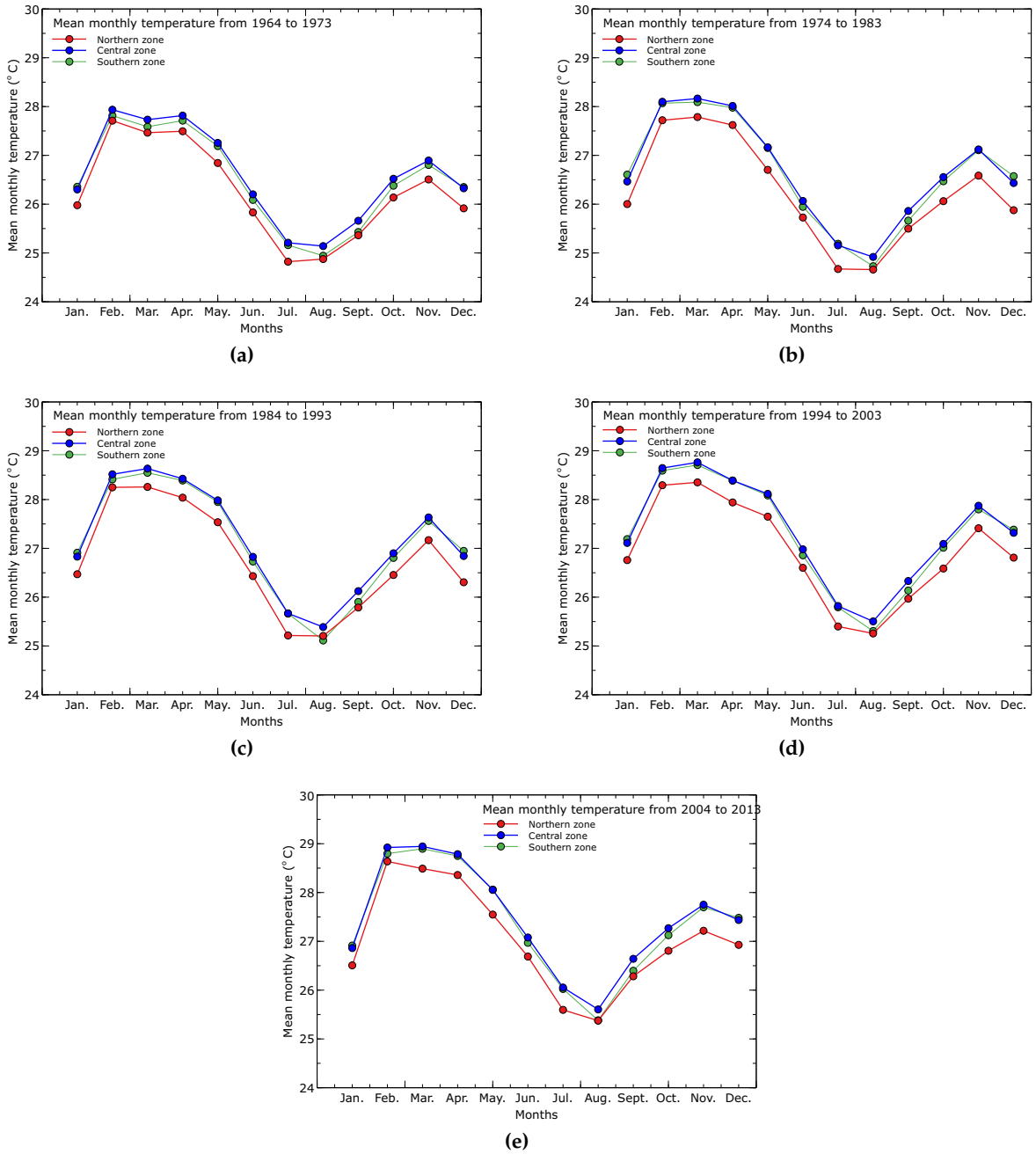

Figure 2.11: Decadal mean monthly temperature climatology from (**a**) 1964 to 1973, (**b**) 1974 to 1983, (**c**) 1984 to 1993, (**d**) 1994 to 2003 and (**e**) 2004 to 2013, respectively in the Pra Basin for the three defined zones (northern, central and southern) after Manu et al. (2023d). The northern zones are at higher elevations, while the southern ones are at lower elevations.

2.6.4 Stable Oxygen-18 and Deuterium Isotopes Plot Against Elevation for Surface Water and Groundwater

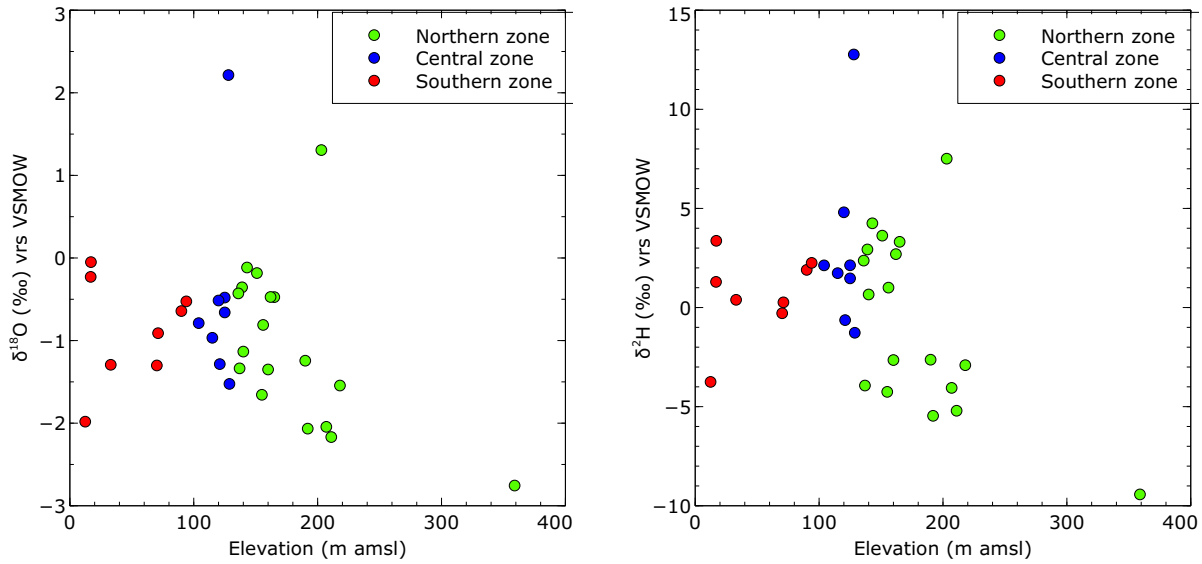

(a) **(b)**

Figure 2.12: Surface water stable oxygen-18 (**a**) and deuterium (**b**) isotopes plot against elevation show no clear correlation between them. The sample located in the highest elevation measured the least stable isotope of oxygen and deuterium ratios.

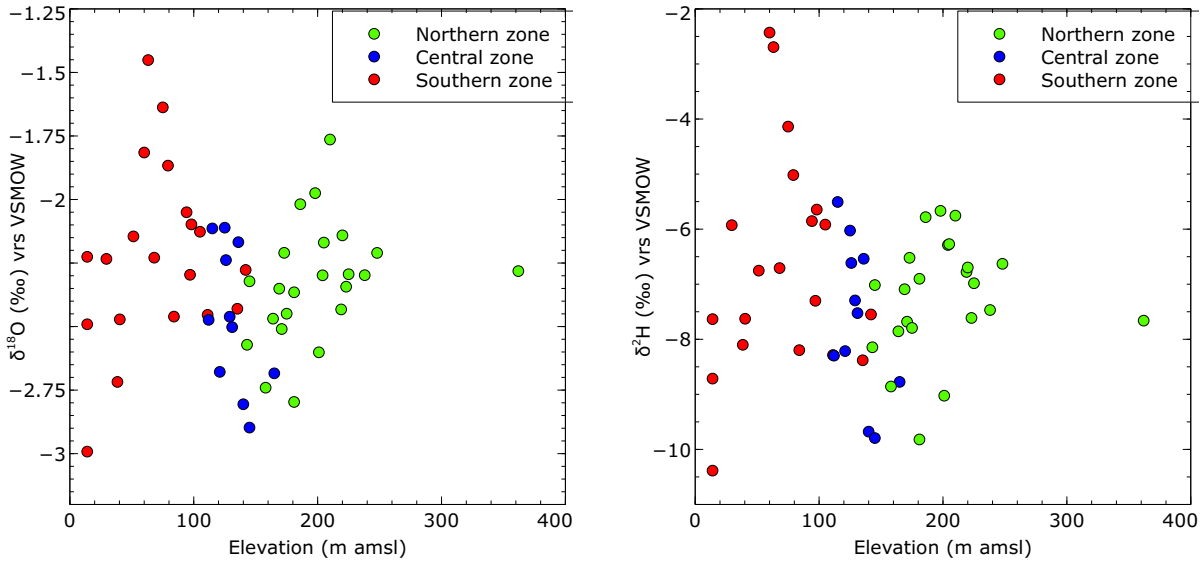

(a) **(b)**

Figure 2.13: Groundwater stable oxygen-18 (**a**) and deuterium (**b**) isotopes plot against elevation show no significant correlation between them. Very few samples in the southern zone (low elevation) showed relative enrichment of the stable oxygen-18 and deuterium isotope ratios.

Chapter 3

Hydrochemical Characterization of Surface Water and Groundwater in the Crystalline Basement Aquifer System in the Pra Basin (Ghana)

ABSTRACT

The quality of groundwater resources in the Pra Basin (Ghana) is threatened by ongoing river pollution from illegal mining. To date, there are very limited data and literature on the hydrochemical characteristics of the basin. For the first time, we provide regional hydrochemical data on surface water and groundwater to gain insight into the geochemical processes and quality for drinking and irrigation purposes. We collected 90 samples from surface water (rivers) and groundwater (boreholes) and analysed them for their chemical parameters. We performed a water quality assessment using conventional water quality rating indices for drinking water and irrigation. Cluster and factor analysis were performed on the hydrochemical data to learn the chemical variations in the hydrochemical data. Bivariate ion plots were used to interpret the plausible geochemical processes controlling the composition of dissolved ions in surface water and groundwater. The water quality assessment using Water Quality Index (WQI) revealed that 74% of surface water and 20% of groundwater samples are of poor drinking quality and, therefore, cannot be used for drinking purposes. For irrigation, surface water and groundwater are of good quality based on Sodium Adsorption Ratio (SAR), Wilcox diagram and United States Salinity (USSL) indices. However, Mn and Fe (total) concentrations observed in most surface water samples are above the acceptable limit for irrigation and therefore require treatment to avoid soil acidification and loss of availability of vital soil nutrients. Manganese and iron (total) are identified as the main contaminants affecting the basin's water quality. The hierarchical cluster analysis highlights the heterogeneity in the regional hydrochemical data, which showed three distinct spatial associations based on elevation differences. Groundwater composition chemically evolves from a Ca–HCO_3 to a Na–HCO_3 and finally to a Na–Cl water type along the flow regime from the recharge to the discharge zone. The bivariate ion plot and the factor analysis underscore silicate weathering, carbonate dissolution and ion exchange as the most likely geochemical processes driving the hydrochemical evolution of the Pra Basin groundwater. Going forward, geochemical models should be implemented to elucidate the dominant reaction pathways driving the evolution of groundwater chemistry in the Pra Basin.

3.1 Introduction

One of the components of the United Nations sustainable development goals is ensuring access to quality water and improved sanitation for all (Katila et al. 2019). This has become necessary due to the increasing pollution of large surface water bodies and the complex nature of some aquifers around the world (Fayiga et al. 2018; Groen et al. 1988; Sasakova et al. 2018; Verlicchi and Grillini 2020). The problem of unregulated anthropogenic activities, such as poor agricultural practices, illegal mining and indiscriminate sewage disposal are major causes of water pollution, especially in many parts of Africa. According to the United Nations, more than 80% of human waste is discharged into rivers untreated, and more than 40% of the world's population is affected by water scarcity (Katila et al. 2019). The situation is worst in many

developing countries, such as Ghana. One of the river basins affected by these activities is the Pra Basin in Ghana. Over the past decade, large river networks that provide water to over four million people have been adversely affected by illegal mining activities (Affum et al. 2016; Amonoo-Neizer and Amekor 1993; Armah et al. 2014; Bempah and Ewusi 2016; Golow and Mingle 2003; Tay et al. 2014). This new development has increased dependence on groundwater as the only available alternative source of water supply. Specific uses of the groundwater in the basin include drinking, industrial, animal watering and mechanized irrigation systems that require good quality for their applications. Therefore, determining the geochemical processes that control the evolution of groundwater and its quality is essential (Gao et al. 2019; Ren et al. 2020; Solangi et al. 2019) to ensure sustainable water resource management in the basin.

Groundwater is protected from contamination by anthropogenic pollutants due to the filtering capacity of the overburden material and is therefore usually preferred to surface water (Yidana et al. 2012b). However, the quality may deteriorate depending on the local environmental conditions (Liu et al. 2018; Wang et al. 2014; Zhang et al. 2007). Several factors contribute to changes in groundwater hydrochemistry, including climate, precipitation, mineralogy of the underlying geology with which the water interacts, aquifer properties and topography. These factors contribute to the spatial and temporal changes in the water composition. Understanding the hydrochemical characteristics of groundwater thus provides insight into the mechanisms and geochemical processes that drive groundwater chemical evolution.

In the study area, research on the hydrochemical characterization of surface water and groundwater is very sparse and the few ones that exist (Loh et al. 2021; Loh et al. 2022; Tay et al. 2017) are poorly coordinated to provide a regional overview for better planning and management of the aquifers in the basin. The complexity characterizing the underlying geology and the enormous land-use changes make it very difficult to understand the processes that determine the quality of surface water and groundwater in a regional setting.

Several researchers have used various conventional approaches to assess the quality of water resources for drinking (Ibrahim et al. 2023; Xia et al. 2022; Zhang et al. 2012) and irrigation (Loh et al. 2021; Panneerselvam et al. 2023) purposes. The Water Quality Index (WQI) has been used extensively in various geological terrains to study surface water and groundwater quality for drinking (Loh et al. 2020; Okofo et al. 2021). Others have been employed to study irrigation water quality, including the USSL, %Na and Wilcox diagram (Loh et al. 2021; Panneerselvam et al. 2023; Yidana and Yidana 2010). In the Pra Basin, Loh et al. (2021) used the WQI, %Na, Wilcox and the United States Salinity Level diagram to assess groundwater quality in the Lake Bosumtwi area of the Pra Basin and concluded that the groundwater is of good quality for drinking and irrigation and demonstrated the utility of these approaches in studying water quality in the terrain.

In the present study, major ions and trace metals are used to provide knowledge about spatial variation in surface water and groundwater quality and geochemical processes in the Pra Basin of Ghana. We deduce the important geochemical processes that govern the evolution of groundwater composition in the basin. Here we employed classical methods, including WQI, %Na, USSL and Wilcox diagram, to assess the water quality for drinking and irrigation. Hierarchical cluster analysis (HCA) was used to establish spatial associations within the hydrochemical dataset. Factor analysis was used to reduce the dimensionality of the data to identify the plausible factors driving groundwater chemical evolution.

3.2 Materials and Methods

3.2.1 Location and Physical Setting

The study area (Figure 3.1A) is in the Pra Basin in Ghana (Figure 3.1B,C). It is one of the basins with an established management board set up by the Water Resources Commission (WRC). The study area lies between the Universal Transverse Mercator (UTM) coordinates 30 N 795477m E, 30 N 624441m E and 30 N 553263m N, 30 N 744975m N. The catchment area consists of the Birim and the main Pra rivers. It covers a total area of about 10,703 km^2 (WRC 2012). The rivers are perennial and cross several towns and serve as the main source of water supply for many communities and industries within the basin. However, recent activities, including illegal mining, have rendered many of these rivers undrinkable, making the groundwater resource the most reliable for water supply (Affum et al. 2016; Amonoo-Neizer and Amekor 1993; Armah et al. 2014; Bempah and Ewusi 2016; Golow and Mingle 2003; Tay et al. 2014).

The main economic activities in the study area are mining and agriculture. It is estimated that over 60% of the people are engaged in agriculture (WRC 2012), with cocoa cultivation being the predominant agricultural activity in the region. Large-scale mining activities have been conducted since the 1950s, however, illegal mining has recently increased throughout the basin in search of economic minerals such as gold, bauxite, diamonds, manganese and iron.

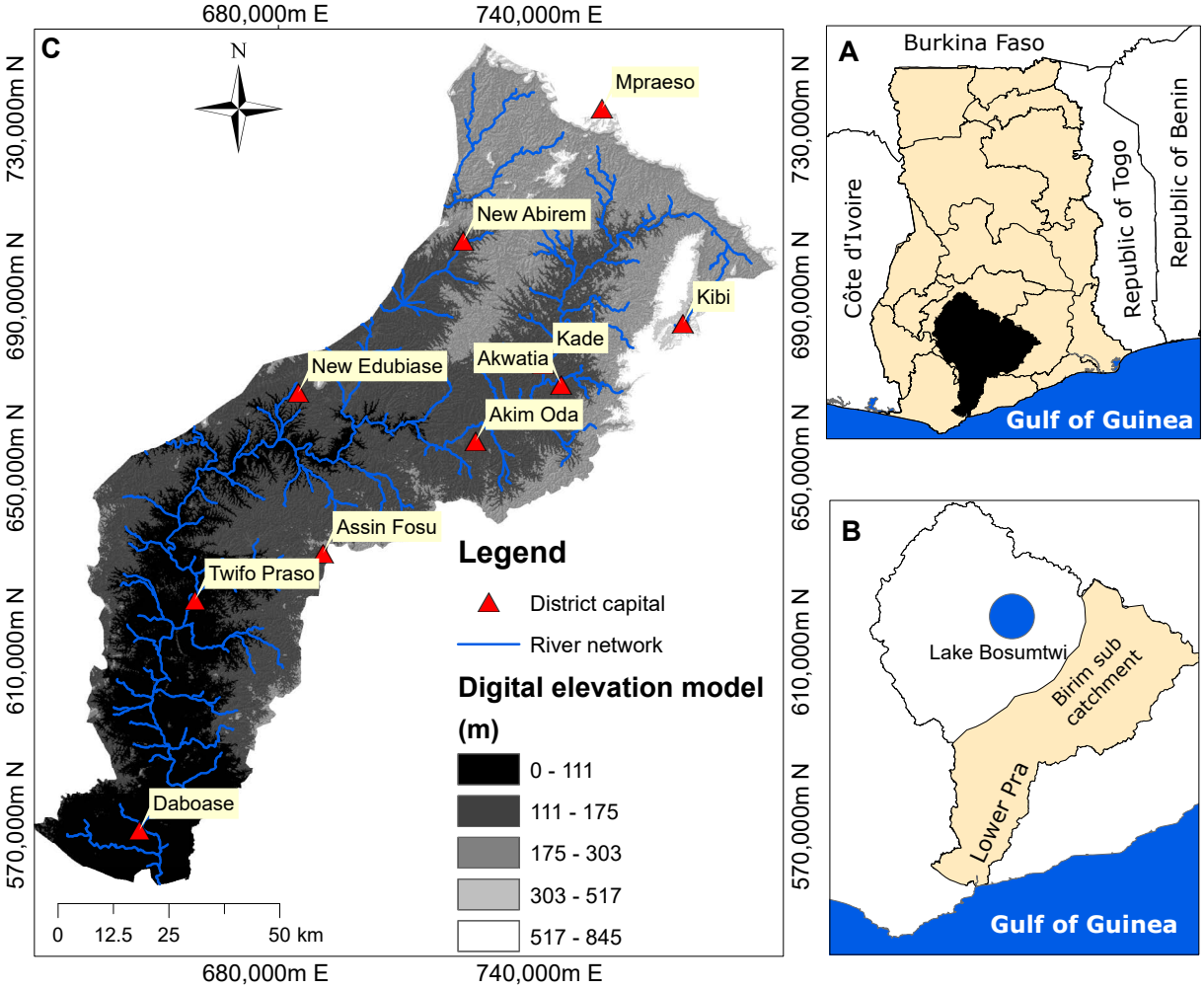

Figure 3.1: The location of the main Pra Basin in Ghana and the international boundaries (**A**), the study area representing the Birim and the Lower Pra catchments of the Pra Basin (**B**), the digital elevation model (DEM) of the study area and the river networks, including some notable districts (**C**).

3.2.2 Geology

The study area consists of two major rock formations, the Birimian Supergroup and the Cape Coast granitoid complex (Figure 3.2). The Birimian underlies the northern area and the Cape Coast granitoid mostly the southern area. There is also the Tarkwain Formation, which is found in a few areas on the eastern and western edges of the study area. The Birimian consists mainly of meta-sediments and includes phyllite, shale and greywacke. On top of the Birimian lies the Tarkwain Formation, which consists of sandstones, conglomerates and argillites. The Cape Coast granitoid is massive and outcrops predominantly in Ghana's southern parts (Kesse 1985; Leube and Hirdes 1986). The Cape Coast type granite comprises quartz, gneiss, foliated biotite and horn–blende–quartz–diorite gneiss (Ganyaglo et al. 2010).

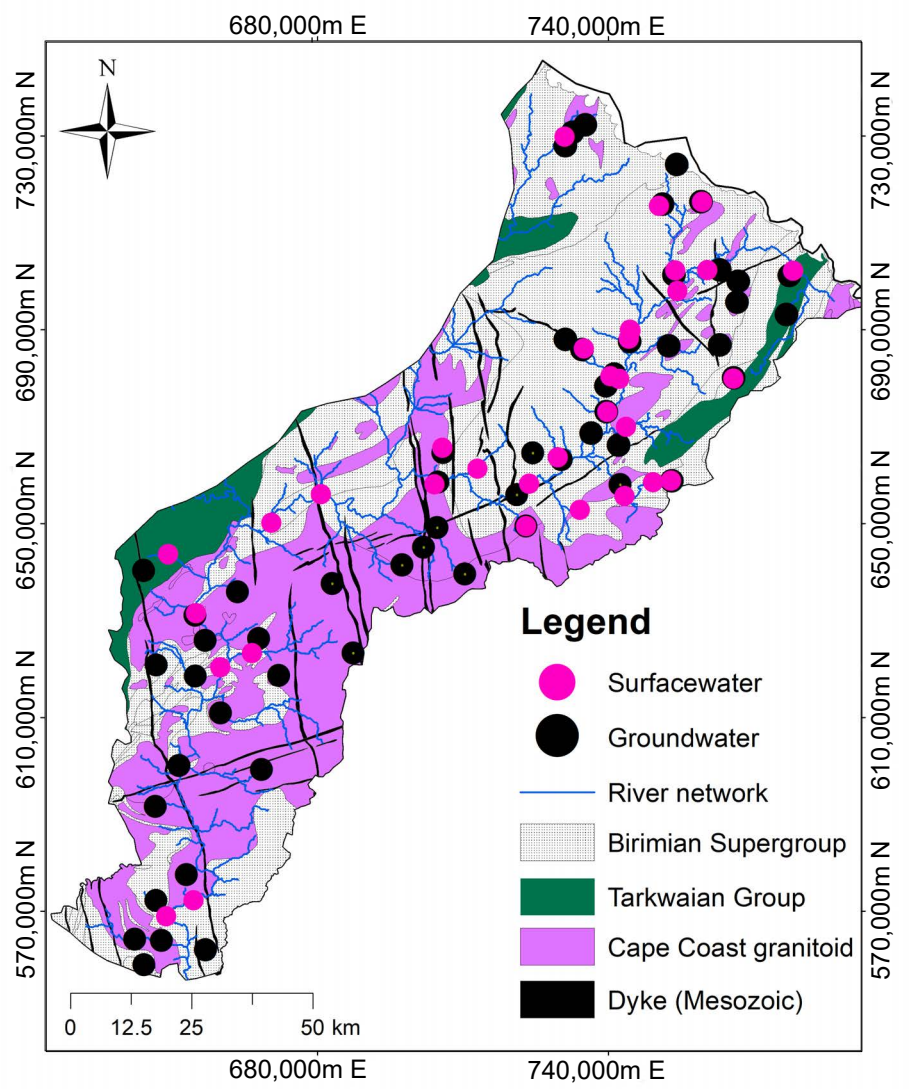

Figure 3.2: Geological map of the study area showing the predominant rock types and the sampling locations. The Birimian Supergroup consist of meta-sediments, mainly phyllite, schists and greywacke. The Tarkwain Group consist of sandstones, conglomerates and argillites, the Cape Coast granitoid of quartz and dioritic gneiss and the Dyke is made of dolerite.

3.2.3 Surface Water and Groundwater Sampling

A total of 90 water samples were taken from rivers (n = 34) and boreholes (n = 56) in the study area. The sampling wells were selected taking into account geology, accessibility and

spatial distribution (Figure 3.2). The sampling was carried out in March 2020. The sampling campaign coincided with the start of the major rainy season, which begins in mid-March and early April. Temperatures during the sampling period ranged from 27 to 30 °C, with a mean of 28 °C. Prior to sampling, the boreholes were first flushed for a minimum of 15 min to remove stagnant water and ensured representative water from the aquifer was reached. A detailed description about materials and sampling procedure are elaborated in Manu et al. (2023e).

3.2.4 Instrumentation and Measurements

The concentrations of cations (Na^+, K^+, Ca^{2+} and Mg^{2+}) and trace metals (Si, Ba, Mn and Fe) were measured by Inductively Coupled Plasma Optical Emission Spectrometry (ICP-OES). The anion concentrations (Cl^-, HCO_3^-, SO_4^{2-}, NO_3^-) were measured by ion chromatography (ICS 3000, Thermo Fisher Scientific) using an AS11 HC column and a conductivity detector. The analytical precision of the ICP-OES and IC was ±5%. Parameters including pH, dissolved oxygen (DO), electrical conductivity (EC) and temperature, were determined in the field using the WTW profiline 3320 series multi-parameter measuring device. Alkalinity (as HCO_3^-)measurements were carried out onsite via HACH digital Titrator Model 16900.

To ensure the reliability of the measurements, duplicate samples of some of the rivers and boreholes were collected, and measurements were conducted to cross-check their corresponding measured samples. The final measurements were subjected to an internal consistency test using percentage charge balance error (CBE). In this study, a CBE < ±3% was achieved and considered sufficient.

3.2.5 Computation of Water Quality Indices

The sodium adsorption ratio (SAR) and the water quality index (WQI) were calculated from the hydrochemical data to assess the quality of the water for irrigation and drinking purposes. A total of 11 chemical parameters including Na^+, K^+, Ca^{2+}, Mg^{2+}, Cl^-, HCO_3^-, SO_4^{2-}, NO_3^-, Ba, Mn and Fe (total) were used to calculate the WQI of the water samples. The computation of the WQI involved four steps (Sahu and Sikdar 2008). In the first step, all chemical parameters were assigned weights (wi) according to their negative impact on human health with reference to the WHO guideline protocol for drinking water (WHO 2017). In step two, the relative weight ($W_i = w_i / \sum w_i$) of each parameter was calculated. The WHO standard for the parameters in drinking water (WHO 2017), their assigned weights and calculated relative weights are presented in Table 3.1. Step 3 involved calculating the quality rating scale (qi), as shown in Equation (3.1):

$$q_i = \frac{C_i}{S_i} \times 100 \tag{3.1}$$

where q_i, C_i and S_i are the quality rating value, the concentration of each parameter and the WHO standard values of each parameter, respectively. Finally, the WQI was computed using Equation (3.2):

$$WQI = \sum W_i \times q_i \tag{3.2}$$

The WQI classification scheme by Sahu and Sikdar (2008) was used to interpret the threshold values acceptable for drinking purposes. The drinking water classification scheme includes excellent water (WQI < 50), good water (WQI between 50 and 100), poor water (WQI

between 100 and 200), very poor water (WQI between 200 and 300) and not unsuitable for drinking (WQI > 300).

Table 3.1: List of parameters used to calculate the WQI, their standard drinking water reference values (WHO 2017), for drinking water, assigned weights (w_i) and relative weights (W_i). Note: All concentrations are in mg/L except pH

Parameter	Standard	Weight (w_i)	Relative Weight (W_i)
pH	7.5	4	0.138
Na^+	200	2	0.069
Ca^{2+}	200	2	0.069
Mg^{2+}	150	2	0.069
Cl^-	250	3	0.103
SO_4^{2-}	250	3	0.103
NO_3^-	10	5	0.172
Mn	0.1	3	0.103
Fe	0.3	3	0.103
Ba	1.3	2	0.069
Total		29	1.0

The SAR was calculated using the equation proposed by Allison and Richards (1954) and Hem (1985) which is contained in Equation (3.3):

$$\mathrm{SAR} = \frac{\mathrm{Na^+}}{\sqrt{\frac{\mathrm{Ca^{2+}+Mg^{2+}}}{2}}} \tag{3.3}$$

Ion concentration in meq/L was adopted for the calculation.

The Wilcox plot was generated by plotting EC vs. $\%Na^+$. The $\%Na^+$ was calculated using Equation (3.4):

$$\%\mathrm{Na^+} = \frac{\mathrm{Na^+ + K^+}}{\mathrm{Ca^{2+} + Mg^{2+} + Na^+ + K^+}} \times 100 \tag{3.4}$$

All ion concentrations are expressed in meq/L.

The USSL diagram was created by plotting the EC against the SAR. The interpretation of irrigation quality from the USSL was based on four classifications, categorized as low, medium, high and very high salinity levels. Water samples falling within the low and medium salinity areas in the plot are considered excellent to good for irrigation.

The chloro–alkali indices were used to study the occurrence of cation exchange in groundwater. Schoeller (1965) proposed two chloro–alkali indices, CAI-I and CAI-II, to assess the presence of such processes in groundwater. The two indices are calculated using Equations (3.5) and (3.6), respectively:

$$\mathrm{CAI-I} = \frac{\mathrm{Cl^- - (Na^+ + K^+)}}{\mathrm{Cl^-}} \tag{3.5}$$

$$\mathrm{CAI-II} = \frac{\mathrm{Cl^- - (Na^+ + K^+)}}{\mathrm{CO_3^{2-} + SO_4^{2-} + HCO_3^- + NO_3^-}} \tag{3.6}$$

All ion concentrations are taken in meq/L. The chloro–alkali indices < 0 indicate the occurrence of cation exchange and > 0 emphasize reverse ion exchange.

3.2.6 Cluster Analysis of the Groundwater Hydrochemical Data

The groundwater hydrochemical data were subjected to multivariate statistical analysis to learn about the spatial associations and factors controlling groundwater chemistry. The data were logarithmically transformed and standardized to their respective z-scores to ensure that all hydrochemical data met the requirements of normal distribution. Factor analysis with the principal component as the extraction criterion was applied to the transformed data (z-scores) to reduce the data in order to establish the relationship between the variables. To optimize the variations between the variables, we used the varimax rotation method to ensure that the data are uncorrelated. The Kaiser Criterion (Kaiser 1960) was applied to remove components that do not provide unique processes in the hydrochemistry. Factors that loaded communalities < 0.5 were excluded from the analysis and the process repeated. The reason for this is that variables that load communalities < 0.5 do not show much influence among generated principal components and, therefore contribute only marginally to the factor model (Yidana et al. 2020).

The hierarchical cluster analysis (HCA) was used to partition the hydrochemical data based on their spatial correlation. Here all the standardized (z-score) hydrochemical parameters, including pH, Na^+, K^+, Ca^{2+}, Mg^{2+}, Cl^-, HCO_3^-, SO_4^{2-}, NO_3^-, Ba, Mn and Fe (total) were included in the HCA. The Statistical Package for Social Science, IBM SPSS Statistics v20 (Statistics 2013) was used for all the statistical analysis. The Squared Euclidean Distance was chosen as the similarity/dissimilarity determinant to partition the data into their respective groupings and subsequently regrouped using the Ward's agglomeration method (Güler and Thyne 2004; Ward Jr 1963). Determining the number of clusters in the HCA analysis is a semi-objective process and requires knowledge of the underlying geological, hydrogeological and prevailing environmental conditions (Loh et al. 2020; Yidana et al. 2020). The output of the number of clusters depends on the position of the critical linkage distance on the dendrogram. It is always a good practice to choose an appropriate linkage distance so as not to generate too many or too few groupings in order not to complicate interpretation or to omit certain important hydrochemical processes. In our case, a linkage distance of 3.5 was chosen and resulted in three clusters. The samples under each cluster and their positions were then plotted and used as the basis to understand the groundwater chemical evolution along the flow regime.

3.3 Results

Overall, the hydrochemical data of the surface water and groundwater samples show large variations across the entire dataset. During the field campaign, we found that most of the surface water samples were turbid with a brownish color mainly due to the impact of illegal mining. All wells sampled are public wells that are active and serve as the main water supply for the communities in the catchment area, however, the quality of the samples is not checked regularly. Information on the historical drill hole logs, including the quality report and drill depths for some of the wells is not available. The hydrochemical data and details about the field and laboratory measurements can be found in Manu et al. (2023e).

3.3.1 Surface Water Chemistry

Figure 3.3a shows the variation in the major ions and trace metal composition of the surface water samples. As can be seen, the order of cation and anion abundance is $Na^+ > Ca^{2+} > K^+ > Mg^{2+}$ and $HCO_3^- > Cl^- > SO_4^{2-} > NO_3^-$, respectively. We have observed that the cations show relatively less variability than the anions. The largest variability in the hydrochemical data is associated with NO_3^- and SO_4^{2-}. The pH of surface water is generally mildly acidic to alkaline with a mean and standard deviation of 7.3 and $\pm$0.3, respectively. The electrical conductivity ranges from 18 to 607 µS/cm with a mean and standard deviation of 157 µS/cm and $\pm$101 µS/cm, respectively. The temperature is less variable and ranges from 28 to 32 °C with a mean and standard deviation of 28.5 °C and $\pm$1.4 °C, respectively. The dissolved oxygen (DO) ranges between 0.3 mg/L and 2.1 mg/L with a mean and a standard deviation of 1.5 mg/L and $\pm$0.5 mg/L, respectively. For trace metals, Fe (total) concentration was relatively higher than that of the Mn. The highest Fe (total) concentration occurs in the southern areas, while the northern areas have high Mn concentrations.

3.3.2 Groundwater Chemistry

Figure 3.3b shows the statistical summary of groundwater chemical composition. The pH of the groundwater is generally acidic to neutral and shows homogeneity in its data set. The order of cation abundance is $Na^+ > Ca^{2+} > Mg^{2+} > K^+$ while that of the anions is $HCO_3^- > Cl^- > NO_3^- > SO_4^{2-}$. Among the major ions, NO_3^- and SO_4^{2-} show the greatest variability in their concentrations. For the trace metals, the Mn concentration is relatively higher than that of Fe (total), with both parameters exhibiting large variations. We observed a significant number of the groundwater samples with measured Fe (total) concentrations below the detection limit. The dissolved oxygen ranges from 0.4 to 2.8 mg/L with a mean and standard deviation of 1.2 mg/L and $\pm$0.5 mg/L, respectively. As for the physical parameters, the temperature ranges from 27 to 31 °C with an average and standard deviation of 28.5 °C and $\pm$1.2 °C, respectively. The electrical conductivity ranges from 33 to 795 µS/cm with a mean and standard deviation of 239.0 µS/cm and $\pm$164 µS/cm, respectively. The highest EC values are associated with the samples in the southern areas, while the northern areas are characteristically low.

3.3.3 Calculation of Surface Water Quality Indices for Drinking and Irrigation

Figure 3.4a shows the spatial distribution of the calculated surface water quality index (WQI). As can be seen, 25 out of 34, representing 74% of the surface water samples, had WQI > 100 and are classified as poor to unsuitable for drinking. Surface water samples from the northern area are influenced by Mn, while Fe (total) influences samples in the central and southern areas. Our analyses show that all major ion concentrations are well within the WHO standard limits for drinking water. However, we find that the Fe (total) concentration in 27 out of 34 samples exceeds the WHO limit of 0.3 mg/L Fe (total) in drinking water, while the Mn concentration in 15 out of 35 samples exceeds the acceptable limit of 0.1 mg/L. The surface water quality is significantly influenced by the high Mn and Fe (total) contents in the surface water samples.

For irrigation purposes, the water quality indices SAR, USSL and the Wilcox diagram show good to excellent surface water quality. Figure 3.4b shows the spatial distribution of the calculated SAR, which is broadly within the acceptable limit of SAR < 10 for irrigation water.

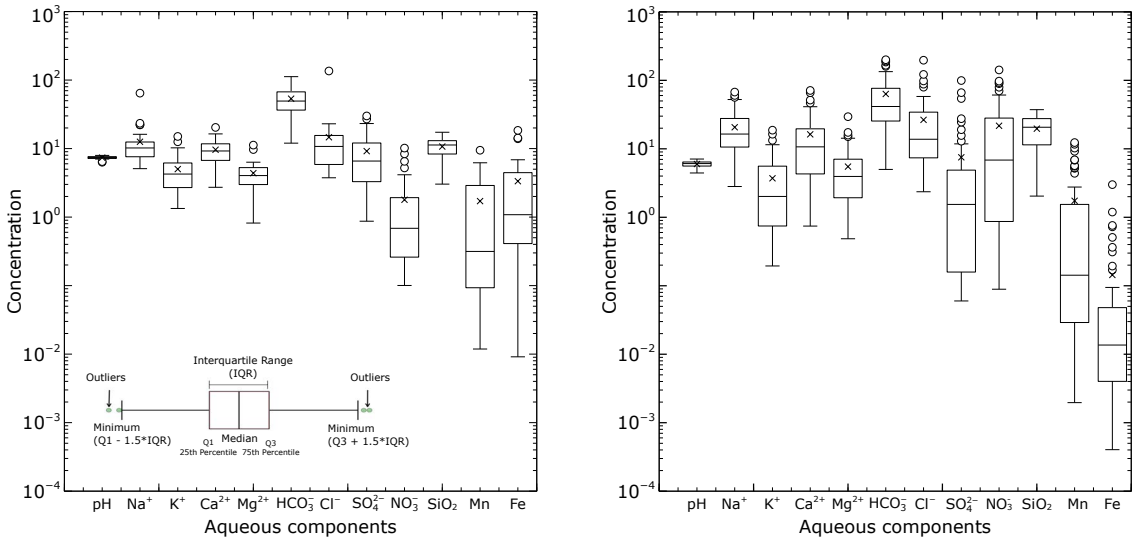

Figure 3.3: The box- and-whisker plots show the relative abundance of major ions, trace metals and silica in surface water (**a**) and groundwater (**b**). The horizontal solid line and the x symbol on the box-and-whisker plot represent the average and the median concentrations, respectively. Outliers are defined by points that fall more than 1.5*IQR above the third quartile or below the first quartile. All the ion concentrations are measured in mg/L except pH.

We see from Figure 3.5a that 32 out of 34 samples fall into the C1 S1 (low salinity, low sodicity) category of irrigation water. Only three samples fall into the C2 S1 category (medium salinity, low sodicity). Based on the Wilcox classification (Figure 3.5b), we find all surface water samples in the excellent to good irrigation water category.

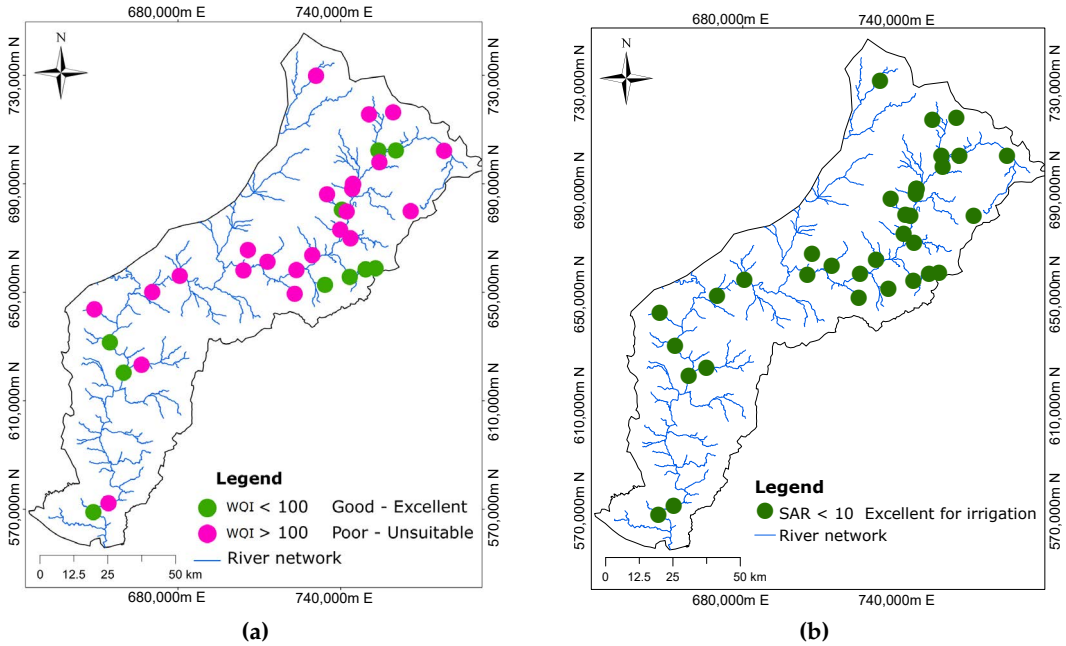

Figure 3.4: Surface water spatial distribution maps of (**a**) Water Quality Index (WQI) and (**b**) Sodium Adsorption Ratio (SAR) for the assessment of water quality for drinking and irrigation purposes

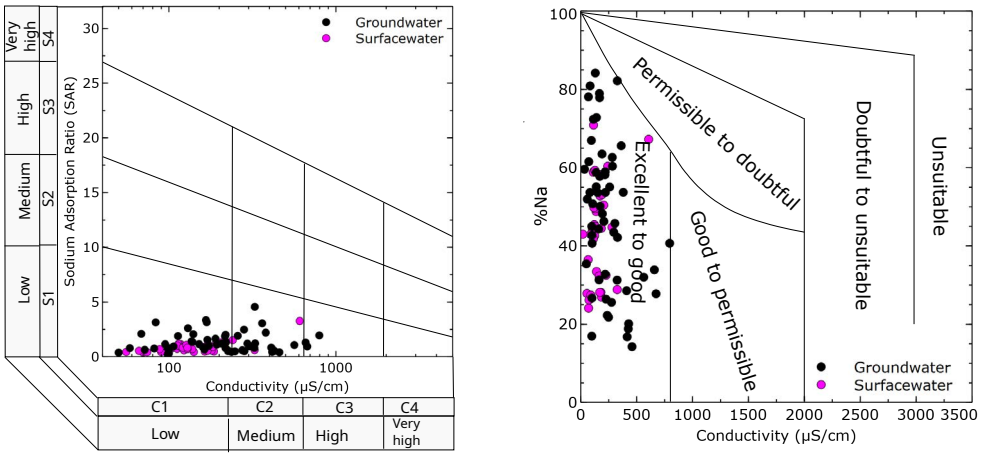

(a) **(b)**

Figure 3.5: Irrigation water classification diagrams showing surface water and groundwater quality acceptable for irrigation (**a**) USSL classification (Allison and Richards 1954) and (**b**) Wilcox classification (Wilcox 1955)

3.3.4 Calculation of Groundwater Quality Indices for Drinking and Irrigation

Figure 3.6a shows the spatial distribution of the WQI used to assess the drinking water quality of the groundwater. As can be seen, a total of 44 out of 56 groundwater samples had a WQI < 100 and fall into the category of good to excellent drinking water. However, twelve samples showed a WQI > 100 and fall into the poor to unsuitable category. Eleven of the samples classified as poor to unsuitable are located in the northern areas of the basin. We find that all major ion concentrations including Na^+, K^+, Ca^{2+}, Mg^{2+}, Cl^-, HCO_3^-, SO_4^{2-} and NO_3^- are well within the limits of the WHO drinking water guidelines (WHO 2017), with the exception of eight samples where NO_3^- exceeded the acceptable limit of 50 mg/L nitrate in drinking water. For trace metals, the Fe (total) concentration in most groundwater samples (50 out of 56) is within the WHO acceptable drinking limit of 0.3 mg/L, while 6 samples were above it. The Mn concentration in twenty samples exceeded the WHO value of 0.4 mg/L Mn in drinking water. All samples with the high Mn concentration are located in the northern parts of the basin.

For irrigation quality assesment, the SAR, USSL and Wilcox diagram show that all groundwater samples fall into the good to excellent irrigation water category. The spatial distribution of the calculated SAR is shown in Figure 3.6b. We see that all groundwater samples have a SAR > 10 and above in the good to excellent irrigation water category. Figure 3.5a shows the distribution of the samples in the USSL diagram. Almost all the groundwater samples are within the the C1 S1 (low salinity—low sodicity) and C2 S2 (medium salinity—low sodicity) categories of irrigation water. Three samples plot within the C3 S1 area representing a high salinity—low sodicity water. Figure 3.5b shows the distribution of the groundwater samples on the Wilcox plot and highlights that all the samples fall in the category of excellent to good quality irrigation water with an electrical conductivity less than 1000 µS/cm.

3.3.5 Hierarchical Cluster Analysis (HCA) of the Groundwater Hydrochemical Data

HCA performed on the groundwater chemical data revealed three clusters that do not show a clear pattern (Figure 3.7A), underscoring that the hydrochemical environment

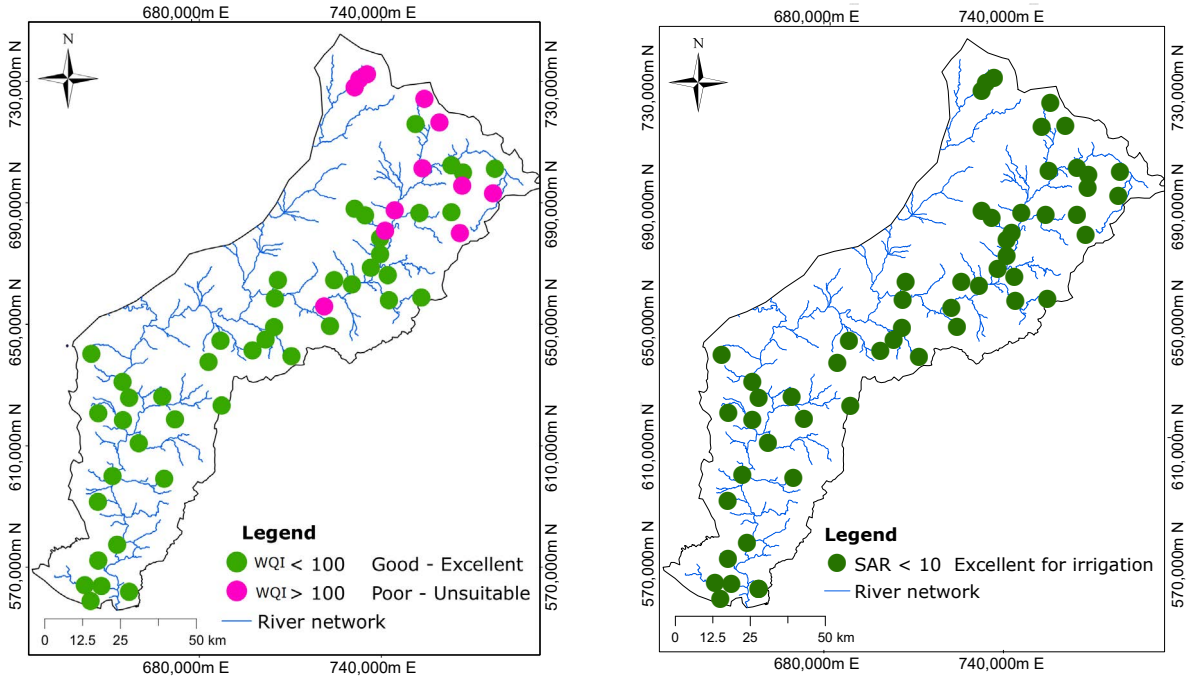

Figure 3.6: Groundwater spatial distribution maps of (**a**) Water Quality Index (WQI) and (**b**) Sodium Adsorption Ratio (SAR) for the assessment of water quality for drinking and irrigation purposes.

is heterogeneous at the basin scale. Here we see that the water compositions are variable across the two major lithologies. The spatial association in hydrochemistry is not identifiable based on the underlying geology.

However, HCA provides three distinct spatial associations, taking into account elevation (Figure 3.7B), consistent with general groundwater flow under the influence of topography. Based on elevation, we see that the northern zone samples are at higher elevations, the central zone is at intermediate, and the southern zone is at lower elevations. These three zonations were defined to facilitate the interpretation of the hydrochemical dataset, which is variable at the basin scale.

3.3.6 Groundwater Chemical Variation Within the Three Defined Zones

Groundwater chemistry exhibits large variability in chemical composition, with the largest variability observed in samples from the southern zone of the area. Figure 3.8a,b shows the box-and-whisker plot of the physical and chemical parameters in the groundwater for the three zones, respectively. The northern zone has the widest spread and variability in pH with an estimated standard deviation of ± 0.74. The southern zone recorded the highest variability in the electrical conductivity with an estimated standard deviation of ± 196 µS/cm. From Figure 3.8a, the groundwater of the northern and southern zones has the widest spread in dissolved oxygen (DO) and exhibits mixed reducing conditions. The central zone has the lowest deviation in DO and exhibits oxic conditions in most groundwater samples.

Our results indicate that Na^+, Ca^{2+} and HCO_3^- are the abundant ions in groundwater. The order of cation occurrence in the northern zone is $Ca^{2+} > Na^+ > Mg^{2+} > K^+$, the central zone is $Na^+ > Ca^{2+} > Mg^{2+} > K^+$ and the southern zone is $Na^+ > Ca^{2+} > Mg^{2+} > K^+$ (Figure 3.8b). For

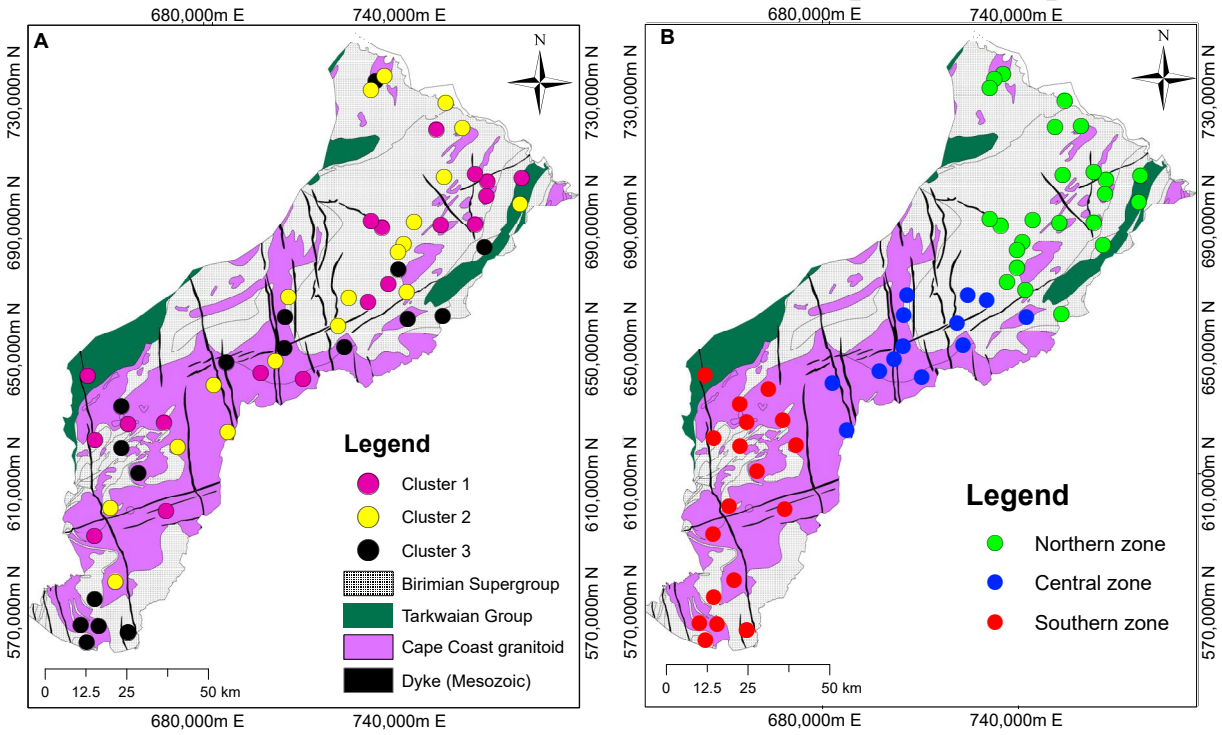

Figure 3.7: Hierarchical cluster analysis (HCA) of the hydrochemical dataset. (**A**) Taking into account only hydrochemical data, three clusters are identified with no apparent geographical proximity, highlighting large variability across the basin. (**B**) Considering elevation for the HCA, three spatially distinct clusters appear, dividing the basin into three zones: northern, central and southern. The elevation is highest in the northern zone and decreases towards the southern zone.

anions (Figure 3.9), the order of abundance is $HCO_3^- > NO_3^- > Cl^- > SO_4^{2-}$ (northern zone), $HCO_3^- > Cl^- > NO_3^- > SO_4^{2-}$ (central zone) and $Cl^- > HCO_3^- > NO_3^- > SO_4^{2-}$ (southern zone). In the northern zone, Ca^{2+} and Na^+ account for about 80% of the total cation concentrations, while HCO_3^- accounts for 65% of the total anion concentrations. In the central zone, Ca^{2+} and Na^+ contribute about 80% of the total cations, with HCO_3^- and Cl^- account for 57% and 24% of the total anions. In the southern zone, Na^+ contributes about 50% while Ca^{2+} accounts for 30% of the cations. Anions in the southern zone consist of 37% HCO_3^-, 32% Cl^- and 20% NO_3^-. All three zones show very low concentrations of K^+ and SO_4^{2-}.

Table 3.2 shows the results of selected correlation coefficients between the hydrochemical parameters in the groundwater and highlights relationships between them. They were tested at a significance level of $p < 0.05$ with $r > 0.7$ and $r < 0.5$ indicating strong and weak correlations (Okofo et al. 2021; Wang 2014), respectively. In the northern zone groundwater samples, there is a strong positive correlation between pH and HCO_3^-, EC and Ca^{2+}, EC and HCO_3^-, Ca^{2+} and HCO_3^- and Na^+ and Cl^-. In the central zone, there is a strong correlation between pH and SiO_4, pH and Ca^{2+}, EC and Ca^{2+}, Ca^{2+} and Cl^-, and Na^+ and Mg^{2+}. The southern zone also shows a strong positive correlation between pH and HCO_3^-, EC and Ca^{2+}, EC and Na^+, EC and Cl^-, Ca^{2+} and Cl^- and Na^+ and Cl^-. These correlations show that several factors combine in the evolution of hydrochemical parameters in the groundwater and provide a potential source for them. Within these relationships, Ca^{2+}, Na^+, Cl^- and HCO_3^- contribute significantly to the EC in groundwater.

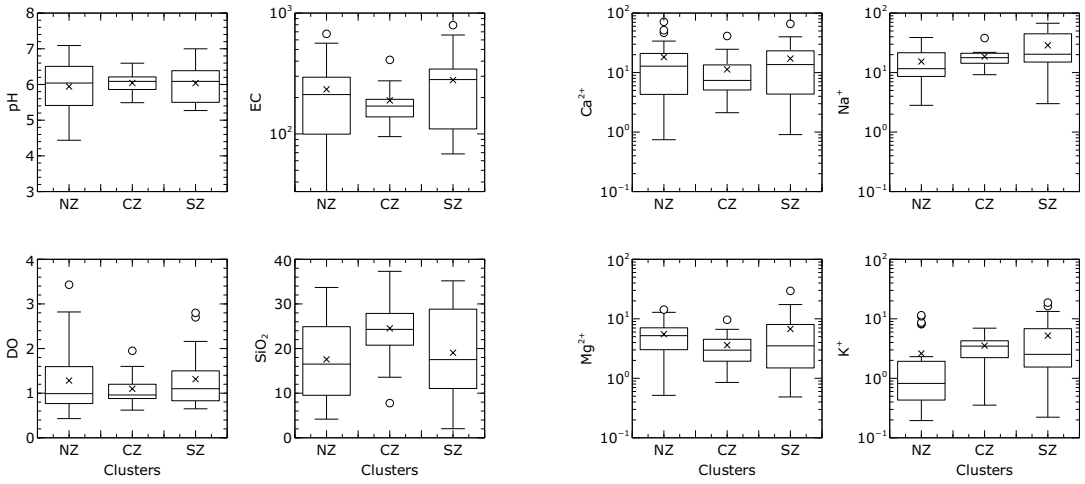

Figure 3.8: Box-and-whisker plots displaying the variations in the (**a**) physical parameters and silica content, and (**b**) major cations in the groundwater. The interpretation of the box-and-whisker plots follows the legend presented in Figure 3.3. The horizontal solid line and the x symbol on the box-and-whisker plot represents the average and the median concentrations, respectively. Outliers are defined by points that fall more than 1.5*IQR above the third quartile or below the first quartile. NZ, CZ and SZ denote the northern zone, central zone and southern zone, respectively. All chemical parameters are measured in mg/L except for pH and EC µS/cm.

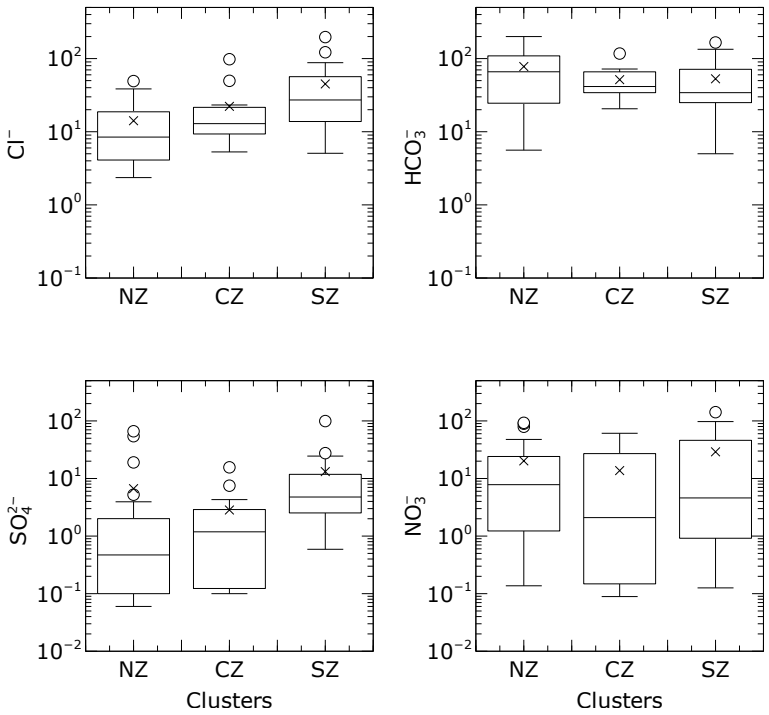

Figure 3.9: Box-and-whisker plots highlighting the variations in the major anions (HCO_3^-, Cl^-, SO_4^{2-} and NO_3^-) in groundwater for the three identified zones. The horizontal solid line and the x symbol on the box-and-whisker plot represents the average and the median concentrations, respectively. Outliers are defined by points that fall more than 1.5*IQR above the third quartile or below the first quartile. NZ, CZ and SZ denote the northern zone, central zone and southern zone, respectively. All chemical parameters are measured in mg/L.

Table 3.2: Correlation coefficients between the hydrochemical parameters in the groundwater, highlighting the relationships between them. They were tested at a significance level of $p < 0.05$ with $r > 0.7$ and $r < 0.5$ indicating stronger and weaker correlations (Okofo et al. 2021; Wang 2014), respectively. Only the correlations with r-values > 0.7 are considered significant and presented here.

Zone	pH-HCO_3^-	pH-SiO_2	pH-Ca^{2+}	EC-Ca^{2+}	EC-Na^+	EC- Cl^-	EC-HCO_3^-	Ca^{2+}-HCO_3^-	Ca^{2+}-Cl^-	Na^+-Cl^-	Na^+-Mg^{2+}
Northern	0.70	-	-	0.93	-	-	0.87	0.87	-	0.88	-
Central	-	0.80	0.75	0.96	-	-	-	-	0.76	-	0.73
Southern	0.79	-	-	0.92	0.72	0.88	-	-	0.76	0.84	-

3.3.7 Groundwater Types

The hydrochemical plot using the trilinear Piper diagram (Piper 1944) shows variable water composition throughout the study area. A qualitative examination of the Piper diagram (Figure 3.10) shows that the samples from the southern zone are the most widespread and have the most diverse water composition. In the northern zone, 21 out of 25 samples are of Ca-HCO_3 water type, while 4 samples have mixed water compositions. Looking at the central zone, 8 out of 13 samples show a mixed water type dominated by Na-HCO_3. The southern zone exhibits a Na–Cl-dominant composition.

We observe from Figure 3.10 that in the northern zone, the alkaline earth metals (Ca^{2+} and Mg^{2+}) exceed the alkalis (Na^+ and K^+) while in the central zone the alkalis dominate the alkaline earth metals. The southern zone shows the dominance of the alkalis over the alkaline earth metals.

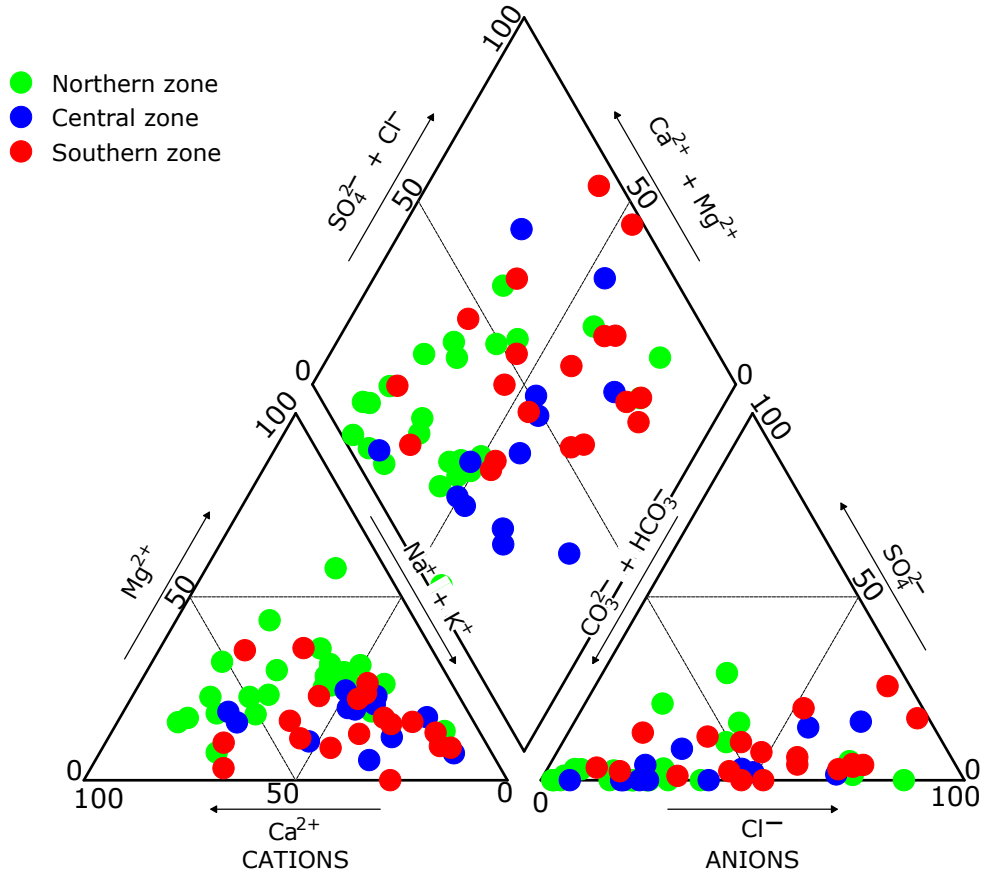

Figure 3.10: Piper diagram presenting the dominant ion species in the groundwater.

3.3.8 Mineral Weathering Processes

Figure 3.11 shows the results from the Gibbs diagram and underlines that the interaction between water and rock is the main mechanism driving the hydrochemistry in the study area. The plot of $Na^+/(Ca^{2+} + Na^+)$ and $Cl^-/(Cl^- + HCO_3^-)$ ratios expressed as meq/L vs. TDS (mg/L) show that most of the samples plot in the rock dominance region, indicating the anion and cation composition of groundwater is derived from weathering processes.

We observe that the groundwater chemistry is driven by a higher $Na^+/(Ca^{2+} + Na^+)$ ratio as a significant number of the points fall on the right side of the plot. The points distribution in the $Cl^-/(Cl^- + HCO_3^-)$ vs. TDS shows an increase in Cl^- relative to HCO_3^- along the flow regime from the north to the south of the basin.

Figure 3.12 shows the binary ion plots of the hydrochemical data and highlights the potential geochemical processes driving groundwater chemistry, including silicate weathering and cation exchange processes. The Na^+ vs. Cl^- plot (Figure 3.12a) shows that 19 of 24 samples from the northern zone, all 13 samples from the central zone and 14 of 19 samples from the southern zone plot in the silicate mineral weathering area. From the chloro–alkaline indices plot (Figure 3.12b), we found that almost all the groundwater samples except seven have negative choloro–alkaline indices values, which are dominantly distributed in the ion exchange area. We observed that one sample from the northern and four from the southern zone are plotted in the reverse ion exchange region. The HCO_3^- vs. Ca^{2+} plot (Figure 3.12c) shows the majority of the samples below the 1:1 line, emphasizing the excess of HCO_3^- over Ca^{2+}.

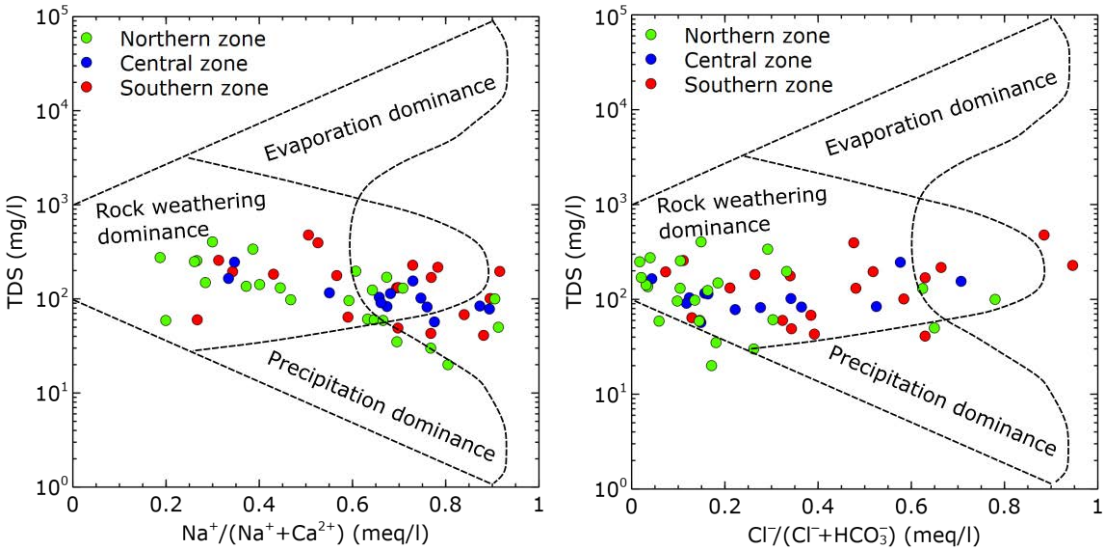

Figure 3.11: Gibbs diagram for groundwater samples used to determine the main controls of water chemistry highlight rock weathering as the main mechanism controlling groundwater chemistry in the Pra Basin.

3.3.9 Factor Analysis

Four factor models were generated, including each of the three zones (northern, central and southern) and the combined dataset with factor scores showing significant correlations explaining the variation in the groundwater chemical composition. In the northern zone, two factors accounted for 78% of the total variation in the dataset as presented in Table 3.3. Factor 1 explained 40% of the variance and loaded positively with pH, Ca^{2+}, HCO_3^- and SiO_2, while Factor 2 loaded significantly with Na^+, Cl^- and SO_4^{2-} and explained about 37% of the total

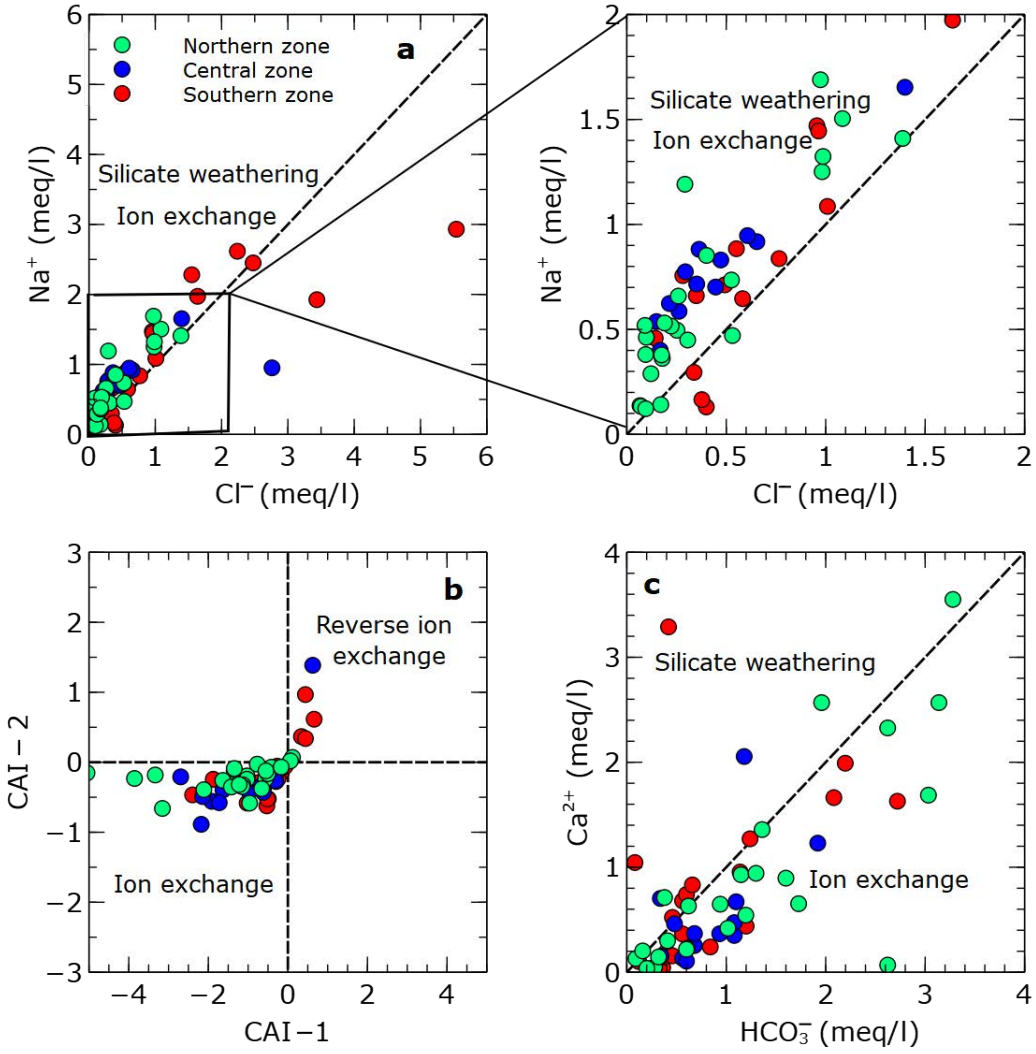

Figure 3.12: Bi-variate ion plots showing the most probable geochemical processes, including silicate weathering (a), and ion exchange (b and c) in the groundwater system.

variation (Table 3.3). Here, Ca^{2+}, HCO_3^- and pH have the highest factor scores and thus have the relatively strongest influence among other parameters.

The central zone produced three factor scores, explaining about 86% of the variance in the hydrochemical data. The extracted factor model is presented in Table 3.3. Out of this Factor 1 and Factor 2 explained 35% and 34% of the variation, while Factor 3 explained 17% of the variation (Table 3.3). There is no clear identification of dominant process(es) influencing groundwater chemistry in the central zone.

In the southern zone, two factors scores explained approximately 80% of the total variance in the hydrochemistry (Table 3.3). Factor 1 explained about 53% of the total variance and was positively loaded with Na^+, K^+, Mg^{2+}, Cl^- and SO_4^{2-}, with Na^+ and Cl^- providing the highest factor scores (Table 3.3). Factor 2 explained 27% and loaded positively with pH and HCO_3^-.

Between the individual factor models, the northern zone is characterized by the dominance of Ca^{2+}, HCO_3^- and pH, the southern zone is dominated by Na^+ and Cl^- according to the factor scores. There is no dominant factor to explain the hydrochemical variation in the central zone. The central zone showed no dominance of ionic species and presented the highest number of factor models highlighting the influence of different processes on the hydrochemistry.

Table 3.3: Rotated Component Matrix (Extraction method: Principal component Analysis, Rotation Method: Varimax with Kaiser Normalization) generated from the factor analysis explaining significant relationships between the hydrochemical parameters. The dash symbols (-) indicate that the parameter loaded a communality less than 0.5 and was deemed statistically insignificant and thus was not considered for the factor analysis.

Northern Zone (n = 24)	pH	Na^+	K^+	Ca^{2+}	Mg^{2+}	HCO_3^-	Cl^-	SO_4^{2-}	SiO_2	% of Variance	Cumulative %
Fact 1	**0.958**	0.155	0.006	**0.845**	-	**0.904**	0.051	0.427	**0.776**	40.773	40.773
Fact 2	0.011	**0.901**	**0.799**	0.453	-	−0.021	**0.938**	**0.666**	0.189	37.702	78.475
Central Zone (n = 13)	**pH**	**Na^+**	**K^+**	**Ca^{2+}**	**Mg^{2+}**	**HCO_3^-**	**Cl^-**	**SO_4^{2-}**	**SiO_2**	**% of Variance**	**Cumulative %**
Fact 1	**0.922**	−0.126	−0.009	**0.719**	0.188	**0.767**	0.025	−0.336	**0.897**	34.773	34.773
Fact 2	−0.247	**0.839**	0.166	0.575	**0.818**	−0.285	**0.874**	**0.711**	−0.043	33.589	68.362
Fact 3	0.052	0.36	**0.952**	−0.318	−0.318	−0.453	0.226	0.423	0.226	17.518	85.880
Southern Zone (n = 19)	**pH**	**Na^+**	**K^+**	**Ca^{2+}**	**Mg^{2+}**	**HCO_3^-**	**Cl^-**	**SO_4^{2-}**	**SiO_2**	**% of Variance**	**Cumulative %**
Fact 1	−0.13	**0.899**	**0.785**	-	**0.896**	0.033	**0.926**	**0.760**	-	52.57	52.57
Fact 2	**0.947**	−0.048	0.248	-	0.231	**0.932**	−0.116	0.120	-	27.30	79.87
Combined (n = 56)	**pH**	**Na^+**	**K^+**	**Ca^{2+}**	**Mg^{2+}**	**HCO_3^-**	**Cl^-**	**SO_4^{2-}**	**SiO_2**	**% of Variance**	**Cumulative %**
Fact 1	−0.060	**0.898**	**0.789**	0.445	-	−0.164	**0.932**	**0.770**	0.294	40.043	40.043
Fact 2	**0.927**	0.141	0.084	**0.805**	-	**0.902**	0.018	0.185	**0.710**	36.054	76.097

The factor analysis performed on the combined dataset resulted in two factor models accounting for 76% of the total variance in the hydrochemical dataset. Factor 1 loaded positively with Na^+, K^+, Cl^- and SO_4^{2-} (Table 3.3) and explained 40% of the variation. Factor 2 explained 36% of the variance and loaded positively with pH, Ca^{2+}, HCO_3^- and S^{4+}. The correlations between the parameters indicate different processes that control the hydrochemistry of the groundwater. The factor model of the combined data set presented the lowest cumulative percentage of variation and brings to bare the heterogeneity in the basin scale data set.

3.4 Discussion

3.4.1 Sampling and Measurements

A total of 90 water samples from surface water (n = 34) and groundwater (n = 56) were successfully analyzed for their chemical parameters. This is the first time such a comprehensive regional-scale hydrochemical study has been conducted in the Pra Basin before and after the ban on illegal mining activities. In general, common practice assumes that the cations and anions, which are the main chemical constituents in groundwater, must fall within the range of at least ±5% of each other (Appelo and Postma 2004; Drever et al. 1988). In this study, the charge balance error (CBE) performed on the chemical data showed that most of the samples fell below ±3%, reflecting good data quality. On the basis of the internal consistency check, the presented hydrochemical data of the surface water and groundwater is considered representative of the field conditions and thus can be used for further analysis.

3.4.2 Assessment of Surface Water Quality for Drinking and Irrigation

The surface water in the Pra Basin is of poor quality for drinking, supposedly due to the illegal mining activities in the area. Our analysis shows that Mn and Fe (total) are the two pollutants affecting surface water quality. To our knowledge, the high concentrations of Mn and Fe (total) might be facilitated by illegal mining involving underground excavation, digging and washing in the rivers in search of mineral resources. In the study area, the saprolite and the duricrust overlying the bedrock contain minerals of pyrite, iron oxides and Mn-rich sediments

(Manu et al. 2013). When exposed to water, these minerals dissolve, releasing Mn and Fe (total) into the water and increasing their concentration in surface water.

Our results agree broadly with the results of Bessah et al. (2021) who studied the surface water quality of the Pra Basin. In their study, the authors sampled surface water from 25 rivers in the Pra Basin and showed that 80% of the samples had Fe (total) concentrations above the WHO standard in drinking water. They found high concentrations of Cu, Hg, As and Fe (total), above the acceptable levels for drinking water. The presence of mercury in the surface waters of the Pra Basin has been attributed to illegal mining activities where the use of mercury to extract gold is common. Darko et al. (2021) also reported turbidity in some nearby rivers ranging from 12 to 4645 NTU, which is above the acceptable limits of 5 NTU in surface water bodies (Darko et al. 2021). Their study also found Fe (total) concentrations as high as 30 mg/L with a mean of 7.7 mg/L, above the WHO standard of 0.1 mg/L for drinking water. The high turbidity and excessive levels of Fe (total) and Hg in the surface water are likely caused by the illegal mining activities pervasive in the Pra Basin.

Irrigation quality indices such as SAR, USSL and the Wilcox diagram classify the surface water as suitable for irrigation. The calculated indices for irrigation were based on the ions including Na^+, K^+, Ca^{2+} and Mg^{2+} as these are known to have negative effects on soil and also on plants when present in excess. We observed very low levels of Na^+, which is good for soil maintenance. Excess sodium in the water affects the hydraulic conductivity of the soil and is an important factor when considering water for irrigation. Generally, water with a SAR < 10 is considered excellent for irrigation (Hem 1985). Based on this criterion, the surface waters can be interpreted as suitable for irrigation. This is confirmed by the USSL and Wilcox plots based on the sodium and electrical conductivity of the water.

Regarding the trace metals (Fe (total) and Mn), our results indicate that surface water may require some treatment before being used for irrigation. In general, irrigation water with Fe (total) and Mn concentrations less than 5 mg/L and 0.2 mg/L (Ayers, Westcot, et al. 1985), respectively, is considered acceptable for irrigation. Excessive levels of these trace metals have been reported as a possible cause of clogging and rusting of irrigation systems (Grabić et al. 2019). In general, Fe is not toxic to plants. However, extreme levels can lead to soil acidification and depletion of essential plant nutrients such as phosphorus and molybdenum (Ayers, Westcot, et al. 1985; Grabić et al. 2019). Manganese, on the other hand, is toxic to some plants in acid soils (Ayers, Westcot, et al. 1985), and its presence must be controlled depending on the type of plants to be irrigated. In this study, 24% of Fe (total) and 47% of Mn concentrations in surface water are above their respective limits in irrigation water and, therefore may require treatment to reduce concentrations to acceptable levels before use.

3.4.3 Assessment of Groundwater Quality for Drinking and Irrigation

Our analysis shows that groundwater quality in the central and southern zones is excellent for drinking, while the northern zone is of poor quality, affected by Mn and Fe. Samples from the central and southern zones are largely from the Cape Coast granitoid aquifers. The granitoid generally consists of silicates. Due to the slow rate of weathering of silicate minerals, the amount of dissolved ions is very low and within WHO guidelines for drinking water. All major ionic concentrations are within the desirable limits of WHO guideline levels in drinking water. In our analysis, we find that without including trace metals, such as Fe (total) and Mn, in the WQI calculations, all samples fall in the good to excellent category, consistent with a comparison

based on WHO guideline values for each major ions. However, considering Mn and Fe (total) in the WQI analysis, we find that 13 samples, all located in the northern zone, are of poor quality and cannot be used for drinking. To the best of our knowledge, the sources of Mn and Fe (total) are likely from the rock and leaching from polluted surface waters. The rocks beneath the northern zone are mostly meta-sediments containing pyrite, iron oxides and Mn-rich minerals (Manu et al. 2013). As water interacts with the rocks in the aquifer, more ions, including Mn and Fe (total), are released into the solution. On the other hand, due to the high Mn and Fe (total) contents in surface waters, it is also likely that they were transported from the surface into the aquifer in areas where the hydraulic connection between groundwater and surface water exists.

Our analysis based on the SAR, USSL and the Wilcox irrigation schemes show that groundwater is of excellent quality for irrigation. In general, crystalline bedrock aquifers produce excellent water quality for crop irrigation (Anku et al. 2009; Chegbeleh et al. 2020; Gibrilla et al. 2011; Kaka et al. 2011; Koffi et al. 2017; Loh et al. 2021; Yidana et al. 2012a). The quality of the water used for irrigation depends on the concentration of ions leaching into the groundwater from the underlying geological material. Such ions include Na^+, K^+, Ca^{2+}, Mg^{2+}, HCO_3^-, Cl^-, SO_4^{2-} and NO_3^-. In this study, the major ion concentrations of the groundwater is generally low and this can be attributed to the slow weathering of the crystalline rocks.

With regard to trace metals (Mn and Fe (total)), the groundwater of the northern zone has relatively higher concentrations of Mn and Fe (total) than those of the central and southern zones. In view of this, water extracted from the northern zone aquifers may require some treatment prior to use. However, the groundwater in the central and southern zones could be used without treatment.

3.4.4 Mechanism Controlling Groundwater Chemistry

Theoretically, three mechanisms controlling the dissolved ions in groundwater can be derived from the Gibbs diagram, depending on rock dominance, precipitation dominance and evaporation dominance. It is evident that most groundwater samples are plotted in the rock-dominance region (Figure 3.11), suggesting that rock weathering is an important mechanism controlling groundwater chemistry in the study area. According to Banks and Frengstad (2006), the ratio of $Na^+/(Na^+ + Ca^{2+})$ in silicate-dominated environments can exceed 0.9, which is the maximum limit in the Gibbs diagram. In such cases, the groundwater chemistry is driven by a high $Na^+/(Na^+ + Ca^{2+})$ ratio and the points on the Gibbs diagram shifts to the right outside of the boomerang. Our results support this hypothesis, as some of our groundwater samples show a $Na^+/(Na^+ + Ca^{2+})$ ratio greater than 0.9, underscoring that silicate weathering is an important process driving ground water chemistry in the area, consistent with several studies that identified the weathering of silicates as a dominant geochemical process in similar rock environments (Chegbeleh et al. 2020; Tay et al. 2017; Yidana et al. 2012b).

3.4.5 Chemical Processes Driving Groundwater Evolution

Bivariate ion plots in Figure 3.12 show that groundwater chemistry is mainly controlled by silicate weathering, carbonate dissolution and ion exchange reactions. From Figure 3.12a we see that there is an excess of Na^+ relative to Cl^-, indicating an additional source of the Na^+ in the solution. Meybeck (1987) reported that a Na^+/Cl^- ratio greater than 1 emphasizes silicate weathering as a source of Na^+. Again, the excess Na^+ in the solution likely comes from ion exchange where the Ca^{2+} in the solution is exchanged for Na^+ from the aquifer matrix. Freeze and Cherry (1979) and Appelo and Postma (2004) underscored that that if Na^+ is

released mainly by silicate weathering, HCO_3^- will be the most abundant anion in groundwater, which is generally the case in the northern and central zones, however in the southern zone Cl^- is the most dominant anion interpreted to originate from the dissolution of marine aerosols from the sea.

From Figure 3.12b,c, we learn that ion exchange and carbonate dissolution do occur in the groundwater system of the Pra Basin. Schoeller (1967) proposed two indices which are used to determine the occurrence of ion exchange in a natural water system. He observed that when ion exchange occurs, the indices will be negative, indicating Na^+-Ca^{2+} ion exchange, and when positive, indicate the reverse. Based on the Chloro-Alkaline Indices plot, we found that the majority of the samples show a negative value, indicating a Na^+-Ca^{2+} exchange. Here Na^+ in the aquifer matrix exchanges with Ca^{2+} in solution, leading to a depletion of Ca^{2+}. A similar trend was observed in the Ca^{2+} vs. HCO_3^- plot as most samples are plotted on the HCO_3^- side. These two plots show that Ca^{2+} is exchanged with Na^+ in our groundwater system, suggesting that cation exchange affects the chemical composition of groundwater in the area. In addition to ion exchange, the points plotted along the 1:1 line in Figure 12c indicate a common source for Ca^{2+} and HCO_3^- that can be attributed to carbonate dissolution. The influence of carbonate dissolution plays a role in the hydrochemical evolution of the groundwater in the northern and central zones of the basin where calcite is found in the rocks (Manu et al. 2013).

3.4.6 Statistical Analysis Explaining the Causes of Spatial Variability in Groundwater Composition

Our analysis based on the HCA shows that hydrochemical variation in groundwater is determined by elevation, while factor scores revealed silicate weathering and carbonate dissolution as the plausible geochemical processes driving groundwater chemistry in the Pra Basin. Three spatially distinct chemical associations were identified from the HCA based on sample locations at either higher, intermediate, or lower elevations. Under natural conditions, groundwater is expected to flow from higher to lower elevations. For this reason, the higher elevation (northern zone) and the lower elevation (southern zone) are interpreted as recharge and discharge zones, respectively. The central zone, marked by an intermediate elevation, is interpreted as a transition zone along the flow path. From this, the groundwater in the study area is most likely to flow in the direction from the northern zone through the central and finally to the southern zone.

Chemically, the groundwater composition in the three defined zones changes from Ca-HCO_3 to a mixed water type dominated by Na–HCO_3 and a dominant Na–Cl water along the flow regime from the recharge to the discharge zone, respectively. In principle, the chemical composition of groundwater in the recharge zone is dominated by Ca–HCO_3, which represents waters that have not interacted much with the rocks and are only in the early stages of evolution (Chebotarev 1955; Chegbeleh et al. 2020). The prevalence of HCO_3^- in the northern zone is partially influenced by the CO_2 of the soil zone and the highly CO_2-charged rainwater. Here the dominance of the Ca^{2+} could be attributed to the dissolution of carbonate, which is identified in the Birimian rocks underlying the northern zone (Manu et al. 2023e; Manu et al. 2013). The latter probably contributes to the HCO_3^- in the water composition of the northern zone. Factor analysis performed on the northern zone water samples revealed two factors, with Factor 1 explaining 40% of the overall variance in hydrochemistry. Factor 1 shows a positive correlation for pH, Ca^{2+}, HCO_3^- and SiO_2, which we interpret as a consequence of silicate weathering and carbonate dissolution. This is consistent with the general mineralogical composition of the rocks

in the area which have been found to contain silicates (albite, K-feldspar, muscovite and biotite) and carbonate minerals (Manu et al. 2013; Nude et al. 2011). The high positive correlation between Ca^{2+} and HCO_3^- indicates the dominance of these ions in groundwater and confirms the Ca–HCO_3 water type preserved in the northern zone.

In the transition zone, which is characterised by intermediate elevations, the chemical composition of the groundwater changes from the Ca–HCO_3 water type to the mixed (predominantly Na–HCO_3) water type. The softening of the water composition in the central zone is likely caused by cation exchange where Ca^{2+} in the water exchanges with the Na^+ from the aquifer material. The cation exchange reaction process releases more Na^+ into the groundwater, making it the most abundant cation in the central zone. Other minor water compositions, including Na–Cl, Ca–Cl, Mg–Cl and Ca–HCO_3, underscore that a mixture of different water compositions from different flow paths is likely to cause the mixed water types observed in this zone. This is corroborated by the factor analysis which revealed three factor models without a dominant process, suggesting that mixed water compositions control groundwater chemistry in the central zone. This is consistent with the general conclusion that the chemical composition of groundwater in the transition zone along the groundwater flow regime is a mixture of different water compositions (Chebotarev 1955).

In the southern zone, the water composition changes from Na–HCO_3 dominant to a Na–Cl water. The Na–Cl water in the southern zone is most likely derived from two sources. The first source will be the general evolution of anions along the groundwater flow path as described by Chebotarev (1955). According to Chebotarev (1955), when water moves through rocks, its chemical composition changes, and the longer the residence time, the more chemically evolved the water becomes. In his theory, the author underlined that along the flow path, HCO_3^- anions dominating the shallow and recharging areas give way to SO_4^{2-} and finally to Cl^-, while Ca^{2+} is displaced by Na^+. On the other hand, due to the proximity of the southern zone to the sea, it is likely that aerosols from the sea also contribute significantly to the composition of the Na–Cl water. This is confirmed by the factor model (Factor 1) generated for the southern zone, which showed a strong positive correlation with Na^+, Cl^- and SO_4^{2-}, suggesting a common source which is most likely from marine aerosols consistent with the findings of Tay et al. (2017). The mineralogical composition of of the rocks in the study area does not support the possible influence of halite and sulfate minerals, as there is no petrographic evidence in the underlying rocks. In view of this, we could assume that the marine aerosol contribution is likely to influence the hydrochemistry of the southern zone groundwater composition.

3.5 Conclusions

Understanding the geochemical processes that control the chemical composition of surface water and groundwater is crucial for the development of appropriate water management strategies. In this current study, 90 water samples from rivers and boreholes were analyzed for their chemical parameters, including major ions and trace metals. The hydrochemical data provide the baseline information and was used to assess the quality and infer geochemical processes that control the hydrochemistry of the water resources in the Pra Basin.

Among the two water sources, groundwater is considered good for drinking and irrigation, except for the northern zone, which may require Mn and Fe (total) treatment. Our analysis shows that surface water has poor quality and cannot be used as drinking water in its current state without treatment. The sources of these trace metals could be traced from the underlying

geology through water–rock interactions and the illegal mining activities through underground excavations facilitating the dissolution of Mn- and Fe-rich minerals contained in the subsurface materials. Based on the SAR, USSL and the Wilcox indices, all the surface water samples are rated excellent for irrigation. However, the high concentrations of Mn and Fe (total) observed in most of the surface water samples may require treatment to avoid soil acidification and loss of essential soil nutrients. Here we conclude that using only the major ionic composition is not sufficient to determine the drinking and irrigation water quality of surface water and groundwater, and therefore trace metals, such as Mn and Fe (total), as well as toxic metals (mercury, arsenic and cyanide) associated with illegal mining and bacteriological contaminants should be considered for the general water quality assessment.

Water–rock interactions control the chemical composition of groundwater. A combined interpretation of ion ratio plots and statistical analysis underlines that groundwater chemical composition changes with elevation with silicate weathering, carbonate dissolution and cation exchange as plausible geochemical processes driving the Pra Basin hydrochemistry. Based on the HCA, three distinct chemical associations are recognized, distinguishable by elevation. From this, we could deduce that ground water in the Pra Basin most likely flows in the direction from higher (northern zone) to lower elevations (southern zone). Along the flow regime, the groundwater composition changes from Ca-HCO_3 (northern zone) to a mixed water type dominated by Na-HCO_3 and finally to Na-Cl. The statistical relationship between Na^+ and Cl^- derived from factor analysis indicated a potential influence from marine aerosols since the underlying geology shows no evidence of halite deposits in the area.

This research is part of an ongoing study aimed at conceptualizing the hydrogeochemical conditions in the Pra Basin to aid in water resource management following the pervasive illegal mining activities in and around the study area. As a next step, we plan to implement geochemical models, including inverse and reaction path models, to elucidate the geochemical processes that drive groundwater chemical evolution. In doing so, the reactions of the water with the host rocks can be examined and quantified to understand the chemical behaviour of the dissolved ions in the groundwater system.

Chapter 4

Water-Rock Interactions Driving Groundwater Composition in the Pra Basin (Ghana) Identified by Combinatorial Inverse Geochemical Modelling

ABSTRACT

The crystalline basement aquifer of the Pra Basin in Ghana is essential to the water supply systems of the region. This region is experiencing the ongoing pollution of major river networks from illegal mining activities. Water management is difficult due to the limited knowledge of hydrochemical controls on the groundwater. This study investigates its evolution based on analyses from a previous groundwater sampling campaign and mineralogical investigation of outcrops. The dominant reactions driving the average groundwater composition were identified by means of a combinatorial inverse modelling approach under the hypothesis of local thermodynamical equilibrium. The weathering of silicate minerals, including albite, anorthite, plagioclase, K-feldspar, and chalcedony, explains the observed median groundwater composition in the transition and discharge zones. Additional site-specific hypotheses were needed to match the observed composition of the main recharge area, including equilibration with carbon dioxide, kaolinite, and hematite in the soil and unsaturated zones, respectively, and the degradation of organic matter controlling the sulfate/sulfide content, thus pointing towards kinetic effects during water–rock interactions in this zone. Even though an averaged water composition was used, the inverse models can "bridge" the knowledge gap on the large basin scale to come up with quite distinct "best" mineral assemblages that explain observed field conditions. This study provides a conceptual framework of the hydrogeochemical evolution for managing groundwater resources in the Pra Basin and presents modelling techniques that can be applied to similar regions with comparable levels of heterogeneity in water chemistry and limited knowledge of aquifer mineralogy. The combinatorial inverse model approach offers enhanced flexibility by systematically generating all plausible combinations of mineral assemblages from a given pool of mineral phases, thereby allowing for a comprehensive exploration of the reactions driving the chemical evolution of the groundwater.

4.1 Introduction

The Pra Basin is one of Ghana's basins with high economic importance. Mineral resources, including gold, bauxite, iron, manganese, diamonds etc., mainly occur there. Several activities, such as large and small-scale plantations, fishing, and illegal mining, are pervasive. These economic activities alter the vegetation and have negatively impacted the water resources (Affum et al. 2016; Amonoo-Neizer and Amekor 1993; Armah et al. 2014; Bempah and Ewusi 2016; Golow and Mingle 2003; Manu et al. 2023d; Tay et al. 2014), especially surface waters. This situation has put much stress on the groundwater resource that the people rely upon for their water supply. However, the groundwater quality and geochemical controls on the regional scale are not well studied.

For this reason, Manu et al. (2023d) carried out a regional field study to assess the quality and characterized the hydrogeochemical properties of the groundwater. The main findings of their study, based on classical interpretations using bivariate ion plots and statistical analysis, include the following: (1) the groundwater is generally of excellent quality for drinking and irrigation, (2) three spatial associations exist, which define the flow regime in the basin based on elevation differences, (3) the composition of the groundwater evolves along the hypothetical flow path from $Ca-HCO_3$ to $Na-HCO_3$ and finally to Na–Cl water types, (4) the water–rock interaction is the mechanism that controls the dissolved ion concentrations, and (5) silicate weathering, carbonate dissolution, and ion exchange are plausible chemical processes governing the groundwater composition. In a related study, Loh et al. (2022) used the stable isotopes data in the Lake Bosumtwi area and highlighted that (1) the groundwater originates from precipitation, and (2) the infiltrating water in the unsaturated zone is affected by evaporation before reaching the saturated zone. Their findings are akin to the previous studies conducted at the local scale at different locations in the Pra Basin (Banoeng-Yakubo et al. 2009a; Loh et al. 2021; Tay et al. 2015). The research results presented so far have mainly offered qualitative interpretations without focusing on the quantitative aspects of the chemical reaction processes. As a result, there is a lack of accurate information about the dissolved or precipitated minerals responsible for the chemical development of the groundwater. Furthermore, the lack of a functional conceptual model for reaction pathways hampers our understanding of how groundwater chemical composition changes along its flow path. To fill these gaps, this study uses geochemical models to provide a more comprehensive understanding of the key hydrochemical reactions driving the groundwater evolution.

Geochemical models are essential for analyzing chemical reactions in natural geological systems such as rocks, minerals, and fluids. These models are based on the principles of thermodynamics, kinetics, mass balance, and fluid dynamics, and they help to quantify geochemical processes, including dissolution, precipitation, sorption, and ion exchange, which control groundwater chemical evolution (Apollaro et al. 2021; Elango and Kannan 2007). Approaches used to study these processes include inverse and forward modelling. Classical inverse geochemical modelling utilizes mass balance to quantify the amounts of reactions of predetermined phases to account for chemical changes observed between two end-member solutions (Plummer et al. 1994). This approach involves defining the known chemical composition of the initial and final solutions and specifying the reacting mineral phases; the model determines the set of mole transfers for the mineral phases that explain the evolution of the final water composition (Parkhurst, Appelo, et al. 1999), irrespective of thermodynamical constraints. Conversely, forward modelling applies local thermodynamic equilibrium to an initial solution in contact with a determined mineral assemblage to predict the final solution and, thus, the amounts of reacting phases needed to reach a local equilibrium (Parkhurst, Appelo, et al. 1999).

Several software packages, including PHREEQC (Parkhurst 1995), Geochemist Workbench (Bethke 2022), TOUGHREACT (Xu et al. 2004) etc., are available to implement geochemical models. Among these codes, PHREEQC (Parkhurst 1995) is one of the most widely used codes to perform geochemical simulations. Its popularity is attributed to factors such as the availability of the source code, its widespread usage among users, and its extensive documentation. Recently, De Lucia and Kühn (2021) proposed a geochemical and reactive transport modelling package (RedModRphree) that leverages the R programming interface

to establish PHREEQC geochemical simulations. The power of the RedModRphree lies in its flexibility to program algorithms associated with geochemical models, including error and sensitivity analysis, parameter calibration and optimization, statistical modelling, and thermodynamic database manipulation (De Lucia and Kühn 2021).

In this study, we utilized geochemical simulations to investigate the chemical evolution of groundwater in the highly heterogeneous geochemical environment of the Pra Basin. Our modelling approach started by defining a conceptual reaction path model based on the findings from the previous works enumerated above. Three conceptual flow paths were adopted following the results of Manu et al. (2023d) and Loh et al. (2022). A combinatorial inverse modelling technique (Section 4.2.7) was employed as an exploratory approach to identify plausible mineral assemblages whose thermodynamical equilibriums could explain the observed composition of groundwater along the flow regime. Unlike classical inverse modelling, which relies solely on mass balance, this technique operates under the assumption of local thermodynamic equilibrium. The best matching mineral assemblages were further calibrated using conceptualized reaction path models that were depicted to include, e.g., the influence of unsaturated zone. Based on the model results, a potential hydrogeochemical evolution model was obtained that identifies the driving hydrochemical processes along the groundwater flow in the Pra Basin. The developed conceptual framework serves as a foundation for further investigation and analysis of the hydrogeochemical dynamics in the basin.

4.2 Materials and Methods

4.2.1 Study Area

The study area consists of the two sub-basins including the Birim and the Lower Pra of the main Pra Basin, located in the southern parts of Ghana. The geographical location, physical setting, climate and major economic activities in the basin are described in Manu et al. (2023d).

4.2.2 Geological Setting

The study area is dominated by two rock formations (Figure 4.1): the Birimian Supergroup and the Cape Coast granitoid (Dzigbodi-Adjimah 1993). The Tarkwain Rock Formation occupies smaller portions and is mostly found on the eastern and western edges of the study domain. The Birimian rocks predominantly underlie the northern portions and the Cape Coast granitoid south of the basin. A detailed study of the mineral and rock composition of the Birimian, Tarkwain, and Cape Coast granitoid rock formations has been copiously discussed in the literature (Kesse 1985; Kesse 1976; Leube et al. 1990). The Birimian metasediments consist of phyllite, schists, greywacke, weakly metamorphosed tuffs, feldspathic sandstones, and Mn- and Si-rich chemical sediments (Kesse 1985; Manu et al. 2013; Nyame 2013). The phyllites have been found to contain pyrite and finely divided carbonaceous matter (Banoeng-Yakubo et al. 2010). Available data suggest that the phyllite and metagreywackes contain significant amounts of calcite (over 15% in some cases) in the Birimian metasediments (Yidana et al. 2012b). High biotite and plagioclase minerals have also been reported in the Birimian rocks (Yidana et al. 2012b). The Tarkwaian rocks consist of sandstones, conglomerates, and argillites, which constitute a clastic sequence of arenaceous and argillaceous sediments (Kesse 1985). Most of the southern parts of Ghana are underlain by the Cape Coast granitoid (Kesse 1985; Leube and Hirdes 1986). The pegmatites of the Cape Coast granites occur as dykes with feldspars, quartz, and micas as the dominant mineral composition (Kesse 1985). The Cape Coast type granitoid also comprises

granitic to quartz dioritic gneiss, which changes from medium-grained, foliated biotite quartz diorite gneiss to horn-blended quartz–diorite gneiss (Ganyaglo et al. 2010).

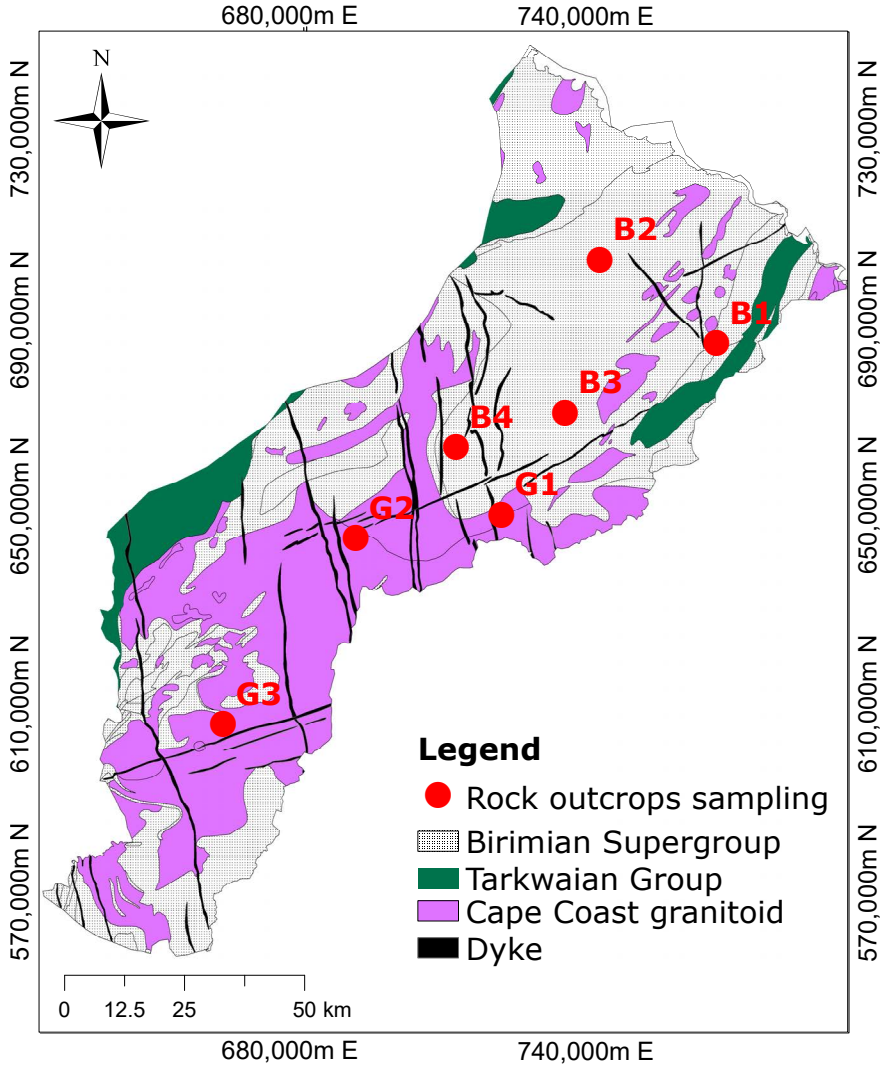

Figure 4.1: Geological map showing the dominant rock formations and the sampling locations. The Birimian rocks are composed of metasediments, while the Cape Coast granitoid is composed of granite, and the Dyke is made of dolerite (modified after Manu et al. (2023d)).

4.2.3 Hydrogeologic Conditions

The study area falls within the Crystalline Basement Granitoid Complex and the Birimian Province in Ghana. In general, the rocks are inherently impermeable; however, secondary porosity results from fractures and faults that control groundwater movement (Banoeng-Yakubo et al. 2010). The hydrogeological units consist primarily of a saprolite overlain by duricrust, saprock, and underlying bedrock. The saprolite is deeply weathered and consists of clay or silt. The saprock is oxidized and forms the transition zone between the saprolite and the bedrock. Groundwater occurs in two distinct hydrogeological units comprising the overburden and the bedrock. The bedrock consists of granitoid and Birimian rocks, which vary in thickness and fracture intensity (Banoeng-Yakubo et al. 2010).

4.2.4 Field Work

Fieldwork was undertaken to sample rocks for mineralogical studies. Figure 4.1 shows the geological map of the study area with the outcrop locations. A total of seven representative samples were collected, comprising four from the Birimian Supergroup and three from the Cape Coast granitoid formation. The description of the measurements and the mineralogical composition identified by the petrographic thin section analyses are described in Manu et al. (2023e).

4.2.5 Modelling Input Data Sources

The data used for the geochemical modelling include major ion chemical compositions from rainwater and groundwater samples, as well as mineralogical information determined by thin section petrography analysis. Three sets of information were required for model setup: (1) the initial solution—in our case, we used chemical data from the rainwater, (2) the final solution, which is the groundwater composition, and (3) the mineralogical information.

In this study, the hydrochemical data of the rainwater (Table 4.1) in close vicinity to the Pra Basin were taken from Akoto et al. (2011) and used as the initial solution. Chemical parameters such as pH, Na^+, K^+, Ca^{2+}, Mg^{2+}, HCO_3^-, Cl^-, and SO_4^{2-} were used for the starting aqueous components in our modelling. In their study, Loh et al. (2022) estimated the evaporation rate of rainwater before groundwater recharge to be between 54% and 60%. In view of this, the initial solution was simulated by evaporating rainwater until the chloride concentration measured in the groundwater was reached. In that way, chloride was used as a conservative tracer unaffected by the chemical reaction processes. This assumption is reasonable, as there is no evidence of halite in the underlying geology to dissolve and alter the Cl^- concentration of the infiltrating water. The final chemical composition of the evaporated rainwater was then used as the initial solution for the combinatorial and reaction path modelling.

The hydrochemical data of the groundwater from Manu et al. (2023d) were adopted in the present study. The median ion concentrations shown in Table 4.1 of the samples were taken to represent each of the three zones (Figure 4.2) along the flow path from the recharge to the discharge zone. The rationale for using the median as the final representative composition was to minimize the error introduced by outliers and the natural variability in the water samples (Thyne et al. 2004). The chemical parameters of groundwater considered for the modelling included pH, Na^+, K^+, Ca^{2+}, Mg^{2+}, HCO_3^-, Cl^-, SO_4^{2-}, Fe, and SiO_2.

The mineral phases were selected from a petrographic study performed on outcrop samples by Manu et al. (2023e). Photomicrographs showing the mineralogical and textural features of the rock samples are presented in Figure 4.3. The mineralogical composition of the Birimian rocks underlying the northern zone consists of biotite, chlorite, quartz, sericite, minor K-feldspar, and calcite (Figure 4.3B1–B3). Iron oxides are visible in hand specimens. Biotite has significantly altered to chlorite, whiles the K-feldspar has altered into sericite. The granitoid is locate principally over the southern zone and comprises quartz, plagioclase, K-feldspar, muscovite, and biotite with accessory chlorite and sericite (Figure 4.3G1–G3). In our study, the presence of albite was confirmed through XRD analysis, while plagioclase was identified through thin section analysis. Additionally, we assumed the presence of anorthite, the calcium end-member of plagioclase, in the system. The mineral phases considered for combinatorial inverse modelling along the three flow paths included primary albite, anorthite, plagioclase, phlogopite, K-mica, K-feldspar, $Fe(OH)_3$, and calcite, as well as secondary kaolinite,

Ca-montmorillonite, chlorite (14A), quartz, pyrite, and chalcedony. Here, the primary and secondary minerals were considered as reactants and products, respectively.

Table 4.1: Hydrochemical data from rainwater and groundwater used for the modelling. The rainwater (RW) and groundwater (comprising northern, central, and southern) data were adopted from Akoto and Adiyiah (2007) and Manu et al. (2023e). ND denotes not determined.

			Median			Range		
Prameter	**Units**	**RW**	**Northern**	**Central**	**Southern**	**Northern**	**Central**	**Southern**
pH	-	4.7	6.5	6.1	6.0	5.9–7.0	5.6–6.4	5.3–6.4
Temp	°C	ND	28.1	28.4	29	26.0–29.0	28.1–29.6	27.8–31.0
Na^{+}	mg/L	0.4	11.9	17.1	44.3	3.1–32.4	9.2–21.8	16.4–67.4
K^{+}	mg/L	0.7	0.7	3.7	6.1	0.3–8.2	0.4–6.3	1.2–16.3
Ca^{2+}	mg/L	0.8	26.4	7.2	14.8	12.6–51.5	2.1–13.5	3.1 -66.0
Mg^{2+}	mg/L	0.3	6.4	2.5	7.2	1.6–12.8	0.9–4.6	1.5–29.4
HCO_3^{-}	mg/L	6.7	108.5	3.7	28.0	37.8–191.0	29.3–67.1	5.0–134.0
Cl^{-}	mg/L	4.5	8.4	12.7	58.1	2.4–49.0	6.0–21.5	17.5–196.7
SO_4^{2-}	mg/L	11.1	1.1	1.6	8.6	0.4–66.0	0.1–4.3	1.6–99.4
Fe(total)	mg/L	ND	0.2	0.01	0.02	0.008–0.8	0.001–0.2	0.006–0.09
SiO_2	mg/L	ND	23.9	23.4	17.5	7.2–33.7	13.6–37.3	11.8–29.7

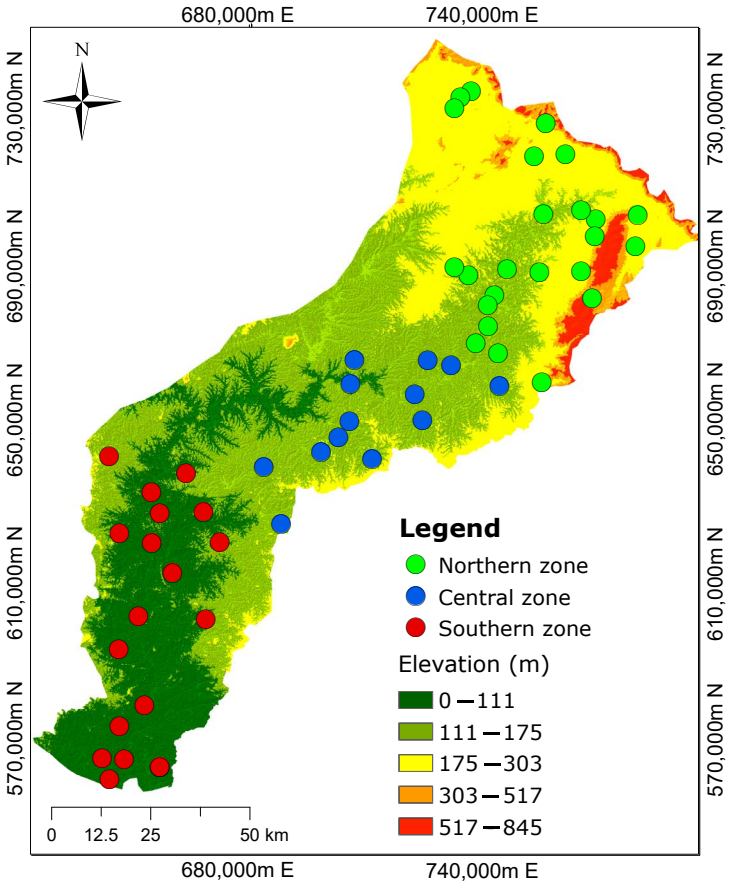

Figure 4.2: Three demarcated zones from the previous study by Manu et al. (2023d) show the spatial distribution of groundwater sampling sites. The northern zone is characterized by high elevations, while the southern zone has low elevations. The groundwater flow is assumed to mimic the topography.

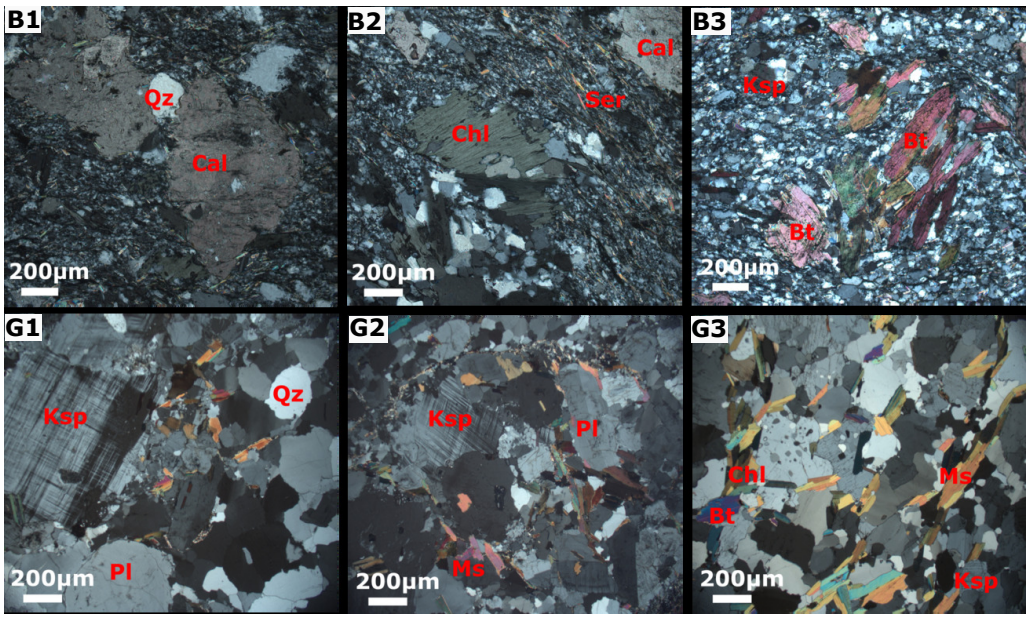

Figure 4.3: Thin sections of rock outcrops (adopted from Manu et al. (2023e)). The first row shows the mineralogy of the Birimian metasediments (**B1**, **B2**,**B3**), including quartz (Qz), biotite (Bt), K-feldspar (Ksp), sericite (Ser), chlorite (Chl), and calcite (Cal). The second row shows the mineral composition of the granitoid (**G1**,**G2**,**G3**) comprising quartz (Qz), K-feldspar (Ksp), plagioclase (Pl), muscovite (Ms), and biotite (Bt).

4.2.6 Geochemical Code and Thermodynamic Data

In this study, the geochemical modelling code PHREEQC (Parkhurst 1995), was chosen for the numerical simulations, with the `phreeqc.dat` as the selected database. The underlying reasons for choosing PHREEQC are threefold: (1) code availability, (2) wider user coverage, and (3) adequate documentation.

Minerals such as plagioclase, biotite, and muscovite were originally not included in the `phreeqc.dat` database. Biotite or "black mica" was introduced in the model as the Mg end-member phlogopite, adopted from the thermodem thermodynamic database (Circone and Navrotsky 1992). Muscovite or "white mica", was introduced as K-mica. For the plagioclase, a fixed stoichiometry of 0.38 Ca/0.62 Na was assumed. Its equilibrium constant was estimated by weight averaging the equilibrium constants of the two end-members, anorthite and albite, using their definitions in `phreeqc.dat`. The chemical equations, along with the thermodynamic equilibrium constants of the added phases in the `phreeqc.dat` database, are presented in Table 4.2 in Appendix 4.7.1. The RedModRphree package (De Lucia and Kühn 2021) was used to set up and perform the combinatorial screening and the calibration of the reaction path models described in the next section. For more detailed information about the RedModRphree setup, see De Lucia and Kühn (2021).

4.2.7 Combinatorial Inverse Modelling Approach

A multi-step inverse modelling approach was devised to successively integrate field observations into models and then to calibrate the latter with known geochemical constraints. Notably, in a preliminary combinatorial inverse approach, all possible mineral assemblages drawn from a pool of potential minerals were screened under local thermodynamic equilibrium conditions aimed at identifying the mineral assemblage that would best explain the changes in composition along the flow path of the groundwater. This was a different goal than with

classical inverse geochemical models, which consist rather in computing the amount of mole transfer from a predetermined mineral assemblage (Appelo and Postma 2005).

Three hypothetical flow paths were defined based on the cluster analysis conducted by Manu et al. (2023d). Flowpath I includes rainwater as the starting point and the northern zone groundwater as the final solution. Flowpath II represents two end-member solutions, the northern and central zones, while Flowpath III represents the water transfer from the central and to the southern zones. The median ion concentrations of the groundwater samples within the three zones postulated by Manu et al. (2023d) were retained as representative and used as target concentrations to rank all computed equilibrium models.

The modelling procedure begins with the definition of the starting solution, which represents evaporated rainwater and has chemical concentrations stated in mol/kgw. The temperature is assumed to be 25 °C, which corresponds to the average temperature of groundwater samples collected in the study region. Certain components, such as iron and silica, were not originally present in the rainfall composition and were labelled as NA (not applicable) to guarantee consistency between the target groundwater concentrations and the predicted results.

The simulation used the `phreeqc.dat` database, which was adjusted to include minerals such as phlogopite and plagioclase, as well as organic matter. Target concentrations, representing the groundwater elemental composition in the northern, central, and the southern zones, were specified in order to compare the modelled results with the observed concentrations. The primary and secondary minerals were defined to dissolve or precipitate when present in the groundwater solution.

The simulation was programmed to generate all potential combinations of 3 to 8 mineral phases drawn from predetermined pools of primary and secondary minerals. Each resulting mineral assemblage was then considered at equilibrium with the initial water, and the final total elemental concentrations of the modelled solutions were ranked by their discrepancy to the target solution. We assumed that any mineral combination resulting in a model solution would be plausible for explaining the observed composition.

In this study, a pool of 14 mineral phases comprising primary albite, anorthite, plagioclase, phlogopite, K-feldspar, K-mica, $Fe(OH)_3$, and calcite, as well as secondary kaolinite, Ca-montmorillonite, chlorite, quartz, pyrite, and chalcedony, were used as the reactants and products for the combinatorial inverse modelling. Pyrite was not included along Flowpath III, as there was no evidence of its presence in the granitoid formation.

Given the large pool of mineral phases, several thousand models were generated. Here, a maximum allowable threshold reactivity of 0.5 mol/kgw was applied to eliminate models where two competing mineral phases or proxies for the same element were present in the system. The reason for this is that, in the case of a complete dissolution of a mineral phase leading to the precipitation of large amounts of a stable phase, physically unrealistic results would be obtained.

The ensemble of computed equilibrium models was compared to the observed concentration range of the aqueous groundwater components, and models that did not fall within the observed concentration ranges were removed. Due to the ill-posed nature of inverse models, there can be multiple solutions that fit the observed data. Therefore, we utilized the relative root mean square error (RRMSE) (Equation (4.1)) of all the aqueous components of

the equilibrium models with respect to the target concentrations in order to rank the matches obtained.

$$\text{RRMSE} = \sqrt{\frac{1}{n}\sum_{i=1}^{n}\left(\frac{y_i - \hat{y}_i}{y_i}\right)^2} \tag{4.1}$$

where i represents the respective ions, y_i represents the observed aqueous concentrations, $\hat{y}_i$ represents the simulated aqueous components, and n is the total number of elements to be matched.

Finally, the contingencies for each mineral phase contained in the 50 best-matching models were calculated. The rationale for the frequency calculations is that, when a mineral phase is present in many high-ranked models, the probability of identifying a reactive mineral phase is greater than the minerals not represented in the same ensemble.

4.2.8 Calibration Based on Reaction Path Scheme

Based on the combinatorial inverse modelling results, the mineral assemblages identified as most probable were further calibrated according to the conceptual reaction path model shown in Figure 4.4. The reaction path modelling was implemented through a five-step approach, as discussed in the following.

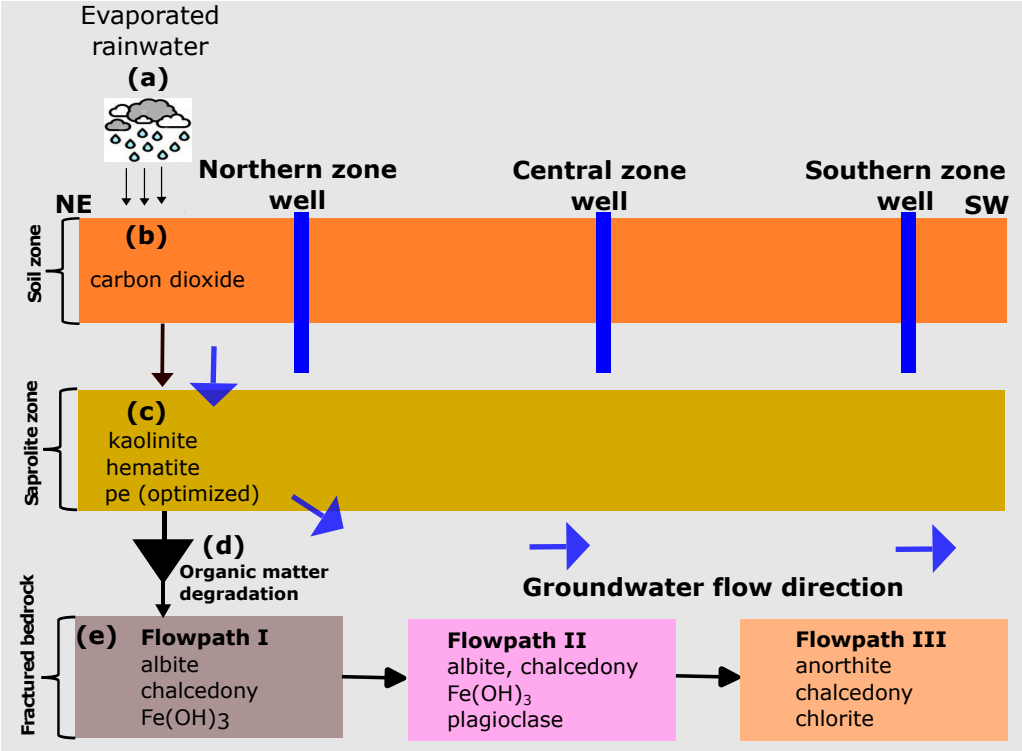

Figure 4.4: Conceptual reaction path models considering the rainwater origin of the groundwater. The northern zone is assumed to be the recharge area at high elevations. Vertical flow in the central and southern zones is assumed to have no significant impact on groundwater chemical evolution.

In step (a), the rainwater composition was subjected to evaporation using the Cl^- concentration in the northern zone groundwater as the target concentration. The final solution after evaporation was saved and used as the starting solution for the reaction path modelling.

Step (b) involved the equilibration of the evaporated solution with CO_2 in the topsoil. Here, we performed a trial and error calibration by adjusting the partial pressure of CO_2 until a reasonable match with the HCO_3^- in the observed concentration was achieved. This approach was deemed necessary due to the lack of soil measurements for carbon dioxide (CO_2) in the current investigation.

In step (c), the solution from step (b) was equilibrated with kaolinite and hematite. The saprolite is deeply weathered and consists of clay and silty clay. The uppermost part comprises red laterite clay and duricrust dominated by cemented iron oxides and silica nodules. In an ideal scenario, the release of Al and Fe into the solution is primarily attributed to primary silicate and Fe-containing minerals. However, to simplify the model, we utilised secondary minerals, namely kaolinite and hematite, to estimate the equilibrium quantities of Al and Fe in the solution. The redox potential of the water in the unsaturated zone was then optimized in order to control the Fe concentration. We used the trial-and-error method to optimize the redox (pe) of the infiltrating water in the unsaturated zone. This method was used because no redox potential (pe) measurements were carried out in the current study. The numerical values determined by manual calibration offered a preliminary estimate of the prevailing redox conditions in the groundwater system.

In step (d), we integrated the organic matter degradation reaction into the batch model to control the sulphate/sulphide content in the groundwater. Based on the hypothesis that organic matter present in the groundwater system under anaerobic conditions is responsible for the lower SO_4^{2-} concentrations, we also assumed that iron oxides present in the meta-sediments underwent further reactions with H_2S, which is formed during the decomposition of the organic matter. These reactions result in the formation of iron sulfide minerals, particularly pyrite, as observed in our study. To represent the organic matter, we used the hypothetical compound CH_2O, as suggested by Pitkaenen et al. (1998). Since the organic matter content in the soil was not measured, we adjusted the CH_2O values until the observed sulphate content in the groundwater was matched.

In step (e), the solution from step (d) was equilibrated with the determined aquifer mineralogy in the three zones identified by combinatorial inverse modelling.

4.3 Results

4.3.1 Mineral Assemblages Identified from the Combinatorial Inverse Modelling

Given the large pool of mineral phases, 12,805 unique models each were generated for Flowpath I and II, and 7007 models were generated for Flowpath III. However, by implementing a threshold reactivity of 0.5 mol/kgw, only 11,788 models for Flowpath I, 11,785 models for Flowpath II, and 6370 models for Flowpath III converged to a physically meaningful solution.

Combinatorial inverse modelling provided sets of potential model solutions that fell within the range of the observed aqueous compositions of the groundwater. The RRMSE values obtained for the 50 best-matching simulations ranged from 2.769 to 2.783 with a mean of 2.777 for Flowpath I, from 0.433 to 0.472 with a mean of 0.458 for Flowpath II, and from 0.329 to 0.395 with a mean of 0.365 for Flowpath III. Based on the RRMSE values, Flowpath I, which comprises the evolution from precipitation to the northern zone groundwater, had the highest RRMSE values exhibiting larger deviations from the median concentrations. In the case of Flowpath I, the inverse equilibrium calculation could not produce a model that matched all the

measured aqueous components in the groundwater (northern zone). In general, Ca^{2+}, Mg^{2+}, HCO_3^-, Cl^-, SO_4^{2-}, and SiO_2 showed fairly good matches between the modelled and the median concentrations adopted in our simulation. Ions including Na^+, K^+, and Fe(total) showed significant variations from the median concentrations, although several models were within the measured compositional range. Figure 4.5A depicts the mineral frequency distribution of the best-matching 50 equilibrium models. The most frequently occurring minerals included $Fe(OH)_3$, chalcedony, plagioclase, pyrite, chlorite, and albite. The best-matched equilibrium simulation yielded three dominant mineral reactions: the dissolution of albite and $Fe(OH)_3$ and the precipitation of chalcedony. It is important to highlight that this mineral assemblage is considered among the potential combinations in the various equilibrium models for further calibration using the reaction path models.

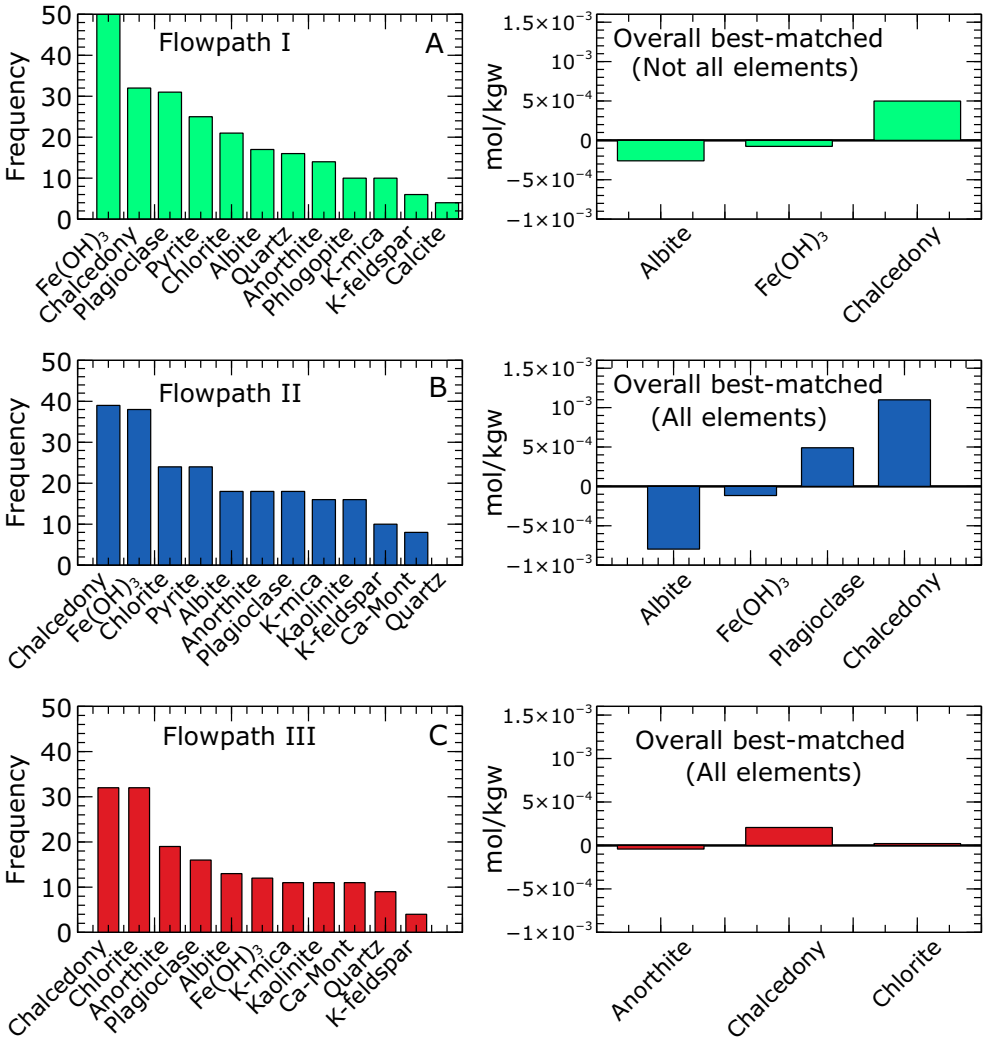

Figure 4.5: Frequency distribution of the 50 best inverse equilibrium models. For the northern zone (Flowpath I), no model matched all the aqueous components; however, the best simulations are shown in (**A**). Simulations matching all the measured aqueous components in the groundwater and mineral reactions for the overall best-matched for the central (Flowpath II) and southern zones (Flowpath III) are shown in (**B**,**C**), respectively. The minerals with a higher number of occurrences underscore the likelihood of a reactive mineral phase. Negative and positive mole transfers indicate mineral dissolution and precipitation, respectively.

For Flowpath II, the inverse equilibrium calculations yielded 188 simulations that matched the observed aqueous components. The mineral frequency distribution of the top 50 matching

models is presented in (Figure 4.5B). The prevalent minerals found to be in equilibrium with the waters in the central zone were chalcedony, $Fe(OH)_3$, chlorite, pyrite, albite, and anorthite. The overall best equilibrium simulation revealed four dominant mineral reactions: the dissolution of albite and $Fe(OH)_3$ and the precipitation of plagioclase and chalcedony.

Regarding Flowpath III, the inverse equilibrium calculation produced 180 simulations that matched the observed aqueous components. The mineral frequency analysis (Figure 4.5C) performed on the top 50 matching models within the range of measured aqueous compositions revealed that chalcedony, chlorite, anorthite, and plagioclase were the most common minerals likely to be in equilibrium with the groundwater in the southern zone. These mineral assemblages aligned with the predicted minerals in the overall best-matched solution. The overall best equilibrium model showed three dominant minerals: anorthite, chalcedony, and chlorite. Notably, anorthite was observed to dissolve, while chalcedony and chlorite precipitated as the system approached equilibrium.

4.3.2 Reaction Path Modelling

Reaction path modelling was applied to mimic the flow path of the water from the recharge area (northern zone) to the discharge zone (southern zone), thus getting into contact with the mineral assemblages deduced from the inverse equilibrium models. Figure 4.6a,b, and c compare the observed and modelled concentrations of aqueous components resulting from subsurface reactions with aquifer materials in the three zones. Generally, all modelled concentrations fell within the range of the observed values. We found that the chemical evolution of the groundwater in the Pra Basin is driven by silicate weathering (albite, anorthite, plagioclase, chalcedony, and chlorite) and that the subsurface reaction path is sufficient to quantify groundwater composition along the flow regime from the recharge (northern zone) to the discharge area (southern zone).

Figure 4.6a presents the modelled groundwater results for the northern zone based on the equilibration of the final calibrated rainwater with the mineral assemblage determined from the combinatorial inverse model along Flowpath I. The modelled concentrations of all aqueous components were within the interquartile range of the observed composition, except for Mg^{2+}, which showed significant deviations from the median. Notably, in our combinatorial inverse modelling, none of the equilibrium simulations matched all the observed aqueous components. Further calibration was required to model the northern zone groundwater, including considerations for rainwater evaporation, the equilibration of CO_2 in the soil zone, the equilibration of kaolinite and hematite, as well as redox optimization in the unsaturated zone, and the degradation of organic matter. The rainwater underwent an evaporation rate of 47%, which doubled all ion concentrations until the chloride (Cl^-) concentration in the groundwater of the northern zone was reached. A partial pressure of $10^{-1.7}$ atm for CO_2 was considered significant in causing an increase in the HCO_3^- concentration of the water infiltrating the soil zone. Since no measurements were available for Fe and SiO_2 in the rainwater, the equilibration of hematite and kaolinite provided initial concentrations of 4.89×10^{-13} mol/kgw for Fe and 2.19×10^{-4} mol/kgw for SiO_2, respectively, for the modelled groundwater. The redox potential (pe) was adjusted until a value of 3.5 was sufficient to produce a Fe concentration of 3.38×10^{-7} mol/kgw that matched the observed northern zone groundwater composition. This value represents a plausible estimation of the redox state of the unsaturated zone process in the groundwater system in the northern parts of the area. Organic matter degradation results indicated that an estimated amount of 4.0×10^{-4} moles was sufficient to produce a

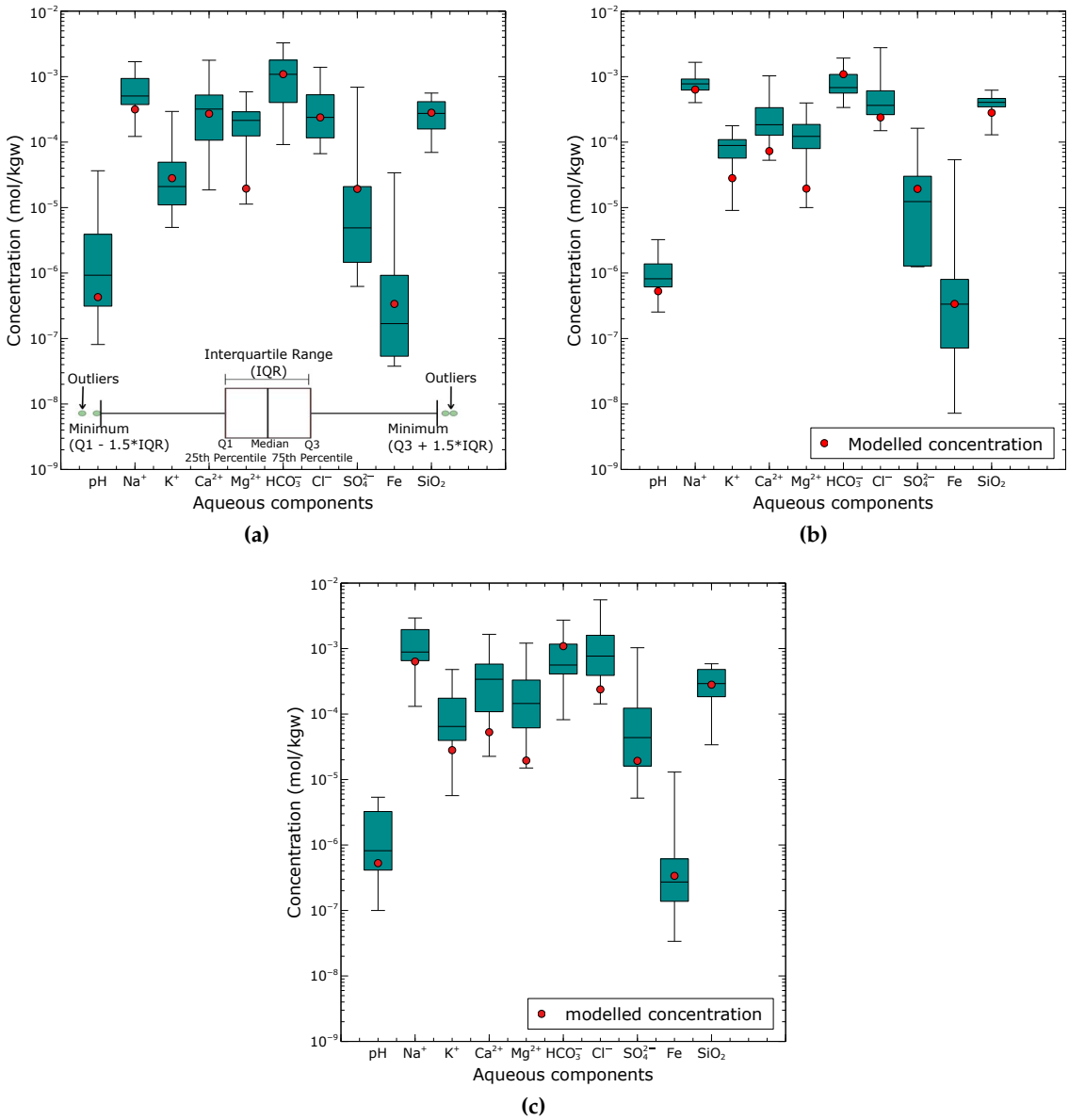

Figure 4.6: Comparison of the predicted aqueous groundwater components (red circles) from the reaction pathway calibration model and the range of observed composition (box plot) for the northern zone (**a**), central zone (**b**), and southern zone (**c**).

SO_4^{2-} concentration in the range of the observed groundwater composition in the northern zone (recharge area).

Figure 4.6b shows the results of the modelled groundwater composition for the central zone (Flowpath II) compared with the observed compositional ranges. Among the simulated aqueous components, pH, Na^+, HCO_3^-, Cl^-, SO_4^{2-}, Fe, and SiO_2 were closest to the observed median composition. In contrast, K^+, Ca^{2+}, and Mg^{2+} showed relatively low values relative to the median. Changes in the redox conditions did not show any significant effect on the simulated water composition.

Figure 4.6c presents the modelled groundwater composition of the southern zone compared with the observed aqueous concentrations. The simulated aqueous concentrations were within the observed compositional range. All aqueous components, except K^+, Ca^{2+}, Mg^{2+}, and Cl^-, showed minimal deviation from the median composition.

4.4 Discussion

The petrographic investigations on the outcrops showed the mineral composition of the rocks in the study area. Our simulation results indicate that the identified minerals are consistent with the general mineralogy of the Birimian meta-sedimentary rocks (Asiedu et al. 2004; Kesse 1985; Manu et al. 2013) and the Cape Coast granitoid (Kesse 1985; Leube and Hirdes 1986). In particular, our analysis indicates the alteration of primary minerals, such as biotite and K-feldspar, into secondary chlorite and sericite, which is consistent with previous studies (Kesse 1985; Manu et al. 2013). The meta-sedimentary rocks were also found to contain some minor traces of calcite, which were believed to have formed from the metamorphism of the sediments. This is broadly consistent with observations by Yidana et al. (2012b), suggesting that the phyllite and metagreywacke associated with the meta-sediments contain about 15% or more calcite.

Our modelling results enabled the identification of plausible minerals and a likely reaction path model that controls the chemical evolution of the groundwater. To the best knowledge of the authors, this is the first time an attempt has been made to provide specific minerals that influence the chemistry of the groundwater rather than use the generalizations derived from the classical interpretations of the hydrochemical data that suggest silicate mineral weathering as the dominant mineral reaction in the study area (Loh et al. 2021; Manu et al. 2023d; Tay et al. 2015). In this study, we found that the mineral phases predicted by our modelling were consistent with petrographic analyses. However, we did notice a discrepancy between our modelling results and observations for the recharge zone (Flowpath I from rainwater to the northern zone). With our inverse equilibrium model, we found no possible matching solution, thereby indicating that the mineral reactions may not be in equilibrium and that kinetic processes may be responsible for the observed discrepancy. Nevertheless, within the simulated results, we could deduce the probable mineralogy consistent with the petrographic results of the outcrop samples. The overall best-matched modelled results showed the equilibration of albite, $Fe(OH)_3$ and chalcedony in this zone. On the other hand, the central and the discharge zone (the other two Flowpaths II and III) resulted in distinct solutions that explain the observed water composition. This suggests that the reactions are predominantly controlled by thermodynamics in these zones. Our model outlines that, among the best-matched simulations, a frequency count can infer the most likely minerals that equilibrate with the groundwater. Groundwater migrating from the northern zone is likely to equilibrate with albite, plagioclase, $Fe(OH)_3$, and chalcedony to produce the groundwater chemical composition of the central zone (Flowpath II). These predicted minerals are consistent with field data indicating the presence of primary albite and plagioclase in the rock formation. Similar results have been reported by Adiaffi et al. (2016). Water flowing from the central to the southern zone (Flowpath III) is equilibrated with anorthite, chalcedony, and chlorite.

Concerning our assumptions, and in particular those of thermodynamic equilibrium, we have to recognize that the northern recharge zone (Flowpath I) requires additional hypotheses and degrees of freedom in order for the calibration to agree with the observations. We argue that the formation water residence time in the rock was probably not long enough to reach equilibrium and that the reactions are kinetically controlled. Given this additional hypothesis, it was necessary to assess the influence of the infiltration processes in the soil and the unsaturated zone before the water entered the aquifer to interact with the rocks. We propose here that the excess HCO_3^- may arise from the reaction between CO_2 in the soil zone and the decomposition of organic matter, which could also account for the decrease in SO_4^{2-} concentration. In principle,

the CO_2 generated through the respiration of plant roots in the soil zone reacts with water (H_2O) to generate a weak carbonic acid that dissociates and releases H^+ into the solution (Appelo and Postma 2004; Freeze and Cherry 1979). The presence of H^+ combines with the CO_3^{2-} complex to form HCO_3^-. In our study, adding this step resulted in a significant increase in HCO_3^- from 2.07×10^{-4} mol/kw to 6.86×10^{-4} mol/kgw, which is well in line with the observed concentration. Regarding the additional SiO_2, the equilibration of the water with kaolinite in the unsaturated zone accounted for this deviation. Adiaffi et al. (2016) observed the same in the southeast of Ivory Coast in the sub-region.

The reduction in sulfate concentration in the groundwater, relative to rainwater, is primarily driven by the degradation of organic matter. The initial solution (rainwater) used in our study shows a high sulfate content and lower pH, which was attributed to the evaporation and oxidation of sulfur dioxide (SO_2) emissions from nearby industries. Remarkably, the sulfate content in the groundwater was found to be factor 10 lower than that of the rainwater. During our fieldwork, we also noted a foul smell of rotten eggs in three borehole samples within the northern zone, which indicated the presence of hydrogen sulfide (H_2S). The amount of H_2S remaining in the solution depends strongly on the amount of Fe (II) in the groundwater solution (Appelo and Postma 2005). Appelo and Postma (2005) emphasized that H_2S can undergo additional reactions with Fe-oxide surfaces, thereby leading to the formation of iron sulfide minerals, such as pyrite, which aligns with our models predicting pyrite as a secondary mineral. These findings suggest that reactions in the soil and the unsaturated zones play a significant role in the chemical evolution of the groundwater prior to recharge. We demonstrated that it is possible to calibrate the mineral assemblages using a reaction path model while taking extra hypotheses into account in the event that the presented combinatorial inverse model technique does not produce a reasonable outcome.

The weathering of silicate minerals controls the enrichment of major cations, including Na^+, K^+, Ca^{2+}, Mg^{2+}, and the anionic HCO_3^- in the groundwater system, with carbonate dissolution playing a subordinate role. Petrographic analysis of the outcrops indicated the predominance of silicate minerals, including plagioclase (albite and anorthite), muscovite (as K-mica), K-feldspar, and biotite (as phlogopite), which was further supported by our inverse equilibrium simulations, which revealed their dominant contribution to the groundwater system. With this in mind, the water–rock interactions along the flow path will likely result from the reactions involving these minerals in the presence of water. Manu et al. (2023d) and Tay et al. (2015) used a combined interpretation of ion plots and principal component analysis and showed that groundwater evolution in the Pra Basin is driven by the weathering of silicate minerals.

The results of the reaction path modelling indicate that the chemical behaviour of Na^+ along the flow path is mainly controlled by albite weathering. This finding is supported by the predicted mineral assemblages from the combinatorial inverse modelling, which indicate albite dissolution in the north and central zones. In the case of Ca^{2+}, our model results indicate that the dissolution of anorthite mainly controls its occurrence in the groundwater. The alteration of biotite into chlorite, as observed in the thin section analysis and further confirmed by the combinatorial inverse model along Flowpath III (southern zone), along with the consistent occurrence of chlorite in the 50 best-matched equilibrium models, play a crucial role in determining the fate of dissolved potassium. Magnesium appears to be the most challenging element in the system, which showed the greatest variation from the median concentration despite being within the reported compositional range. The dissolution of primary biotite (as

phlogopite) identified by the petrographic analysis is the most likely source that could explain the release of Mg^{2+} into the groundwater. However, just a handful of our equilibrium models predicted its occurrence, thus implying that additional processes, such as cation exchange, may contribute to the chemical behaviour of the Mg^{2+} in the aquifer system.

In relation to dissolved Fe, our equilibrium models consistently suggested the presence of $Fe(OH)_3$ as a chemically relevant mineral controlling the behaviour of Fe in the system. This is evident from its frequent occurrence among the overall best-matched simulations. On the other hand, chloride and sulfate exhibited conservative behaviour along the flow path from the recharge to the discharge point, which can be attributed to the absence of halite or sulfate-containing minerals in the area. While sulfate could potentially be released from pyrite oxidation, our equilibrium models predicted pyrite as a secondary mineral, thus aligning with the field observations.

In contrast, the influence of carbonate mineral dissolution on groundwater chemistry was minimal, as demonstrated by our models. Although calcite is present in the terrain, based on our petrographic analysis, it rarely occurred in our simulated results, thus suggesting that it is a secondary mineral in the groundwater system. Our results are consistent with previous studies (Loh et al. 2021; Manu et al. 2023d; Okofo et al. 2021; Tay 2012; Tay et al. 2015) and provide a strong conclusion that the weathering of silicate minerals is the primary factor driving groundwater chemistry in the Pra Basin.

The water chemistry in the Pra Basin is heterogeneous. A recent cluster analysis performed by Manu et al. (2023d) revealed that the hydrochemical variation was indistinguishable based on geology, which led to the division into three clusters based on elevation differences. Hence, this makes understanding the factors controlling hydrochemistry quite difficult. To address this challenge, we had to work with an average description, and we assumed the median concentrations of the clusters as representations of the chemical composition. Our modelling results show that some aqueous components, such as K^+, Ca^{2+}, and Mg^{2+}, differed significantly from the target median ion composition. Despite these significant deviations from the median composition, all the simulated aqueous components fell within the range of the observed compositional values. This suggests that even based on an averaged heterogeneous water composition and scarce information about the mineralogy, distinct and concise reaction paths can be determined.

By leveraging aquatic chemistry, we have been able to bridge the knowledge gap and produce plausible predictions of mineralogy controlling the chemical evolution of the groundwater on a large basin scale. Even though an averaged water composition was used, the inverse models could come up with distinct "best" mineral assemblages reflecting the underlying geology. Our models produced plausible mineral assemblages, which varied across different zones of the flow path. However, we must acknowledge that we only collected a few outcrop samples at random locations in the terrain, which limited our knowledge of the minerals in the area. Therefore, we inferred the secondary minerals based on our understanding of possible weathering products of primary minerals, such as plagioclase, albite, and K-feldspar, without requiring detailed analysis. This allowed us to constrain the mineral phases in our model setup and predict their likely formation, which aligned with the observed composition. Overall, we conclude that knowing about aquatic chemistry is more critical than accurate knowledge of mineralogy, because it is easier to sample and measure.

A conceptual hydrogeochemical model for the Pra Basin was constructed based on the results of the combinatorial inverse and reaction path models (Figure 4.7). It shows the principal

assumption that the groundwater flows from a higher elevation in the northern zone through the centre of the basin to a lower elevation in the southern zone, which follows the topography. Rainwater is the main source of groundwater recharge, and its chemistry is affected by industrial activities in the area. The acidity of the rainwater is potentially controlled by SO_2 from fossil fuel combustion, which oxidizes and precipitates as dilute sulfuric acid. The chemistry of the rainwater is altered by evaporation, thus leading to changes in ion concentration and a subsequent decrease in the pH. Organic matter degradation is the primary mechanism driving sulfate/sulfide content in the groundwater. We assumed that, as water infiltrates the unsaturated zone, the equilibration of secondary hematite and kaolinite represents the "limiting concentration" for the unknown sources of Fe and Al. Groundwater chemistry changes along the subsurface flow path from the recharge to the discharge zones due to water–rock interactions. The influence of the vertical flow along the flow path has a negligible impact on the chemical composition of the groundwater. The groundwater in the northern, central, and southern zones could be reproduced under local thermodynamic equilibrium conditions. In the northern zone (recharge area), the dissolution of albite and $Fe(OH)_3$, along with the precipitation of chalcedony, are the most likely reactions affecting the dissolved ions. Similarly, the most probable reactions in the central zone are the dissolution of albite and $Fe(OH)_3$, as well as the precipitation of plagioclase and chalcedony. In the southern zone, which serves as the discharge area, anorthite has been observed to dissolve, while chalcedony and chlorite precipitate. These reaction patterns highlight the key processes occurring in each zone to maintain the chemical balance of the groundwater system.

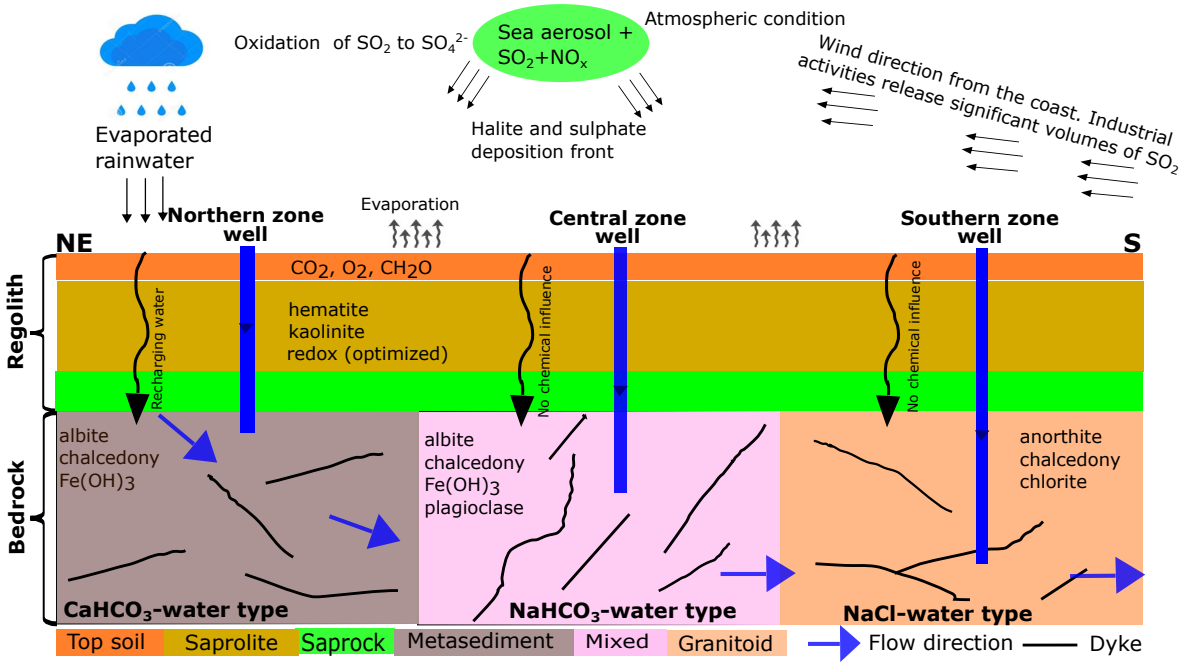

Figure 4.7: Conceptual model of hydrogeochemical evolution and groundwater flow path in the crystalline basement aquifer system of the Pra Basin in Ghana. Groundwater is assumed to flow from the northeast to the south of the basin.

4.5 Model Limitations

The use of average groundwater compositions to represent different zones along a flow regime and thermodynamic equilibrium assumptions to generate realistic mineral assemblages may have drawbacks. Because the hydrochemical data in this study exhibits a high degree of

variability, employing the average water composition may oversimplify the variability in each of the three zones. As a result, if the water composition range is too wide, there may be significant differences between the simulated and observed values.

In addition, since some reactions are likely to be kinetically controlled, the model assumption based on thermodynamic equilibrium may not accurately reflect the true natural state. This could alter the predicted mineral assemblages by affecting mineral dissolution and precipitation rates.

It is important to mention that the modelling approach used in this study considered pure phases from a stoichiometric perspective. However, this can result in discrepancies for certain elements, particularly in the case of clay minerals such as chlorite.

Another drawback of our model is the absence of cation exchange, which can have a considerable impact on the amounts of Na^+, K^+, Ca^{2+}, and Mg^{2+} in the simulated groundwater. We found significant differences in the concentrations of K^+, Ca^{2+}, and Mg^{2+} in the final simulated groundwater solution, especially in the southern zone. These disparities may be linked to the influence of cation exchange, which likely controls the amount of these minerals in the aquifer system.

4.6 Conclusions

The present study successfully implemented sequential geochemical numerical simulations to understand the chemical evolution of groundwater in a heterogeneous basin-scale environment. A combinatorial inverse modelling approach was employed to determine the most likely mineral assemblage in equilibrium. The mineral assemblages were further calibrated through reaction path modelling to elucidate the changes in groundwater composition along the flow path. Our findings allow for the following conclusions:

1. The plausible mineral assemblages that best explain the chemical composition of the groundwater in the Pra Basin have been identified. These mineral assemblages, including albite, chalcedony, and $Fe(OH)_3$ for the northern zone, albite, chalcedony, $Fe(OH)_3$, and plagioclase for the central zone, and anorthite, chalcedony, and chlorite for the southern zone, were found as plausible mineral assemblages governing the dissolved ions in the groundwater, and these assemblages align with petrographic information from outcrops.
2. Groundwater chemistry is governed by silicate mineral weathering, with the dissolution of carbonate minerals playing a subordinate role. Based on the results of the combinatorial inverse modelling, it is clear that the majority of the mineral phases commonly found in the models are silicates, including primary albite, anorthite, plagioclase, phlogopite, K-mica, and K-feldspar, as well as secondary chlorite, kaolinite, chalcedony, and quartz. Our model results rarely predicted the occurrence of calcite in the 50 best-matched solutions, thus suggesting that carbonate minerals have less impact on the basin's groundwater composition.
3. The degradation of organic matter primarily controls the reduction in sulfate in the groundwater. This is supported by the observed foul smell of rotten eggs in some of the sampled wells, which indicated the presence of hydrogen sulfide (H_2S). Additionally, our modelling results indicate the formation of pyrite, which occurs when H_2S produced from organic matter degradation reacts with the dissolved Fe(II) in the groundwater.
4. The simulation results revealed that accurate knowledge of aquifer mineralogy is less important than aquatic chemistry, which fortunately is easier to sample and measure.

Average water compositions are sufficient to successfully "bridge" the knowledge gap on the large basin scale to come up with distinct "best" mineral assemblages. By leveraging aquatic chemistry, we were able to produce plausible predictions of the mineralogy on a large basin scale with limited knowledge of the mineral compositions obtained from the petrographic analysis of some outcrops in the study area.

5. Equilibrium-based thermodynamic concepts of water–rock interactions were used to quantify the observed hydrochemical variations. However, we acknowledge that the northern zone (Flowpath I), which is assumed to be the recharge area, required additional hypotheses to match the observed composition, thus pointing towards kinetic effects during water–rock interactions. The results of our models emphasized the equilibration of the initial rainwater with the partial pressure of CO_2 ($10^{-1.7}$ atm), followed by the subsequent equilibration of the resulting solution with kaolinite, hematite, and redox optimization (pe = 3.5). Additionally, the calibrated model accounted for the reaction with 4.0×10^{-4} moles of organic matter.
6. A combined interpretation of the combinatorial inverse and reaction path models allowed for the successful development of a conceptual framework of the hydrochemical evolution for the Pra Basin. Based on our models, the main source of groundwater recharge in the Pra Basin is rainwater that has undergone some degree of evaporation. Our hypothesis of geochemical equilibrium among specific mineral assemblages explains the chemical evolution of groundwater from the point of recharge to the point of discharge. Our modelling results indicate that specific reactions play a crucial role in controlling the groundwater evolution in different zones of the basin. In the northern zone, the equilibration of albite, $Fe(OH)_3$, and chalcedony is highlighted as the primary reaction influencing the groundwater chemistry. The equilibration involving albite, $Fe(OH)_3$, plagioclase, and chalcedony is identified as an important factor for the central zone. In the southern zone, the equilibrium of anorthite, chalcedony, and chlorite is significant for understanding the groundwater composition.

Overall, our study provides a concept of the chemical evolution of groundwater in a basin-scale environment. Our findings have implications for the groundwater resource management in the Pra Basin, and our numerical modelling workflow can be applied in similar regions with large heterogeneity in water chemistry and limited knowledge of aquifer mineralogy.

4.7 Appendix

4.7.1 Additional Mineral Phases Included in the `phreeqc.dat` Thermodynamic Data Base

Below is the list of mineral phases, their governing equations, and the thermodynamic equilibrium constants used in the combinatorial inverse and reaction path modelling. The data were adopted from the `phreeqc.dat` thermodynamic database. The fixed stoichiometry plagioclase equation and equilibrium constant was derived by weighted averaging of the sodium plagioclase (albite) and the calcium plagioclase (anorthite) using the observed geochemical data from the available outcrops.

Table 4.2: List of additional phases included in the `phreeqc.dat` database for the simulations.

Mineral	**Chemical Equation**	$\mathbf{log_{10}K_{25}}$
Phlogopite	$KMg_3(AlSi_3)O_{10}(OH)_2 + 10\,H^+ = 1\,Al^{+3} + 1\,K^+ + 3\,Mg^{+2} + 3\,H_4SiO_4$	41.08
Plagioclase	$Na_{0.62}Ca_{0.38}Al_{1.38}Si_{2.62}O_8 + 8H_2O = 0.62Na^+ + 0.38Ca^{+2} + 1.38Al(OH)_4^- + 2.62H_4SiO_4$	−18.65
Organic matter	$CH_2O + H_2O = 4\,e^- + 4\,H^+ + CO_2$	4.80

Chapter 5

Discussion

A baseline hydrochemical and isotopic data for the Pra Basin have been presented in this dissertation. While there have been localized studies in specific areas like the Lower Pra, Lake Bosumtwi, Obuasi, Kumasi, and some parts of the eastern region of Ghana (Duncan 2020; Duncan et al. 2018; Ganyaglo et al. 2010; Golow and Mingle 2003; Loh et al. 2021; Loh et al. 2022; Okofo et al. 2021; Tay et al. 2017; Tay et al. 2015; Tay et al. 2014), the findings in this dissertation fill the knowledge gap by providing regional data on the Birim and the Lower Pra sub-catchments for a more holistic understanding of surface water and groundwater quality and their evolution in the Pra Basin. The hydrochemical data including pH, Na^+, K^+, Ca^{2+}, Mg^{2+}, Cl^-, HCO_3^-, SO_4^{2-}, NO_3^-, Ba, Fe, Mn, dissolved oxygen (DO), temperature and electrical conductivity of 90 water samples sourced from boreholes (56) and rivers (34) are presented. Stable oxygen ($\delta^{18}O$) and hydrogen (δ^2H) isotope ratios are also provided for all the sampled waters. This dissertation also contains mineralogical and chemical information from outcrop samples from the terrain. All the data mentioned can be found in Manu et al. (2023e) as well in the Appendices 2.6 and 4.7 in **Chapter 2** and **Chapter 3**, respectively.

The overall research objective is to gain insight into the processes that determine the hydrogeochemical evolution of groundwater quality in the Pra Basin. The specific objectives include (1) determining the origin, recharge processes and flow path of groundwater and quantifying the recharge amount using the Chloride Mass Balance (CMB) and Water Table Fluctuation (WTF) methods, (2) assessing the hydrochemistry of the Pra Basin to understand the regional variability in quality and the geochemical processes affecting its evolution, (3) determine the plausible mineral assemblages driving the chemical evolution of groundwater in the Pra Basin. The publications presented in the previous chapters elucidate the sources and quantification of groundwater recharge (**Chapter 2**), the regional hydrochemical variability (**Chapter 3**), mechanisms governing the chemical development and plausible mineral assemblages that control the groundwater evolution (**Chapter 4**). A combined interpretation of the results allowed the development of a conceptual hydrogeochemical model that significantly improves the current knowledge of the hydrochemistry in the basin. It became clear that surface water is unsuitable for drinking and irrigation purposes, while groundwater can be used. The chemical composition of groundwater is governed by water-rock interactions, with silicate weathering being the dominant process. Mineral assemblages, including albite, anorthite, plagioclase, chalcedony and potassium feldspar, are identified as plausible minerals that explain the field conditions under the local thermodynamic equilibrium hypothesis. The following points arise for the discussion of the main findings to assess the water quality and its chemical evolution in the Pra Basin:

1. Water quality and groundwater recharge dynamics.
2. Complexities of identifying the conceptual groundwater flow path.
3. A novel model for the assessment of water quality evolution.
4. Implications for water resources management in the Pra Basin.

5.1 Water Quality and Groundwater Recharge Dynamics

As presented in this work, groundwater quality was found to be of generally good quality for drinking and irrigation purposes, except in the northern zone where elevated Mn and Fe levels predominate, requiring treatment before use. Conversely, surface water quality has deteriorated and is no longer suitable for drinking. Nevertheless, it can be used for irrigation with filter systems to reduce water turbidity. It is important to note that the quality assessment of this study is based solely on the analysis of the major ions, including Na^+, K^+, Ca^{2+}, Mg^{2+}, Cl^-, HCO_3^-, SO_4^{2-}, NO_3^-, Ba, Mn and Fe (total). A known problem is the lack of data on mercury (not measured in this study), often used by illegal miners in gold extraction. Existing literature indicates a potential risk of mercury contamination in surface waters in areas where illegal mining activities occur (Donkor et al. 2006; Duncan 2020; Faseyi et al. 2022a; Faseyi et al. 2022b; Klubi et al. 2018). Therefore, it is important to consider heavy metals such as lead (Pb), mercury (Hg), cadmium (Cd) and copper (Cu) to improve the basin's water quality assessment. Another problem is the lack of seasonal data on water quality parameters. The study carried out a one-time sampling in 2021 and determined the regional quality status for this year alone. Since groundwater recharge occurs through surface infiltration of precipitation and surface water, the water quality will likely continue to deteriorate due to the transport of contaminants, which may contradict this study's conclusions. In view of this, additional sampling campaigns are essential to ensure adequate water management and generate seasonal water quality data, thereby improving the understanding of water quality's temporal and spatial dynamics across the catchment. Despite the limited parameters used in the assessment, all major ionic components in the surface water and groundwater meet WHO standard limits for drinking water (WHO 2017), except elevated Fe and Mn levels, which primarily affect water quality in the northern zone.

Concerning groundwater recharge, this study emphasizes the significant potential for water supply throughout the entire Pra Basin (Manu et al. 2023b). This claim is based on the results of the Chloride Mass Balance (CMB) and Water Table Fluctuation (WTF) methods used to estimate recharge. There may be inaccuracies in recharge estimates due to the inherent assumptions in their application (Eriksson and Khunakasem 1969; Marei et al. 2010). In the utilization of the CMB, the assumption was made that the unsaturated zone contains no chloride in storage (McNamara 2005; Obuobie et al. 2010), which may not hold, especially in the southern zone closer to the sea. In this region, research has shown that groundwater chemistry is influenced by marine aerosols (Ganyaglo et al. 2010; Manu et al. 2023b) deposited on the land surface, which is likely to accumulate in the unsaturated zone. Elevated chloride concentrations could lead to underestimating groundwater recharge using the CMB method (Duah et al. 2021; Obuobie et al. 2010). Regarding the WTF, no specific information on the specific yield of the underlying geology was available, and its value was derived from literature (Duah et al. 2021), introducing potential errors in the estimated recharge values (Obuobie et al. 2012a).

Despite these limitations, the estimated recharge values can be useful in constructing a numerical groundwater flow model where recharge estimates serve as initial constraints. The classical methods, such as CMB and WTF, do not consider other components of the catchment's water balance, including evaporation and contributions from surface fluxes. It is envisaged that groundwater flow models would provide reliable results for a more precise estimate of groundwater recharge. Such models can potentially account for various water use scenarios, including the impact of climate change on recharge from precipitation and its impact on regional

groundwater levels. Furthermore, groundwater usage scenarios for domestic, irrigation and industrial purposes and their influence on the available amount of groundwater in the study area could be investigated. These aspects, which are not addressed in the present study, are essential for understanding groundwater availability in the catchment. As a result, the study's assertion that groundwater is abundant lacks conclusive evidence and is inadequate for implementing a comprehensive regional water management plan for the basin.

5.2 Complexities of Identifying the Conceptual Groundwater Flow Path

Figure 3.3 illustrates the chemical distribution of water samples, demonstrating considerable variability in major ion concentration. This study employed multivariate statistical analysis to make sense of this diverse chemical data. In **Chapter 3**, an unsupervised hierarchical clustering analysis (HCA) and principal component analysis (PCA) were utilized to uncover natural associations and potential chemical reaction influences on the water samples. The results of the HCA (Figure 3.7A and B) underlined three groupings unrelated to the lithology and without clear spatial groupings, posing challenges in discerning a feasible flow path essential for the understanding of the evolution of the groundwater chemistry in the study area. To address this, an assumption was made based on the structural orientation of the underlying geology, trending northeast to southwest (Kesse 1985), and the premise that groundwater flow mirrors the topography, suggesting a similar trend in the study region. The assumption was driven by the lack of accessible lithological records and groundwater head data to map the groundwater flow path accurately. Furthermore, insights from the Piper plot (Figure 3.10) supported this hypothesis, suggesting a potential evolution based on the prevalent water types, $Ca-HCO_3$, $Na-HCO_3$, and NaCl—in distinct regions of the basin, namely the northern (recharge zone), central (transition zone), and southern (discharge zone) parts. This is further corroborated by the results of the PCA (see Table 3.3), which revealed a strong positive correlation between Ca^{2+} and HCO_3^- in the northern recharge zone and Na^+ and Cl^- in the southern discharge zone (Manu et al. 2023a). Given these considerations, surface elevation data were integrated as an additional feature to refine the cluster analysis. This modification was intended to categorize the highly variable chemical data based on differences in elevation and serve as a proxy for this study's hypothesized groundwater flow path. Here, the median water composition for the samples within each of the three identified groups was adopted as representative samples for the three zones along the flow path. In this context, the cluster analysis results are significant as they determine the most likely median composition for the simulation. Inaccurate results from the clustering analysis could potentially introduce bias into the representation of the samples, consequently leading to errors in the model output. Therefore, ensuring the accuracy and reliability of the clustering analysis is paramount to obtaining better results from the simulation. Although the HCA was used, there is potential for further exploration with other unsupervised machine learning algorithms, such as K-Means, K-Medoids, Gaussian Mixture, and Density-Based Spatial Clustering of Applications with Noise (DBSCAN), to refine the partitioning of data points within each cluster, thus enhancing the quality of the representative samples used. For example, the K-Medoids clustering technique is known for its robustness in dealing with nonlinear clusters and its resilience to outliers (Arora, Varshney, et al. 2016). Exploring these additional clustering techniques could provide deeper insights into the chemical variability and spatial distribution of the groundwater samples.

It's important to note that the assumed conceptual flow path for the model implementation may have some drawbacks regarding the limited understanding of the flow regime and the hydrogeology of the basin. The Pra Basin is characterized by metamorphosed sedimentary rocks in the northern and central regions (Banoeng-Yakubo et al. 2010). These rocks derive their permeability from extensive fractures, typical of the Birimian meta-sediments. Considering these intricacies, a more resilient method integrating groundwater dating using environmental tracers (SF6, CFC-11, CFC-12) could provide valuable insights into the groundwater flow dynamics of the basin (Okofo et al. 2022; Zango et al. 2023). This approach would categorize water into distinct age groups, facilitating the identification of recharge and discharge source points within the regional flow system. Moreover, employing numerical groundwater flow modelling—a state-of-the-art tool—could enhance comprehension of the basin flow dynamics, particularly in assessing the continuity between the Birimian meta-sediments and the granitoid. It's essential to recognize that the regionalization of the conceptual framework thus far has been conducted as a test case, given the absence of available lithological and groundwater head records of the underlying geology.

5.3 A Novel Model for the Assessment of Water Quality Evolution

This dissertation integrates field observations and numerical simulations to understand the hydrogeochemical evolution of groundwater in the Pra Basin of Ghana. Specifically, the geochemical reaction module PHREEQC (Parkhurst and Appelo 2013) was coupled with R (De Lucia and Kühn 2021) and in combination with the thermodynamic database phreeqc.dat for simulation purposes. First, inverse geochemical modelling was applied to identify and quantify the likely mineral assemblages and reactions responsible for changes in groundwater chemical composition along a hypothetical flow path. Subsequently, the resulting mineral assemblages were further refined through reaction path modelling to simulate the compositional changes in the groundwater. The simulated aqueous components are additionally verified against field observations to establish the final calibrated mineral assemblages relevant to the chemical evolution process.

A novel combinatorial inverse modelling was developed to identify plausible mineral assemblages driving the chemical evolution of groundwater. In the classical inverse modelling approach, the calculations are based on a purely mass balance between the species involved in the reactions. This study used classical inverse modelling to determine the plausible mineral assemblages that dissolved or precipitated to explain chemical changes between end-member compositions. However, one major challenge was that there was no mole balance for Cl^- and SO_4^{2-}, preventing the models from converging to a reasonable solution. This was mainly caused by the absence of the mineral phases containing Cl^- and SO_4^{2-}. To address this issue, one approach taken was the inclusion of mineral phases containing Cl^- and SO_4^{2-}, such as halite and gypsum, which are originally not found in the terrain by the petrographic analysis performed on the outcrop samples (Manu et al. 2023c). This approach was adopted by Garrels and MacKenzie (1967), one of the original inverse models performed on the Siera Spring Waters. In their study, the authors emphasized the other mineral reactions and the differences between a shorter and a longer flow path without necessarily accounting for the influence of halite and gypsum. In this context, a fundamental question arises: why introduce mineral phases that do not match the mineralogical composition of the underlying geology or increase the

uncertainty of an element to provide enough degrees of freedom of adjustment to achieve a mole balance? To obtain a model solution without including phases containing Cl^- and SO_4^{2-}, the combinatorial inverse modelling, which works under the assumption of local thermodynamic equilibrium, was developed to "successively integrate field observations into models and then calibrate them with known geochemical boundary conditions" (Manu et al. 2023c). In a combinatorial modelling approach, all combinations of plausible mineral assemblages are computationally screened, given a known aquifer mineralogy. Based on the assumption of local thermodynamic equilibrium, it is hypothesized that groundwater with longer residence time is more likely to have enough ions dissolved in the solution to be in equilibrium. Within the central and southern zones, where groundwater is presumed to have undergone substantial interactions with aquifer materials, the combinatorial inverse simulations yielded optimal model outcomes (see Figure 4.5) that fairly explain the observed field conditions (Manu et al. 2023c).

Combinatorial inverse modelling results show that water-rock interactions can generally be quantified assuming local thermodynamic equilibrium, except for the recharge zone, where alternative hypotheses are required to reproduce the observed composition. Petrographic studies of outcrop samples revealed the distribution of silicate minerals, including albite, plagioclase, potassium feldspar, biotite, and muscovite, as primary minerals that likely undergo alteration to produce secondary products such as kaolinite, chlorite, and quartz. The mineral assemblages determined from the combinatorial inverse modelling coincide with the observed field conditions and predict the aqueous components that agree fairly well with the observations. The ionic chemical composition of groundwater was found to be generally low. This is consistent with the general knowledge that the weathering of silicates is a slow process that requires a significant amount of time for the ions to dissolve into the solution (Appelo and Postma 2005; Merkel et al. 2005). These observations largely support previous studies (Loh et al. 2021; Okofo et al. 2021; Tay et al. 2015) that used classical bivariate ion diagrams, suggesting that silicate weathering is the primary process driving groundwater chemical evolution in the Pra Basin. However, no model solution adequately matched all observed aqueous components in the northern zone, identified as the recharge zone. This suggests that equilibrium conditions cannot explain chemical evolution and that other processes, such as kinetic reactions, may exert control over the chemical reactions in the northern recharge zone. Additional hypotheses were tested using reaction path modelling to overcome this apparent contradiction. This involves the reaction of initially evaporated rainwater with CO_2 in the soil zone, which increased the HCO_3^- ions in the infiltrated water, followed by the equilibration with kaolinite and hematite in the saprolite zone, acting as limiting reactions to control SiO_2 and Fe concentrations during infiltration in the unsaturated zone and organic matter degradation to control the sulfate concentration in the groundwater. By incorporating these processes and ensuring equilibrium with the identified optimal mineral composition obtained from combinatorial inverse modelling, the model reproduced the observed concentrations satisfactorily (Manu et al. 2023c).

Model calibration using reaction path modelling consistently reproduces the observed composition, with modelled results within the observed composition range. However, significant deviations were observed for Ca^{2+}, Mg^{2+}, Na^+ and K^+ compared to the average composition assumed for the simulation (see Figure 4.6). These differences may be due to several factors, including interactions with surface water and the non-stoichiometric nature of real minerals as opposed to pure end-members presented in the thermodynamic models. Moreover, the consideration of surface water mixing along the flow path, which may result from discharge into groundwater as baseflow, was not considered in the simulation. Stable

isotope analysis of surface water and groundwater and water level fluctuations in monitored groundwater and precipitation patterns highlight a possible interaction between the two water sources. Nevertheless, further studies are needed to understand these interactions adequately. The results of the reaction path model show that the cations consistently exhibit underestimation with respect to the median composition, which can likely be improved by incorporating surface water mixing.

In addition, it is worth noting that the idealized mineral phases in the PHREEQC thermodynamic database (phreeqc.data) are rare in nature, as naturally occurring minerals may contain some trace and common elements (Merkel et al. 2005), which are likely to influence the final simulated composition. In an ideal approximation, the activities of the pure end-member minerals in the solid phase are no longer treated as a unit but are equal to the mole fraction. For example, this study used the albite and anorthite end members in a specific stoichiometric coefficient with the average equilibrium constants to generate a plagioclase phase, which was not originally included in the phreeqc.dat database. The problem is that, in most cases, this idealized approximation is not very good and may not represent the correct chemical reactions needed to achieve better-matching results. Although there are some corrections for the non-ideal behaviour in PHREEQC under the solid solutions feature, this requires additional data that may or may not be available. This is largely because some solid solutions may sometimes exclude certain mixing combinations, for example, Na-K-Ca fractions in feldspars. In this case, the underestimation of the Na^+, K^+, and Ca^2+ cations can be partially attributed to this phenomenon.

5.4 Implications for Water Resources Management in the Pra Basin

The primary goal of water resource management is to ensure an adequate supply of water of the required quality standards to support human livelihood and aquatic ecosystems while maintaining overall ecological balance. Water quality for drinking and irrigation purposes was assessed for surface water and groundwater in the Pra Basin. The water quality assessment presented in Manu et al. (2023d) provides basic information at the regional level for further hydrochemical assessment including water quality monitoring and reactive transport modelling. It has been found in Manu et al. (2023d) that surface water for irrigation and drinking purposes is of poor quality. Contrary to the surface water, groundwater quality for drinking and irrigation purposes has been found to be of good quality (Manu et al. 2023d); However, in the northern zone of the study area, high levels of manganese and iron were found in some groundwater samples, indicating possible contamination from the polluted surface water. Hence, including trace metals like iron, manganese, and particularly mercury is crucial for a comprehensive evaluation of water quality intended for drinking and irrigation within the basin. As demonstrated by Manu et al. (2023d), these elements play a pivotal role in rendering the water unfit for utilization. Such an all-encompassing assessment of water quality holds significant potential in facilitating meticulous planning and sustainable management strategies for ensuring water supply in the region.

As highlighted in Manu et al. (2023b), the study underscored the vast groundwater recharge potential that can serve as a viable alternative following the deterioration of the surface water quality, which historically served as the primary source of water supply in the basin. The research by Obuobie et al. (2012b), employing the Falkenmark indicator

method, assessed the vulnerability of the Pra Basin to water stress conditions. The authors concluded that even without considering climate change, the basin was already water-stressed and was projected to attain water scarcity by 2020 and absolute scarcity by 2050. Notably, their analysis focused on surface water resources and the impact of climate change. Given the current scenario of widespread surface water pollution due to illegal mining activities, the source of the water supply has been shifted to groundwater resources (Asare 2021; Bessah et al. 2021; Darko et al. 2021; Donkor et al. 2006; Duncan 2020; Faseyi et al. 2022b; Klubi et al. 2018). This study (Manu et al. 2023b) has demonstrated the availability of substantial and quality groundwater reserves suitable for drinking purposes. Despite the lack of a quantitative assessment of regional groundwater using groundwater flow models, the presented groundwater recharge estimates using the Chloride Mass Balance (CMB) and Water Table Fluctuation (WTF) methods can aid in water planning and allocation strategies. While Manu et al. (2023b) provides valuable insights into groundwater recharge, groundwater flow models offer accurate quantitative recharge estimates in regional groundwater water budget assessment (Okofo and Martienssen 2022; Yidana et al. 2011). Consequently, the groundwater recharge estimates presented by Manu et al. (2023b) could serve as boundary conditions for these models. In the context of the Pra Basin, previous studies such as Yidana et al. (2011) and Oriakhi and Okonofua (2022) have demonstrated significant promise in harnessing groundwater resources through the utilization of calibrated steady-state groundwater flow models.

The northern zone of the study area is identified as the main recharge zone (Manu et al. 2023c). Isotope analysis revealed that groundwater recharge occurs mainly through precipitation, which evaporates from the land surface and seeps into the unsaturated zone. following the hypothetical flow path from north to south of the basin, the consistent predictions of the groundwater composition by the reaction path model provide robust substantiation to the assertion that the primary recharge zone lies within the northern domain (Manu et al. 2023c). This hypothetical groundwater flow path is consistent with the country's general northeast-southeast structural pattern (Banoeng-Yakubo et al. 2010; Kesse 1985). For water management reasons, the northern zone, as a recharge zone, requires measures to regulate activities, particularly widespread illegal mining, to prevent contamination of the aquifers from the polluted surface water

Chapter 6

Conclusions and outlook

Knowledge of the chemical evolution of groundwater is essential to ensure a safe and high-quality water supply for mankind. The chemical composition of groundwater is significantly influenced by a combination of natural geochemical processes and human activities that can impact water quality. Among the natural sources, water-rock interactions play a crucial role and include processes such as mineral dissolution and precipitation, cation exchange and sorption. Understanding these processes requires a state-of-the-art geochemical modelling workflow capable of quantifying the reactions and identifying plausible minerals that are involved. In many cases, multivariate statistics and classical ion plots are used to provide interpretations of hydrochemical data by inferring the mechanisms and processes on the basis of mere graphical interpretations. The main objective of this present work is to improve the knowledge of the hydrochemical processes driving the evolution of groundwater quality in the Pra Basin of Ghana. For that purpose, geochemical simulations based on the conceptual framework derived from the classical and statistical interpretations of the hydrochemical and isotopic data of surface water and groundwater are used. The three specific objectives that have been achieved are (1) the determination of the origin, recharge processes and estimation of groundwater recharge, (2) the assessment of the hydrochemistry of the Pra Basin to provide insight into spatial variation in surface water and quality and in geochemical processes affecting its evolution, and (3) the determination of plausible mineral assemblages and their reactions that control groundwater chemical evolution. The results presented in this thesis are the first step in providing regional hydrochemical and isotopic data and interpretations to aid in the sustainable management of water resources in the Pra Basin of Ghana.

Groundwater recharge occurs mainly in the northern zone and flows preferentially towards the southern parts of the basin (Chapter 2) and (Chapter 4). A linear regression analysis of the surface water and groundwater stable isotopes and the local meteoric waterline (LMWL) shows that groundwater samples are plotted close to the LMWL, suggesting that groundwater recharge occurs mainly from precipitation. This is reflected in the seasonal variation in the rise in water levels, which is mainly caused by precipitation. The estimated groundwater recharge for the basin averages 228 million m^3, exceeding the annual water requirement of 143.6 million m^3 for the entire Pra Basin, demonstrating huge groundwater potential for exploitation. The simulated groundwater compositions using the local thermodynamic equilibrium hypothesis along the defined flow regime (north-south) show good agreement with the observed concentration ranges and demonstrate a north-south groundwater flow regime from the recharge to the discharge zone.

Regarding water quality, groundwater is considered suitable for drinking and irrigation in most parts of the catchment area, except for the northern recharge zone, where high Mn and Fe concentrations are present in some boreholes. On the other hand, surface water was found to be of poor quality (Chapter 2). It was observed that the groundwater in the northern zone, designated as the main recharge zone, partially contains high levels of Mn and Fe, which can be interpreted as a consequence of possible contamination from the polluted surface water. This is inconclusive and may require further investigation to determine the influence of the

geology, which contains some significant amounts of Fe and Mn oxides. It is anticipated that the dissolution of these minerals might result in the leaching of Fe and Mn through water-rock interactions, leading to their excesses in the groundwater.

Water-rock interactions govern the chemical evolution of the groundwater in the Pra Basin. The initial statistical analyzes of the highly variable chemical data from the water samples using the cluster and factor analysis revealed three distinct groupings (referred to as northern, central and southern zones) representing three hydrochemical environments (Chapter 2). The combined interpretation of the combinatorial inverse and the reaction path models underlined the dominant contribution of silicate minerals, including albite, anorthite, plagioclase, potassium feldspar and chalcedony, as plausible mineral assemblages driving the dissolved ions in the groundwater (Chapter 4).

To assess water quality in the Pra Basin, a new model was developed that can be applied to other regions with similarly high levels of chemical variability in water chemistry. The models integrate field data, including water composition and mineral phases, to perform combinatorial screening under the local thermodynamic equilibrium hypothesis and determine plausible mineral assemblages that explain the chemical changes in water composition. This approach differs from the classical inverse geochemical models, which are based on calculating the mole transfer from a given mineral assemblage. This new model holds enormous potential for studying the chemical evolution of groundwater in a large basin-scale hydrochemical environment.

With rivers and other water resources facing pollution and the changing climate posing challenges, the reliance on groundwater as a dependable water supply in the region has grown significantly. To ensure sustainable management of groundwater, the implementation of integrated water resource management practices is urgently needed. This approach would require a clear understanding of the entire aquatic ecosystem, mainly determined by the quality and quantity of water resources available. This study provides basic information on water quality and its evolution and, therefore, requires additional work to fully achieve integrated water resource management objectives. Future investigations should focus on an integrated approach, implementing numerical groundwater and reactive transport models to understand surface water and groundwater interactions. The following points explain the specific works that need to be considered to improve further the knowledge of the dynamics of water resources in the catchment:

- So far, only the stable isotopes of groundwater have been used to understand the processes, including evaporation, mixing and transpiration impact on the infiltrating water before entering the aquifer. However, due to the complex and diverse nature of the terrain, establishing a dominant groundwater recharge process has proven difficult. Future research efforts should include the assessment of groundwater age dating and residence time. To achieve this, the integration of tracers such as sulfur hexafluoride (SF6) and chlorofluorocarbons (CFC-11, CFC-12) would be crucial to allow another dimension of delineation of the recharge and discharge areas and the impact of climate on groundwater recharge.
- Concerning assessing water quality for drinking and irrigation purposes, the current study concludes that groundwater is good quality for drinking and irrigation purposes except in the northern zone, which requires some treatment, while surface water is of poor quality. However, the data used in the analysis are measurements of the major ions as well as Fe (total) and Mn from a single sampling campaign.

Therefore, it is recommended that another sampling campaign be considered to compare the seasonal impact on water quality in the catchment. In all analyses, the study did not include measurements of Hg, a common metal used in gold extraction by illegal miners. Obtaining this information helps in the holistic assessment of the water quality in the catchment area.

- For quantitative groundwater assessment, we used classical Chloride Mass Balance (CMB) and Water Table Fluctuation (WTF) methods to provide estimates of groundwater recharge for the basin. These methods do not consider the contribution of surface water and evapotranspiration to obtain the best possible estimate of the regional water balance. Therefore, it is recommended to develop a fully integrated regional groundwater flow model to understand the water regime of the catchment better. This will facilitate the simulation of different water use scenarios and the assessment of climate change impacts on groundwater recharge.
- Incorporating reactive transport models would increase our understanding of the fate and transport of pollutants within the basin. Until now, all simulations in this study have been run under the local thermodynamic equilibrium hypothesis for geochemical reactions within a static system without considering hydraulic dynamics such as advection and dispersion. Introducing reactive transport models will offer an exciting opportunity to quantitatively assess the influx of pollutants from contaminated surface waters into the aquifer.

References

ADDAI M. O., YIDANA S. M., CHEGBELEH L.-P., ADOMAKO D. and BANOENG-YAKUBO B. (2016): Groundwater recharge processes in the Nasia sub-catchment of the White Volta Basin: Analysis of porewater characteristics in the unsaturated zone. *Journal of African Earth Sciences* 122, 4–14.

ADIAFFI B., MARLIN C., COULIBALY Y., OGA Y. M. S. and PICHON R. (2016): Hydrogeochemistry of Bedrock Groundwater in SE Ivory Coast. *Int. J. Emerg. Technol. Adv. Eng.* 6 (12), 1–14.

ADOMAKO D., MALOSZEWSKI P., STUMPP C., OSAE S and AKITI T. (2010): Estimating groundwater recharge from water isotope (δ2H, δ18O) depth profiles in the Densu River basin, Ghana. *Hydrological Sciences Journal–Journal des Sciences Hydrologiques* 55 (8), 1405–1416.

ADSIZ C., SKRZYPEK G. and MCCALLUM J. (2023): The measurement of ambient air moisture stable isotope composition for the accurate estimation of evaporative losses. *MethodsX* 11, 102265.

AFFUM A. O., DEDE S. O., NYARKO B. J. B., ACQUAAH S. O., KWAANSA-ANSAH E. E., DARKO G., DICKSON A., AFFUM E. A. and FIANKO J. R. (2016): Influence of small-scale gold mining and toxic element concentrations in Bonsa river, Ghana: A potential risk to water quality and public health. *Environmental Earth Sciences* 75 (2), 178.

AFRIFA G. Y., SAKYI P. A. and CHEGBELEH L. P. (2017): Estimation of groundwater recharge in sedimentary rock aquifer systems in the Oti basin of Gushiegu District, Northern Ghana. *Journal of African Earth Sciences* 131, 272–283.

AHIALEY E., SERFOH-ARMAH Y and KORTATSI B. (2010): Hydrochemical Analysis of Groundwater in the Lower Pra Basin of Ghana.

AKITI T. (1986): Environmental isotope study of ground water in crystalline rocks of the Accra plains (Ghana), In: 4th Working Meeting on Isotopes in Nature. *Proceedings of an Advisory Group Meet- ing, IAEA, Vienna*.

AKOTO O and ADIYIAH J (2007): Chemical analysis of drinking water from some communities in the Brong Ahafo region. *International Journal of Environmental Science & Technology* 4 (2), 211–214.

AKOTO O, DARKO G and NKANSAH M. (2011): Chemical composition of rainwater over a mining area in Ghana. *International Journal of Environmental Research* 5 (4), 847–854.

ALLISON G. and LEANEY F. (1982): Estimation of isotopic exchange parameters, using constant-feed pans. *Journal of Hydrology* 55 (1), 151–161.

ALLISON L. E. and RICHARDS L. A. (1954): *Diagnosis and improvement of saline and alkali soils*. 60. Soil and Water Conservative Research Branch, Agricultural Research Service ...

AMONOO-NEIZER E. H. and AMEKOR E. (1993): Determination of total arsenic in environmental samples from Kumasi and Obuasi, Ghana. *Environmental health perspectives* 101 (1), 46–49.

ANDREASEN M., ANDREASEN L. A., JENSEN K. H., SONNENBORG T. O. and BIRCHER S. (2013): Estimation of regional groundwater recharge using data from a distributed soil moisture network. *Vadose Zone Journal* 12 (3).

ANKU Y. S., BANOENG-YAKUBO B., ASIEDU D. K. and YIDANA S. M. (2009): Water quality analysis of groundwater in crystalline basement rocks, Northern Ghana. *Environmental Geology* 58 (5), 989–997.

APOLLARO C, FUOCO I, BLOISE L, CALABRESE E, MARINI L, VESPASIANO G and MUTO F (2021): Geochemical modeling of water-rock interaction processes in the Pollino National Park. *Geofluids* 2021, 1–17.

APPELO C. A. J. and POSTMA D. (2004): *Geochemistry, groundwater and pollution*. CRC press: London, United Kingdom.

APPELO C. and POSTMA D. (2005): Geochemistry, groundwater and pollution. 2nd. *Ed. Balkema, Rotterdam*.

ARMAH F. A., QUANSAH R. and LUGINAAH I. (2014): A systematic review of heavy metals of anthropogenic origin in environmental media and biota in the context of gold mining in Ghana. *International Scholarly Research Notices* 2014.

ARORA P., VARSHNEY S. et al. (2016): Analysis of k-means and k-medoids algorithm for big data. *Procedia Computer Science* 78, 507–512.

ASANTE-ANNOR A., ACQUAH J. and ANSAH E. (2018): Hydrogeological and hydrochemical assessment of basin granitoids in Assin and Breman Districts of Ghana. *Journal of Geoscience and Environment Protection* 6 (9), 31–57.

ASARE E. A. (2021): Impact of the illegal gold mining activities on Pra River of Ghana on the distribution of potentially toxic metals and naturally occurring radioactive elements in agricultural land soils. *Chemistry Africa* 4 (4), 1051–1068.

ASIEDU D. K., DAMPARE S. B., SAKYI P. A., BANOENG-YAKUBO B., OSAE S., NYARKO B. J. B. and MANU J. (2004): Geochemistry of Paleoproterozoic metasedimentary rocks from the Birim diamondiferous field, southern Ghana: Implications for provenance and crustal evolution at the Archean-Proterozoic boundary. *GEOCHEMICAL JOURNAL* 38 (3), 215–228. DOI: 10.2343/geochemj.38.215

AYERS R. S., WESTCOT D. W. et al. (1985): *Water quality for agriculture*. Vol. 29. Food and Agriculture Organization of the United Nations Rome.

BANKS D. and FRENGSTAD B. (2006): Evolution of groundwater chemical composition by plagioclase hydrolysis in Norwegian anorthosites. *Geochimica et Cosmochimica Acta* 70 (6), 1337–1355.

BANOENG-YAKUBO B, YIDANA S., AJAYI J., LOH Y and ASIEDU D (2010): Hydrogeology and groundwater resources of Ghana: a review of the hydrogeology and hydrochemistry of Ghana. Potable Water and Sanitation.

BANOENG-YAKUBO B, YIDANA S., AKABZAA T and ASIEDU D (2008): Groundwater flow modeling in the akyem area, southeastern, ghana.

BANOENG-YAKUBO B., YIDANA S. M., ANKU Y., AKABZAA T. and ASIEDU D. (2009a): Water quality characterization in some Birimian aquifers of the Birim Basin, Ghana. *KSCE Journal of Civil Engineering* 13 (3), 179–187.

BANOENG-YAKUBO B., YIDANA S. M. and NTI E. (2009b): An evaluation of the genesis and suitability of groundwater for irrigation in the Volta Region, Ghana. *Environmental Geology* 57 (5), 1005–1010.

BANOENG-YAKUBU B, YIDANA S., AJAYI J., LOH Y and ASEIDU D (2011): Hydrogeolog y and groundwater resources of Ghana: a review of the hydrogeology an d hydrochemistry of Ghana. *Potable Water and Sanitation* 142.

BARNES C. and ALLISON G. (1988): Tracing of water movement in the unsaturated zone using stable isotopes of hydrogen and oxygen. *Journal of Hydrology* 100 (1-3), 143–176.

BEMPAH C. K. and EWUSI A. (2016): Heavy metals contamination and human health risk assessment around Obuasi gold mine in Ghana. *Environmental monitoring and assessment* 188 (5), 261.

BENNEH G and DICKSON K. (1995): A New Geography of Ghana, Revised edition.

BERGESEN H. O., PARMANN G. and THOMMESSEN Ø. B. (2018): United Nations Framework Convention on Climate Change (UNFCCC). *Yearbook of International Cooperation on Environment and Development 1998–99*. Routledge, 73–77.

BESSAH E., RAJI A. O., TAIWO O. J., AGODZO S. K., OLOLADE O. O., STRAPASSON A. and DONKOR E. (2021): Assessment of surface waters and pollution impacts in Southern Ghana. *Hydrology Research* 52 (6), 1423–1435.

BETHKE C. M. (2022): *Geochemical and biogeochemical reaction modeling*. Cambridge university press: London, United Kingdom.

CARRIER M.-A., LEFEBVRE R, RACICOT J and ASARE E. B. (2008): Northern Ghana hydrogeological assessment project.

CHACHA N., NJAU K. N., LUGOMELA G. V. and MUZUKA A. N. (2018): Groundwater age dating and recharge mechanism of Arusha aquifer, northern Tanzania: application of radioisotope and stable isotope techniques. *Hydrogeology Journal* 26 (8), 2693–2706.

CHEBOTAREV I. (1955): Metamorphism of natural waters in the crust of weathering—1. *Geochimica et Cosmochimica Acta* 8 (1-2), 22–48.

CHEGBELEH L. P., AKURUGU B. A. and YIDANA S. M. (2020): Assessment of Groundwater Quality in the Talensi District, Northern Ghana. *The Scientific World Journal* 2020.

CHENINI I., ZGHIBI A. and KOUZANA L. (2015): Hydrogeological investigations and groundwater vulnerability assessment and mapping for groundwater resource protection and management: state of the art and a case study. *Journal of African Earth Sciences* 109, 11–26.

CIRCONE S. and NAVROTSKY A. (1992): Substitution of [6, 4] Al in phlogopite: high-temperature solution calorimetry, heat capacities, and thermodynamic properties of the phlogopite-eastonite join. *American Mineralogist* 77 (11-12), 1191–1205.

CRAIG H. (1961): Isotopic variations in meteoric waters. *Science* 133 (3465), 1702–1703.

CRAIG H., GORDON L. I. et al. (1965): Deuterium and oxygen 18 variations in the ocean and the marine atmosphere.

DAPAAH-SIAKWAN S and GYAU-BOAKYE P (2000): Hydrogeologic framework and borehole yields in Ghana. *Hydrogeology Journal* 8 (4), 405–416.

DARKO H. F., KARIKARI A. Y., DUAH A. A., AKURUGU B. A., MANTE V. and TEYE F. O. (2021): Effect of small-scale illegal mining on surface water and sediment quality in Ghana. *International Journal of River Basin Management*, 1–12.

DASSI L. (2010): Use of chloride mass balance and tritium data for estimation of groundwater recharge and renewal rate in an unconfined aquifer from North Africa: a case study from Tunisia. *Environmental Earth Sciences* 60 (4), 861–871.

DAVISSON M., SMITH D., KENNEALLY J and ROSE T. (1999): Isotope hydrology of southern Nevada groundwater: stable isotopes and radiocarbon. *Water Resources Research* 35 (1), 279–294.

DAWSON T. E., MAMBELLI S., PLAMBOECK A. H., TEMPLER P. H. and TU K. P. (2002): Stable isotopes in plant ecology. *Annual review of ecology and systematics* 33 (1), 507–559.

DE LUCIA M. and KÜHN M. (2021): Geochemical and reactive transport modelling in R with the RedModRphree package. *Advances in Geosciences* 56, 33–43.

DELIN G. N., HEALY R. W., LORENZ D. L. and NIMMO J. R. (2007): Comparison of local-to regional-scale estimates of ground-water recharge in Minnesota, USA. *Journal of Hydrology* 334 (1-2), 231–249.

DICKSON K. B., BENNEH G. and ESSAH R. (1988): *A new geography of Ghana*. Vol. 34. Longman London.

DOGRAMACI S., SKRZYPEK G., DODSON W. and GRIERSON P. F. (2012): Stable isotope and hydrochemical evolution of groundwater in the semi-arid Hamersley Basin of subtropical northwest Australia. *Journal of Hydrology* 475, 281–293.

DONKOR A., BONZONGO J., NARTEY V. and ADOTEY D. (2006): Mercury in different environmental compartments of the Pra River Basin, Ghana. *Science of the Total Environment* 368 (1), 164–176.

DORLEKU M., AFFUM A., TAY C. and NUKPEZAH D (2019): Assessment of nutrients levels in groundwater within the Lower Pra Basin of Ghana. *Ghana Journal of Science* 60 (1), 24–36.

DORLEKU M., NUKPEZAH D and CARBOO D (2018): Effects of small-scale gold mining on heavy metal levels in groundwater in the Lower Pra Basin of Ghana. *Applied Water Science* 8, 1–11.

DRAGON K. (2021): Identification of groundwater conditions in the recharge zone of regionally extended aquifer system with use of water chemistry and isotopes (Lwowek region, Poland). *Journal of Hydrology: Regional Studies* 34, 100787.

DREVER J. I. et al. (1988): *The geochemistry of natural waters*. Vol. 437. Prentice hall Englewood Cliffs: New Jersey, USA.

DUAH A. A., AKURUGU B. A., DARKO P. K., MANU E. and MAINOO P. A. (2021): Groundwater recharge and potential exploitation in the Densu basin, Southwestern Ghana. *Journal of African Earth Sciences* 183, 104332.

DUNCAN A. E. (2020): The dangerous couple: illegal mining and water pollution—a case study in Fena River in the Ashanti Region of Ghana. *Journal of Chemistry* 2020, 1–9.

DUNCAN A. E., DE VRIES N. and NYARKO K. B. (2018): Assessment of heavy metal pollution in the main Pra River and its tributaries in the Pra Basin of Ghana. *Environmental nanotechnology, monitoring & management* 10, 264–271.

DZIGBODI-ADJIMAH K. (1993): Geology and geochemical patterns of the Birimian gold deposits, Ghana, West Africa. *Journal of geochemical exploration* 47 (1-3), 305–320.

ELANGO L and KANNAN R (2007): Rock–water interaction and its control on chemical composition of groundwater. *Developments in environmental science* 5, 229–243.

ERIKSSON E. and KHUNAKASEM V. (1969): Chloride concentration in groundwater, recharge rate and rate of deposition of chloride in the Israel Coastal Plain. *Journal of Hydrology* 7 (2), 178–197.

FAN Y., CHEN Y., LI X., LI W. and LI Q. (2015): Characteristics of water isotopes and ice-snowmelt quantification in the Tizinafu River, north Kunlun Mountains, Central Asia. *Quaternary International* 380, 116–122.

FASEYI C., MIYITTAH M., SOWUNMI A. and YAFETTO L (2022a): Water quality and health risk assessments of illegal gold mining-impacted estuaries in Ghana. *Marine Pollution Bulletin* 185, 114277.

FASEYI C., MIYITTAH M., YAFETTO L, SOWUNMI A. and LUTTERODT G (2022b): Pollution fingerprinting of two southwestern estuaries in Ghana. *Heliyon* 8 (8).

FAYIGA A. O., IPINMOROTI M. O. and CHIRENJE T. (2018): Environmental pollution in Africa. *Environment, development and sustainability* 20 (1), 41–73.

FELLMAN J. B., DOGRAMACI S., SKRZYPEK G., DODSON W. and GRIERSON P. F. (2011): Hydrologic control of dissolved organic matter biogeochemistry in pools of a subtropical dryland river. *Water Resources Research* 47 (6).

FINCH J. (1998): Estimating direct groundwater recharge using a simple water balance model–sensitivity to land surface parameters. *Journal of Hydrology* 211 (1-4), 112–125.

FREEZE R. A and CHERRY J. (1979): *Groundwater*. Prentice Hall Inc. Englewood Cliffs, New Jersey, USA.

GANYAGLO S. Y., BANOENG-YAKUBO B., OSAE S., DAMPARE S. B., FIANKO J. R. and BHUIYAN M. A. (2010): Hydrochemical and isotopic characterisation of groundwaters in the eastern region of Ghana. *Journal of Water Resource and Protection* 2 (3), 199.

GAO Z., WANG Z., WANG S., WU X., AN Y., WANG W. and LIU J. (2019): Factors that influence the chemical composition and evolution of shallow groundwater in an arid region: a case study from the middle reaches of the Heihe River, China. *Environmental Earth Sciences* 78 (14), 1–15.

GARRELS R. M. and MACKENZIE F. T. (1967): Origin of the chemical compositions of some springs and lakes. ACS Publications.

GEBRU T. A. and TESFAHUNEGN G. B. (2019): Chloride mass balance for estimation of groundwater recharge in a semi-arid catchment of northern Ethiopia. *Hydrogeology Journal* 27 (1).

GIBRILLA A, BAM E., ADOMAKO D, GANYAGLO S, OSAE S, AKITI T., KEBEDE S, ACHORIBO E, AHIALEY E, AYANU G et al. (2011): Application of water quality index (WQI) and multivariate analysis for groundwater quality assessment of the Birimian and Cape Coast Granitoid Complex: Densu River Basin of Ghana. *Water Quality, Exposure and Health* 3 (2), 63–78.

GIBRILLA A., FIANKO J. R., GANYAGLO S., ADOMAKO D., STIGTER T. Y., SALIFU M., ANORNU G., ZANGO M. S. and ZAKARIA N. (2022): Understanding recharge mechanisms and surface water contribution to groundwater in granitic aquifers, Ghana: Insights from stable isotopes of δ2H and δ18O. *Journal of African Earth Sciences* 192, 104567.

GIBSON J. and REID R (2010): Stable isotope fingerprint of open-water evaporation losses and effective drainage area fluctuations in a subarctic shield watershed. *Journal of Hydrology* 381 (1-2), 142–150.

GOLOW A. and MINGLE L. (2003): Mercury in river water and sediments in some rivers near Dunkwa-on-Offin, an alluvial goldmine, Ghana. *Bulletin of environmental contamination and toxicology* 70 (2), 0379–0384.

GONFIANTINI R. (1986): Environmental isotopes in lake studies. *Handbook of environmental isotope geochemistry*.

GRABIĆ J., VRANEŠEVIĆ M., ZEMUNAC R., BUBULJ S., BEZDAN A. and ILIĆ M. (2019): Iron and Manganese in Well Water: Potential Risk for Irrigation Systems. *Acta Horticulturae et Regiotecturae* 22 (2), 93–96.

GROEN J, SCHUCHMANN J. and GEIRNAERT W (1988): The occurence of high nitrate concentration in groundwater in villages in Northwestern Burkina Faso. *Journal of African Earth Sciences (and the Middle East)* 7 (7-8), 999–1009.

GÜLER C. and THYNE G. D. (2004): Hydrologic and geologic factors controlling surface and groundwater chemistry in Indian Wells-Owens Valley area, southeastern California, USA. *Journal of Hydrology* 285 (1-4), 177–198.

HARBAUGH A. W., BANTA E. R., HILL M. C. and MCDONALD M. G. (2000): Modflow-2000, the u. S. Geological survey modular ground-water model-user guide to modularization concepts and the ground-water flow process.

HEALY R. W. and COOK P. G. (2002): Using groundwater levels to estimate recharge. *Hydrogeology journal* 10, 91–109.

HEM J. D. (1985): *Study and interpretation of the chemical characteristics of natural water*. Vol. 2254. Department of the Interior, US Geological Survey.

IBRAHIM H., YASEEN Z. M., SCHOLZ M., ALI M., GAD M., ELSAYED S., KHADR M., HUSSEIN H., IBRAHIM H. H., EID M. H. et al. (2023): Evaluation and prediction of groundwater quality for irrigation using an integrated water quality indices, machine learning models and GIS approaches: A representative case study. *Water* 15 (4), 694.

JUNNER N. (1940): Geology of the gold coat and Western Togoland. *Bull. Gold Coast Geol. Surv.* 11, 40.

KAISER H. F. (1960): The application of electronic computers to factor analysis. *Educational and psychological measurement* 20 (1), 141–151.

KAKA E., AKITI T., NARTEY V., BAM E. and ADOMAKO D (2011): Hydrochemistry and evaluation of groundwater suitability for irrigation and drinking purposes in the southeastern Volta River basin: Manya Krobo area, Ghana. *Elixir Agriculture* 39, 4793–4807.

KANKAM-YEBOAH K., OBUOBIE E., AMISIGO B. and OPOKU-ANKOMAH Y. (2013): Impact of climate change on streamflow in selected river basins in Ghana. *Hydrological Sciences Journal* 58 (4), 773–788.

KATILA P, COLFER C., DE J., GALLOWAY G, PACHECO P and WINKEL G (2019): Sustainable Development Goals:

KESSE G. O. (1985): *The mineral and rock resources of Ghana*. AA Balkema Publishers, Accord, MA.

KESSE G.O N. (1976): The manganese ore deposits of Ghana. , *Ghana Geological Survey Bulletin* 44.

KLUBI E., ABRIL J. M., NYARKO E. and DELGADO A. (2018): Impact of gold-mining activity on trace elements enrichment in the West African estuaries: The case of Pra and Ankobra rivers with the Volta estuary (Ghana) as the reference. *Journal of Geochemical Exploration* 190, 229–244.

KOFFI K. V., OBUOBIE E., BANNING A. and WOHNLICH S. (2017): Hydrochemical characteristics of groundwater and surface water for domestic and irrigation purposes in Vea catchment, Northern Ghana. *Environmental Earth Sciences* 76 (4), 185.

KORTATSI B. K. (2007): Hydrochemical framework of groundwater in the Ankobra Basin, Ghana. *Aquatic Geochemistry* 13 (1), 41–74.

LEE J.-Y., YI M.-J. and HWANG D. (2005): Dependency of hydrologic responses and recharge estimates on water-level monitoring locations within a small catchment. *Geosciences Journal* 9 (3), 277–286.

LEUBE A and HIRDES W (1986): The early Proterozoic (Birimian and Tarkwaian) of Ghana and some aspects of its associated gold mineralizations. *Ext. abstr. Geocongress* 86, 315–319.

LEUBE A., HIRDES W., MAUER R. and KESSE G. O. (1990): The early Proterozoic Birimian Supergroup of Ghana and some aspects of its associated gold mineralization. *Precambrian research* 46 (1-2), 139–165.

LI P.-y., QIAN H., WU J.-h. and DING J. (2010): Geochemical modeling of groundwater in southern plain area of Pengyang County, Ningxia, China. *Water Science and Engineering* 3 (3), 282–291.

LIGATE F., IJUMULANA J., AHMAD A., KIMAMBO V., IRUNDE R., MTAMBA J. O., MTALO F. and BHATTACHARYA P. (2021): Groundwater resources in the East African Rift Valley: Understanding the geogenic contamination and water quality challenges in Tanzania. *Scientific African* 13, e00831.

LIU J., GAO Z., WANG M., LI Y., MA Y., SHI M. and ZHANG H. (2018): Study on the dynamic characteristics of groundwater in the valley plain of Lhasa City. *Environmental Earth Sciences* 77 (18), 1–15.

LOH Y. S. A., ADDAI M. O., FYNN O. F. and MANU E. (2021): Characterisation and quality assessment of surface and groundwater in and around Lake Bosumtwi impact craton (Ghana). *Sustainable Water Resources Management* 7 (5), 1–18.

LOH Y. S. A., AKURUGU B. A., MANU E. and ALIOU A.-S. (2020): Assessment of groundwater quality and the main controls on its hydrochemistry in some Voltaian and basement aquifers, northern Ghana. *Groundwater for Sustainable Development* 10, 100296.

LOH Y. S. A., FYNN O. F., MANU E., AFRIFA G. Y., ADDAI M. O., AKURUGU B. A. and YIDANA S. M. (2022): Groundwater-surface water interactions: application of hydrochemical and stable isotope tracers to the lake bosumtwi area in Ghana. *Environmental Earth Sciences* 81 (22), 1–15.

LOVE A., HERCZEG A., ARMSTRONG D, STADTER F and MAZOR E (1993): Groundwater flow regime within the Gambier Embayment of the Otway Basin, Australia: evidence from hydraulics and hydrochemistry. *Journal of Hydrology* 143 (3-4), 297–338.

MACE R. E., CHOWDHURY A. H., ANAYA R. and WAY S.-C. T. (2000): A numerical groundwater flow model of the upper and middle Trinity Aquifer, Hill Country area. *Texas Water Development Board Open File Report 00-02*.

MANU E., DE LUCIA M. and KÜHN M. (2023a): Hydrochemical Characterization of Surface Water and Groundwater in the Crystalline Basement Aquifer System in the Pra Basin (Ghana). *Water* 15 (7), 1325.

MANU E., DE LUCIA M. and KÜHN M. (2023b): Isotopic characterization of surface water and groundwater, emphasising origin and recharge processes in the Pra Basin (Ghana). *Water (In review)*.

MANU E., DE LUCIA M. and KÜHN M. (2023c): Water–Rock Interactions Driving Groundwater Composition in the Pra Basin (Ghana) Identified by Combinatorial Inverse Geochemical Modelling. *Minerals* 13 (7), 899.

MANU E., DE LUCIA M. and KÜHN M. (2023d): Hydrochemical characterization of groundwater in the crystalline basement aquifer system in the Pra Basin (Ghana). *Water* 15 (7), 1325.

MANU E., VIETH-HILLEBRAND A, RACH O., SCHLEICHER A. M., TRUMBULL R, STAMMEIER J. A., GOTTSCHE A. and KÜHN M (2023e): Hydrochemistry and stable oxygen (δ18O) and hydrogen (δ2H) isotopic composition of surface water and ground water and mineralogy, in the Pra Basin (Ghana) West Africa. *GFZ Data Services*. DOI: 10.5880/GFZ.3.4.2023.002

MANU J., HAYFORD E., ANANI C., KUTU J. M. and ARMAH T. (2013): Aspects of the chemical composition of the Birimian gold fluid. *Journal of Earth Sciences and Geotechnical Engineering* 3 (4), 87–106.

MAREI A., KHAYAT S., WEISE S., GHANNAM S., SBAIH M. and GEYER S. (2010): Estimating groundwater recharge using the chloride mass-balance method in the West Bank, Palestine. *Hydrological sciences journal* 55 (5), 780–791.

MCNAMARA J. P. (2005): An assessment of the potential for using water and chloride budgets to estimate groundwater recharge in granitic, mountain environments. *Final report: Retrieved 30 April 2023 from https://www2.deq.idaho.gov/admin/LEIA/api/document/download/4654*.

MERKEL B. J., PLANER-FRIEDRICH B. and NORDSTROM D. K. (2005): Groundwater geochemistry. *A practical guide to modeling of natural and contaminated aquatic systems* 2.

MEYBECK M. (1987): Global chemical weathering of surficial rocks estimated from river dissolved loads. *American journal of science* 287 (5), 401–428.

MWRWH (2007): *National water policy*. Ministry of Water Resources, Works and Housing: Accra, Ghana.

NUDE P., HANSON J., DAMPARE S., AKITI T., OSAE S, NYARKO E., ZKARIA N and ENTI-BROWN S (2011): Geochemistry of Pegmatites associated with the cape coast granite complex in the Egyaa and Akim Oda areas of southern Ghana. *Ghana Journal of Science* 51, 89–100.

NYAME F. K. (2013): Origins of B irimian (ca 2.2 G a) mafic magmatism and the P aleoproterozoic 'greenstone belt'metallogeny: a review. *Island Arc* 22 (4), 538–548.

OBUOBIE E., DIEKKRUEGER B., AGYEKUM W. and AGODZO S. (2012a): Groundwater level monitoring and recharge estimation in the White Volta River basin of Ghana. *Journal of African Earth Sciences* 71, 80–86.

OBUOBIE E., DIEKKRUEGER B. and REICHERT B. (2010): Use of chloride mass balance method for estimating the groundwater recharge in northeastern Ghana. *International Journal of River Basin Management* 8 (3-4), 245–253.

OBUOBIE E., KANKAM-YEBOAH K., AMISIGO B., OPOKU-ANKOMAH Y. and OFORI D. (2012b): Assessment of vulnerability of river basins in Ghana to water stress conditions under climate change. *Journal of Water and Climate Change* 3 (4), 276–286.

OKOFO L. B., ADONADAGA M.-G. and MARTIENSSEN M. (2022): Groundwater age dating using multi-environmental tracers (SF6, CFC-11, CFC-12, δ18O, and δD) to investigate groundwater residence times and recharge processes in northeastern ghana. *Journal of Hydrology* 610, 127821.

OKOFO L. B., ANDERSON N. A., BEDU-ADDO K. and ARMOO E. A. (2021): Hydrochemical peculiarities and groundwater quality assessment of the Birimian and Tarkwaian aquifer systems in Bosome Freho District and Bekwai Municipality of the Ashanti Region, Ghana. *Environmental Earth Sciences* 80 (24), 1–22.

OKOFO L. B. and MARTIENSSEN M. (2022): A three-dimensional numerical groundwater flow model to assess the feasibility of managed aquifer recharge in the Tamne River basin of Ghana. *Hydrogeology Journal* 30 (4), 1071–1090.

OKWIR G., KUMAR S., PRAMOD K. S., GAO H. and NJAU K. N. (2023): Conceptualization of groundwater-surface water interaction with evidence from environmental isotopes and hydrogeochemistry in lake Babati Basin in Northern Tanzania. *Groundwater for Sustainable Development* 21, 100940.

ORIAKHI O and OKONOFUA E. (2022): Simulation of Steady State Groundwater Flow in the Lower Pra Basin, Ghana. *Journal of Applied Sciences and Environmental Management* 26 (3), 479–485.

PANNEERSELVAM B., RAVICHANDRAN N., KALIYAPPAN S. P., KARUPPANNAN S. and BIDORN B. (2023): Quality and Health Risk Assessment of Groundwater for Drinking and Irrigation Purpose in Semi-Arid Region of India Using Entropy Water Quality and Statistical Techniques. *Water* 15 (3), 601.

PARKHURST D. L. (1995): *User's guide to PHREEQC: A computer program for speciation, reaction-path, advective-transport, and inverse geochemical calculations*. US Department of the Interior, US Geological Survey, 95–4227.

PARKHURST D. L. and APPELO C. (2013): Description of input and examples for PHREEQC version 3—a computer program for speciation, batch-reaction, one-dimensional transport, and inverse geochemical calculations. *US geological survey techniques and methods* 6 (A43), 497.

PARKHURST D. L., APPELO C. et al. (1999): User's guide to PHREEQC (Version 2): A computer program for speciation, batch-reaction, one-dimensional transport, and inverse geochemical calculations. *Water-resources investigations report* 99 (4259), 312.

PENG T.-R., HUANG C.-C., WANG C.-H., LIU T.-K., LU W.-C. and CHEN K.-Y. (2012): Using oxygen, hydrogen, and tritium isotopes to assess pond water's contribution to groundwater and local precipitation in the pediment tableland areas of northwestern Taiwan. *Journal of Hydrology* 450, 105–116.

PIPER A. M. (1944): A graphic procedure in the geochemical interpretation of water-analyses. *Eos, Transactions American Geophysical Union* 25 (6), 914–928.

PISCIOTTA A., TIWARI A. K. and DE MAIO M. (2019): An integrated multivariate statistical analysis and hydrogeochemical approaches to identify the major factors governing the chemistry of water resources in a mountain region of northwest Italy. *Carbonates and Evaporites* 34, 955–973.

PITKAENEN P., LUUKKONEN A., RUOTSALAINEN P., LEINO-FORSMAN H. and VUORINEN U. (1998): *Geochemical modelling of groundwater evolution and residence time at the Kivetty site*. Tech. rep. Posiva Oy.

PLUMMER L. N., PRESTEMON E. C. and PARKHURST D. L. (1994): An interactive code (NETPATH) for modeling net geochemical reactions along a flow path, version 2.0. *Water-Resources Investigations Report* 94, 4169.

REN X., GAO Z., AN Y., LIU J., WU X., HE M. and FENG J. (2020): Hydrochemical and isotopic characteristics of groundwater in the Jiuquan East Basin, China. *Arabian Journal of Geosciences* 13 (13), 1–17.

RISSER D. W., GBUREK W. J. and FOLMAR G. J. (2005): *Comparison of methods for estimating ground-water recharge and base flow at a small watershed underlain by fractured bedrock in the eastern United States*. Vol. 5038. US Department of the Interior, US Geological Survey.

ROY A., KEESARI T., MOHOKAR H., PANT D., SINHA U. K. and MENDHEKAR G. (2020): Geochemical evolution of groundwater in hard-rock aquifers of South India using statistical and modelling techniques. *Hydrological Sciences Journal* 65 (6), 951–968.

RUIDAS D., PAL S. C., SAHA A., CHOWDHURI I. and SHIT M. (2022): Hydrogeochemical characterization based water resources vulnerability assessment in India's first Ramsar site of Chilka lake. *Marine Pollution Bulletin* 184, 114107.

SAHU P. and SIKDAR P. (2008): Hydrochemical framework of the aquifer in and around East Kolkata Wetlands, West Bengal, India. *Environmental Geology* 55 (4), 823–835.

SASAKOVA N., GREGOVA G., TAKACOVA D., MOJZISOVA J., PAPAJOVA I., VENGLOVSKY J., SZABOOVA T. and KOVACOVA S. (2018): Pollution of surface and ground water by sources related to agricultural activities. *Frontiers in Sustainable Food Systems* 2, 42.

SCANLON B. R., HEALY R. W. and COOK P. G. (2002): Choosing appropriate techniques for quantifying groundwater recharge. *Hydrogeology journal* 10, 18–39.

SCHOELLER H (1965): Qualitative evaluation of groundwater resources. *Methods and techniques of groundwater investigations and development. UNESCO* 5483.

SCHOELLER H (1967): Qualitative evaluation of ground water resources (in methods and techniques of groundwater investigations and development), water resources series, 33.

SHEFFIELD J., GOTETI G. and WOOD E. F. (2006): Development of a 50-year high-resolution global dataset of meteorological forcings for land surface modeling. *Journal of climate* 19 (13), 3088–3111.

SINHA B. and SHARMA S. K. (1988): *Natural ground water recharge estimation methodologies in India*. Springer.

SOLANGI G. S., SIYAL A. A. and SIYAL P. (2019): Analysis of Indus Delta groundwater and surface water suitability for domestic and irrigation purposes. *Civil Eng J* 5 (7), 1599–1608.

STATISTICS I. (2013): IBM Corp. Released 2013. IBM SPSS Statistics for Windows, Version 22.0. Armonk, NY: IBM Corp. *Google Search*.

SUKHIJA B., NAGABHUSHANAM P and REDDY D. (1996): Groundwater recharge in semi-arid regions of India: an overview of results obtained using tracers. *Hydrogeology Journal* 4, 50–71.

SZILAGYI J., HARVEY F. E. and AYERS J. F. (2003): Regional estimation of base recharge to ground water using water balance and a base-flow index. *Groundwater* 41 (4), 504–513.

TAY C., HAYFORD E. and HODGSON I. (2017): Application of multivariate statistical technique for hydrogeochemical assessment of groundwater within the Lower Pra Basin, Ghana. *Applied water science* 7 (3), 1131–1150.

TAY C. K. (2012): Hydrochemistry of groundwater in the Savelugu–Nanton District, northern Ghana. *Environmental earth sciences* 67 (7), 2077–2087.

TAY C. K., DORLEKU M. and KORANTENG S. S. (2018): Hydrochemical evolution of ground and surface water within the Amansie and Adansi districts of the Ashanti region, Ghana. *West African Journal of Applied Ecology* 26 (1), 108–133.

TAY C. K. and HAYFORD E. (2016): Levels, source determination and health implications of trace metals in groundwater within the Lower Pra Basin, Ghana. *Environmental Earth Sciences* 75 (18), 1236.

TAY C. K., HAYFORD E., HODGSON I. O. and KORTATSI B. K. (2015): Hydrochemical appraisal of groundwater evolution within the Lower Pra Basin, Ghana: a hierarchical cluster analysis (HCA) approach. *Environmental Earth Sciences* 73 (7), 3579–3591.

TAY C. K., KORTATSI B. K., HAYFORD E. and HODGSON I. O. (2014): Origin of major dissolved ions in groundwater within the Lower Pra Basin using groundwater geochemistry, source-rock deduction and stable isotopes of 2 H and 18 O. *Environmental earth sciences* 71 (12), 5079–5097.

THYNE G., GÜLER C. and POETER E. (2004): Sequential analysis of hydrochemical data for watershed characterization. *Groundwater* 42 (5), 711–723.

TODD D. (1980): *Groundwater hydrology*. Wiley, New York.

TURNER B. F., GARDNER L., SHARP W. E. and BLOOD E. (1996): The geochemistry of Lake Bosumtwi, a hydrologically closed basin in the humid zone of tropical Ghana. *Limnology and Oceanography* 41 (7), 1415–1424.

UUGULU S and WANKE H (2020): Estimation of groundwater recharge in savannah aquifers along a precipitation gradient using chloride mass balance method and environmental isotopes, Namibia. *Physics and Chemistry of the Earth, Parts a/b/c* 116, 102844.

VERLICCHI P. and GRILLINI V. (2020): Surface water and groundwater quality in South Africa and mozambique—Analysis of the Most critical pollutants for drinking purposes and challenges in water treatment selection. *Water* 12 (1), 305.

WANG R., BIAN J.-M. and GAO Y. (2014): Research on hydrochemical spatio-temporal characteristics of groundwater quality of different aquifer systems in Songhua River Basin, eastern Songnen Plain, Northeast China. *Arabian Journal of Geosciences* 7 (12), 5081–5092.

WANG S. (2014): Hydrochemical and isotopic characteristics of groundwater in the Yanqi Basin of Xinjiang province, northwest China. *Environmental Earth Sciences* 71 (1), 427–440.

WARD JR J. H. (1963): Hierarchical grouping to optimize an objective function. *Journal of the American statistical association* 58 (301), 236–244.

WELHAN J. and FRITZ P (1977): Evaporation pan isotopic behavior as an index of isotopic evaporation conditions. *Geochimica et Cosmochimica Acta* 41 (5), 682–686.

WHO (2017): Guidelines for drinking-water quality, 4th ed.; Incorporating the First Addendum; World Health Organisation: Geneva, Switzerland, 541p.

WILCOX L. (1955): *Classification and use of irrigation waters*. 969. US Department of Agriculture: Washington DC, USA.

WRC (2012): Pra River Basin—integrated water resources management plan. https://www.wrc-gh.org/documents/reports/ (accessed January 22, 2023).

WU Q., WANG G., ZHANG W., CUI H. and ZHANG W. (2016): Estimation of groundwater recharge using tracers and numerical modeling in the North China Plain. *Water* 8 (8), 353.

XIA C., LIU G., MENG Y. and JIANG F. (2022): Reveal the threat of water quality risks in Yellow River Delta based on evidences from isotopic and hydrochemical analyses. *Marine Pollution Bulletin* 177, 113532.

XIAO Y., SHAO J., FRAPE S. K., CUI Y., DANG X., WANG S. and JI Y. (2018): Groundwater origin, flow regime and geochemical evolution in arid endorheic watersheds: a case study from the Qaidam Basin, northwestern China. *Hydrology and Earth System Sciences* 22 (8), 4381–4400.

XU T., SONNENTHAL E., SPYCHER N. and PRUESS K. (2004): *TOUGHREACT user's guide: A simulation program for non-isothermal multiphase reactive geochemical transport in variable saturated geologic media*. Tech. rep. Lawrence Berkeley National Lab.(LBNL), Berkeley, CA (United States).

YIDANA S. M., ALFA B., BANOENG-YAKUBO B. and OBENG ADDAI M. (2014): Simulation of groundwater flow in a crystalline rock aquifer system in Southern Ghana–an evaluation of the effects of increased groundwater abstraction on the aquifers using a transient groundwater flow model. *Hydrological Processes* 28 (3), 1084–1094.

YIDANA S. M., BANOENG-YAKUBO B., ALIOU A.-S. and AKABZAA T. M. (2012a): Groundwater quality in some Voltaian and Birimian aquifers in northern Ghana—application of mulitvariate statistical methods and geographic information systems. *Hydrological sciences journal* 57 (6), 1168–1183.

YIDANA S. M., BANOENG-YAKUBO B. and SAKYI P. A. (2012b): Identifying key processes in the hydrochemistry of a basin through the combined use of factor and regression models. *Journal of earth system science* 121 (2), 491–507.

YIDANA S. M., DZIKUNOO E. A., ALIOU A.-S., ADAMS R. M., CHAGBELEH L. P. and ANANI C. (2020): The geological and hydrogeological framework of the Panabako, Kodjari, and Bimbilla formations of the Voltaian supergroup–Revelations from groundwater hydrochemical data. *Applied Geochemistry* 115, 104533.

YIDANA S. M., GANYAGLO S., BANOENG-YAKUBO B. and AKABZAA T. (2011): A conceptual framework of groundwater flow in some crystalline aquifers in Southeastern Ghana. *Journal of African Earth Sciences* 59 (2-3), 185–194.

YIDANA S. M., OPHORI D. and BANOENG-YAKUBO B. (2008): Hydrochemical evaluation of the Voltaian system—the Afram Plains area, Ghana. *Journal of environmental management* 88 (4), 697–707.

YIDANA S. M., OPHORI D., BANOENG-YAKUBO B. and SAMED A. A. (2012c): A factor model to explain the hydrochemistry and causes of fluoride enrichment in groundwater from the middle voltaian sedimentary aquifers in the Northern Region, Ghana.

YIDANA S. M. and YIDANA A. (2010): Assessing water quality using water quality index and multivariate analysis. *Environmental Earth Sciences* 59 (7), 1461–1473.

YIDANA S. (2013): The stable isotope characteristics of groundwater in the Voltaian Basin–An evaluation of the role of meteoric recharge in the basin. *Journal of Hydrogeology and Hydrol. Eng* 2, 2.

ZAGHLOOL E. et al. (2020): Geochemical Modeling and Statistical Analysis for Groundwater Evolution Assessment in Wadi Qasab, Sohag, Eastern Desert, Egypt. *Journal of Geoscience and Environment Protection* 8 (09), 33.

ZANGO M. S., ANIM-GYAMPO M., GIBRILLA A., PELIG-BA K. B. and OKOFO L. B. (2023): Groundwater recharge and dating in crystalline basement aquifers of Vea catchment: An integrated environmental tracers' approach. *Scientific African* 19, e01505.

ZHANG B., SONG X., ZHANG Y., HAN D., TANG C., YU Y. and MA Y. (2012): Hydrochemical characteristics and water quality assessment of surface water and groundwater in Songnen plain, Northeast China. *Water research* 46 (8), 2737–2748.

ZHANG G., DENG W., YANG Y. and SALAMA R. (2007): Evolution study of a regional groundwater system using hydrochemistry and stable isotopes in Songnen Plain, northeast China. *Hydrological Processes: An International Journal* 21 (8), 1055–1065.

ZHANG L, DAWES W., HATTON T., REECE P., BEALE G. and PACKER I (1999): Estimation of soil moisture and groundwater recharge using the TOPOG_IRM model. *Water Resources Research* 35 (1), 149–161.

ZHU C., WINTERLE J. R. and LOVE E. I. (2003): Late Pleistocene and Holocene groundwater recharge from the chloride mass balance method and chlorine-36 data. *Water Resources Research* 39 (7).

Publications of the candidate

Journal publications

Manu, E., De Lucia, M. and Kühn, M. 2023b. Hydrochemical Characterization of Surface Water and Groundwater in the Crystalline Basement Aquifer System in the Pra Basin (Ghana). *Water*, 15(7), p.1325. DOI: 10.3390/w15071325

Manu, E., De Lucia, M. and Kühn, M. 2023a: Water–Rock Interactions Driving Groundwater Composition in the Pra Basin (Ghana) Identified by Combinatorial Inverse Geochemical Modelling. *Minerals*, 13(7), p.899. DOI: 10.3390/min13070899

Manu, E., De Lucia, M. and Kühn, M. 2023c. Stable Isotopes and Water Level Monitoring Integrated to Characterize Groundwater Recharge in the Pra Basin, Ghana: *Water*, 15(21), p.3760. DOI: 10.3390/w15213760

Manu, E., Afrifa, G.Y., Ansah-Narh, T., Sam, F. and Loh, Y.S.A. 2022: Estimation of natural background and source identification of nitrate-nitrogen in groundwater in parts of the Bono, Ahafo and Bono East regions of Ghana. *Groundwater for Sustainable Development*, 16, p.100696. DOI: 10.1016/j.gsd.2021.100696

Loh, Y.S.A., Fynn, O.F., **Manu, E.**, Afrifa, G.Y., Addai, M.O., Akurugu, B.A. and Yidana, S.M. 2022: Groundwater-surface water interactions: application of hydrochemical and stable isotope tracers to the lake bosumtwi area in Ghana. *Environmental Earth Sciences*, 81(22), p.518. DOI: 10.1007/s12665-022-10644-x

Afrifa, G.Y., Chegbeleh, L.P., Sakyi, P.A., Yidana, S.M., Loh, Y.A.S., Ansah-Narh, T. and **Manu, E.** 2022: Quantifying nitrate pollution sources and natural background in an equatorial context: a case of the Densu Basin, Ghana. *Hydrological Sciences Journal*, 67(13), pp.1941-1953. DOI: 10.1080/02626667.2022.2114357

Loh, Y.S.A., Addai, M.O., Fynn, O.F. and **Manu, E.** 2021: Characterisation and quality assessment of surface and groundwater in and around Lake Bosumtwi impact craton (Ghana). *Sustainable Water Resources Management*, 7, pp.1-18. DOI: 10.1007/s40899-021-00563-3

Duah, A.A., Akurugu, B.A., Darko, P.K., **Manu, E.** and Mainoo, P.A. 2021: Groundwater recharge and potential exploitation in the Densu basin, Southwestern Ghana. *Journal of African Earth Sciences*, 183, p.104332. DOI: 10.1016/j.jafrearsci.2021.104332

Obiri-Nyarko, F., Duah, A.A., Karikari, A.Y., Agyekum, W.A., **Manu, E.** and Tagoe, R., 2021: Assessment of heavy metal contamination in soils at the Kpone landfill site, Ghana: Implication for ecological and health risk assessment. *Chemosphere*, 282, p.131007. DOI: 10.1016/j.chemosphere.2021.131007

Loh, Y.S.A., Akurugu, B.A., **Manu, E.** and Aliou, A.S. 2020: Assessment of groundwater quality and the main controls on its hydrochemistry in some Voltaian and basement aquifers, northern Ghana. *Groundwater for Sustainable Development*, 10, p.100296. DOI: 10.1016/j.gsd.2019.100296

Mainoo, P.A., **Manu, E.**, Yidana, S.M., Agyekum, W.A., Stigter, T., Duah, A.A. and Preko, K. 2019: Application of 2D-Electrical resistivity tomography in delineating groundwater potential zones: Case study from the Voltaian Super Group of Ghana. *Journal of African Earth Sciences*, 160, p.103618. DOI: 10.1016/j.jafrearsci.2019.103618

Manu, E., Agyekum, W.A., Duah, A.A., Tagoe, R. and Preko, K. 2019: Application of vertical electrical sounding for groundwater exploration of Cape coast municipality in the central region of Ghana. *Arabian Journal of Geosciences*, 12, pp.1-11. DOI: 10.1007/s12517-019-4374-4

Data publication

Manu, E. Vieth-Hillebrand, A., Rach, O., Schleicher, A.M., Trumbull, R., Stammeier, J.A., Gottsche, A. and Kühn, M. 2023d: Hydrochemistry and stable oxygen (δ^{18}O) and hydrogen (δ^{2}H) isotopic composition of surface water and groundwater and mineralogy, in the Pra Basin (Ghana) West Africa: *GFZ Data Serv*. DOI: 10.5880/GFZ.3.4.2023.002

Book chapter

Agyekum, W.A., Duah, A.A., Okrah, C. and **Manu, E.** 2017: Groundwater recharge studies and trends in the Lower Volta River Basin, Ghana. *Dams, Development and Downstream Communities*, p.117.

Acknowledgements

I would like to thank the German Academic Exchange Service (DAAD) for awarding me the scholarship (Grant No. 57460308) to pursue my PhD studies in Germany. I am also grateful to the GFZ German Research Centre for Geoscience for their timely financial support. Without their immeasurable support, this would not have been possible.

I extend my heartfelt gratitude to my primary supervisor and section leader, Prof. Dr. Michael Kühn, for graciously welcoming me into his esteemed research group, Fluid Systems Modelling, at the GFZ German Research Centre for Geosciences and the Institute of Geoscience at the University of Potsdam. His insightful guidance, invaluable ideas, and constructive feedback have propelled me towards the successful culmination of my thesis. I am also indebted to Dr. Marco De Lucia for his support of computational programming and consistent encouragement. Additionally, I thank Prof. Dr. Maria-Theresia Schafmeister (Universität Greifswald) and Prof. Bruce Kofi Banoeng-Yakubo (University of Ghana) for graciously agreeing to review and evaluate my thesis. Their expertise and contributions have greatly enriched the quality of my work.

I express my sincere appreciation to Dr.-Ing. Thomas Kempka, my initial point of contact, for his invaluable guidance and support throughout the DAAD scholarship application process. His meticulous review of my research proposal and continuous assistance were pivotal in shaping the early stages of my research journey. I also would like to extend my gratitude to the entire Fluid Systems Modelling section workgroup members. The collaborative and welcoming atmosphere within the group significantly contributed to my motivation and dedication to completing my PhD. Special thanks to Dr. Svenja Steding, Dr. Morgan Tranter, Dr. Theresa Henning, and Dr. Maria Wetzel for generously sharing their expertise and offering guidance when needed.

I would also like to acknowledge the unwavering support of Jenny Meistring, Dr. Christopher Otto, and Dr. Natalie Nakaten for their willingness to accommodate my family's private appointments. I am deeply indebted to the dedicated members of the research team from the CREAM project at the Water Research Institute of Ghana, whose support proved invaluable during my field campaigns. I sincerely thank Dr. Emmanuel Obuobie and Bismark Akurugu for their assistance. Additionally, I express sincere appreciation to my field driver, Mr. Danso, whose commitment was indispensable to the success of the fieldwork. I would also like to thank Dr. Yvonne Sena Akosua Loh from the Department of Earth Science at the University of Ghana for her encouragement.

I am deeply moved by my profound gratitude for my three exceptional children - Angel, Ivan, and Jeremy - whose constant presence served as an unyielding source of motivation, keeping me resolutely focused on my academic pursuit. To my beloved wife, Mrs. Ewurabena Asantewaa Manu, I extend my heartfelt appreciation for her unwavering support and companionship throughout this journey. My gratitude also extends to my parents, Madam Cecilia Aryeh and the late Mr. Kwaku Ofiri, whose investment in my education laid the foundation for my accomplishments.

Lastly, I offer my deepest thanks to the Lord Almighty, whose divine protection and guidance paved the way for the achievement of this significant milestone.

Selbstständigkeitserklärung

Hiermit erkläre ich, Evans Manu, dass ich als Autor der vorliegenden Dissertation mit dem Titel "*Hydrogeochemische Charakterisierung der Wasserressourcen im Pra-Becken (Ghana) zur Qualitätsbewertung und Wasserbewirtschaftung: Feldbeobachtungen und Geochemische Modellierung*", die Arbeit selbstständig und ohne unerlaubte Hilfe angefertigt habe.

Ferner versichere ich, keine anderen als die angegebenen Quellen und Hilfsmittel benutzt zu haben. Alle Ausführungen, die anderen Schriften wörtlich oder inhaltlich entnommenen wurden, sind als solche kenntlich gemacht. Die vorliegende Arbeit wurde in keinem anderen Promotionsverfahren angenommen oder abgelehnt.

_____

Potsdam, 18.12.2023